Analysis of Molecular Interaction and Its Effect on Light- Harvesting and Emitting Organic Systems at the Nanoscale

by

Taesu Kim

A dissertation submitted in partial fulfillment
of the requirements for the degree of
Doctor of Philosophy
(Macromolecular Science and Engineering)
in The University of Michigan
2019

Doctoral Committee:

      Professor Theodore Goodson III, Chair
      Professor Jinsang Kim
      Assistant Professor Charles McCrory
      Professor Emeritus Richard E. Robertson

Taesu Kim

tnskim@umich.edu

ORCID iD: 0000-0002-7128-6312

DEDICATION

I dedicate this dissertation to my parents, spouse and children for their unwavering support and

encouragement.

ACKNOWLEDGEMENTS

TABLE OF CONTENTS

LIST OF FIGURES

LIST OF TABLES

ABSTRACT

Organic electronics is a branch of modern electronics, and it deals with organic materials, such as polymers or small molecules. Its high flexibility, ease of manufacturing, low cost and environmental impact gathered huge interest from industry and academia. While there have been great progress in the area of organic electronic materials, many challenges limit the potentials of various organic systems. The intrinsic structural and electronic inhomogeneity of the solid state aggregates of organic molecules limit their performance and lower their stability. Mismatch between the light absorption and the exciton transport length in organic photovoltaic cells is the critical point of the issue. To solve this problem a better understanding of the excitation transport properties on a local level is essential. However it is difficult to probe the exited dynamics due to fast decay and short transport length of exciton. To better investigate these materials, superior spatial and temporal resolved spectroscopy is essential. In this dissertation, various spectroscopic methods have been introduced to analyze the exciton dynamics in local level. Interferometric two-photon near-field scanning optical microscopy has been introduced to show the organic macromolecular and aggregate systems assembled in different molecular structural orientation. A focus will be placed on the combination of fs-laser interferometry and NSOM microscopy. ~100fs temporal and ~50nm spatial resolution of the system efficiently highlight the structure-functional relationship, discriminate the heterogeneity and measure the coherent excited state dynamic of the molecular system aggregates. Additionally, the ultra-fast excited state behavior of selected organic

electronic materials has been studied using fluorescence upconversion and transient absorption spectroscopy. These investigations inform us of how these photophysical interactions occur in several systems, including light -harvesting and -emitting systems.

CHAPTER I

Introduction and Background

1-1.   Organic Electronics

Organic electronics is an important class of material, as these materials that have has gained prominence due to their versatile functionality such as flexibility, transparency, relatively low cost for production and light weight[1-3]. While the Ching Tang's first practical organic solar cell and light emitting diode power conversion efficiency and EQE (External Quantum Efficiency) were both only 1%[4,5], many scientists and industrial companies have shown great interest in the materials' extendible potential application. Since then a huge amount of time, money and human resources have been invested to promote and expand the field of organic electronic devices. Now, it is not uncommon anymore to use the materials in display, light harvesting, sensor and other semiconductor application[1,3]. The organic photovoltaic power conversion efficiency is close to 15%[6,7] and the external quantum efficiency for OLED (Organic Light Emitting Diode) has already exceeded 30% without special light coupling optical structure[8]. There are countless papers utilizing the benefits of organic system in electronic applications[1-3, 6, 7, 8]. While there have been great progress in the area of organic electronics, many challenges remain unaddressed which limit our

ability in achieving the potentials of various organic materials[1, 3, 9]. It is clear that there is still a need to enhance the relatively low efficiency and device stability in comparison to Si, GaAs[3]. These problems limit the application of organic electronic devices in specific area. Countless scientists and engineers have worked over decades to solve the limitations, and uncover the design rule for expanding the field of the organic applications. They reveal that charge transport, molecular rigidity, conformation and vibration is very important to enhance the materials properties[10]. These properties in organic molecules have highly been affected by its intermolecular interaction and excited state dynamics of the molecules. Organic electronic devices are known to intrinsically possess structural and electronic inhomogeneity which limits their performance. Relatively low efficiency and stability might result from the inhomogeneity of the organic molecular arrangement in comparison with the well-organized inorganic materials[1, 11].To this regard, a better understanding of the excitation transport properties on a local level opens a path to solving the problem. Therefore, in this dissertation, the importance of the localized molecular interactions of organic electronic materials has been investigated using various spectroscopic methods such as NSOM microscope, ultra-fast photon-echo, up-conversion fluorescence and transient analysis.

1-2.   Organic Light Harvesting

Energy liberation is a long-standing human desire. Energy generation processes and facilities spend huge resource such as money, time, materials and manpower, and cause critical problems of environmental disruption threatening human wellbeing. Sunlight is the most abundant energy

resource. Although the first photovoltaic device for the energy liberation goes back to the ancient Egypt, scientific approach using semiconductor was introduced by Charles Fritts in 1883. The efficiency of the first photovoltaic by Charles Fritts is just 1%. However, many scientists and business men have focused on the potential application. There has been a huge progress in the field. Now the maximum efficiency is over 40% using solid state semiconductor which was achieved by Boeing Spectrolab. This feature is similar in the organic light harvesting development. After several decades from Tang's first 1% organic light harvesting devices, a desire for low-cost, flexible and transparent technologies has facilitated development of the organic photovoltaic cells. Organic photovoltaic materials and devices for solar energy conversion have been researched extensively in the last 2 decades, and remarkable progresses have been achieved, with recorded PCE(Power Conversion Efficiencies) ~15% for organic solar cells[6,7]. However there is still need to enhance the PCE to a level close to that of solid state semiconductor. In order to harvest and utilize sunlight enough for photo voltaic application it is essential to understand the photoinduced electron behavior. The active layer of a photovoltaic cell plays the most important role for efficient light harvesting and generation of the electronic power from the sun-light. Free charge carriers are generated from sun light in the active layer. More importantly, these carriers have to efficiently arrive at the electrode for high PCE (Power Conversion Efficiency). However heterogeneity of the organic molecular system in the layer may experience short exciton transport length while the distance is much longer than in lattice structure of inorganic materials because of the strongly bound CT(Charge Transfer) exciton[1]. To solve this problems, the well-known bulk heterojunction donor-acceptor structure has been introduced[12, 13]. It has been shown experimentally that the rate of photoinduced electron transfer (k_{ET}) decreases exponentially with the distance (R_{DA}) between donor and acceptor [10, 14].

$$k_{ET} = k_0 \exp(-\beta R_{DA}) \ldots\ldots\ldots\ldots\ldots\ldots\ldots\ldots\ldots\ldots\ldots\ldots\ldots\ldots\ldots\ldots\ldots\ldots(1\text{-}1)$$

Where k_0 is the electron transfer rate at the boundary between the donor and acceptor materials and β is the attenuation factor. It is noteworthy that the electron transfer rate is critically affected by the donor-acceptor distance based on the equation. This limitation has restricted the design rule for the organic photovoltaic systems. That lowers the donor-acceptor distance dependence of the electron transfer rate is one of the most important issues that researchers are facing now. As conventional understanding, Förster resonance energy transfer (FRET) between the donor and acceptor is a dominant process to the exciton transfer, then, diffusion allows the exciton transfer in the materials. Recently, coherent energy transfer has been introduced for the natural light-harvesting systems. Many results supporting coherent energy transfer extend the exciton diffusion length[15-17], however, there is no direct observation of the coherent energy transportation on artificial light harvesting materials. It is very important to better utilize the organic light harvesting materials and develop new methods to analyze the materials. In this regime, developing new methodology is one of the most important issues, presenting the design rule and utilizing of the materials better. To achieve the purpose, it is essential to analyse the exciton dynamics in ns resolution and fs-time scale due to its time scale and spatial restriction. The affordable solution for the nm scale spatial resolution and fs-time has been proposed by combining the NSOM microscope and fs-laser in this dissertation. I also introduce the methodology of the combination of the two systems, and the experimental results.

1-3.   Organic Light Emitting Diode

Organic light-emitting diode (OLED)) is a very important class of display device, which has properties such as a high color quality and rapid electrical response time over their liquid crystal display counterparts (LCD)[1, 3, 18]. These superior qualities and operational features for display have attracted many interests in industry as well as academia since the Forrest group was able to harvest triplet-excited states in OLEDs via phosphorescence[19-21]. Now the device is rapidly replacing the predominant LCD (Liquid crystal display) market. However, OLED's burn-in and high price in comparison with the LCD are the most critical issues to replace the current dominant LCD display[22]. Many fascinating OLED materials has been introduced to solve the problem[23]. Among them, TADF(Thermally Activated Delayed Fluorescence) is the idea that room thermal energy may facilitate the non-emissive triplet conversion into emissive singlets in a RISC (Reverse InterSystem Crossing) mechanism if the energy level difference between the triplet-singlet manifold is sufficiently small ($\Delta EST < 0.2$ eV)[23-25]. OLEDs using organic TADF emitters have been able to pair the most applicable materials for solving the issues. TADF does not use the expensive rare-earth metal such as Ir, Pt and Rb. Small ΔE_{st} of the materials enables triplet to singlet RISC by assistance of the thermal energy[23-25]. In this regime, singlet and triplet have been used for the luminescence in the same time, hence, high efficiency is achievable. High efficient TADF materials shows almost ideal EQE (External Quantum Efficiency) (EQE) of 25% in comparison to their phosphorescent counterpart without any additional coupling optics[8]. This efficiency is near ideal. However, the key challenge precluding its commercialization is their poor device operational stability.

 It is still very poor in stability even in comparison with the PhOLED(Phosphorescence OLED). It is essential to solve the problem for expanding its application not only academia but also in real

world application. It was interesting to note that while many studies have been published in understanding how the RISC of the TADF emitters may influence the EQE of the devices not to many studies have been done in understanding the effect of aggregation on the TADF stability. However, so far many research efforts in TADF OLED are mostly focusing on improvement of the efficiency[26-27] of TADF materials, while there are some reports to handle the molecular stability issue[28-30]. Empirical hypothesis based on the device life time measurement results has been proposed to investigate the TADF molecular stability. Nakanotani et al. shows that increasing TADF emitter ratio in EML (Emmisive layer) has increased the operational stability of the OLED[28]. Lin-Song Cui et al. also shows the n-type host increases the device stability[29]. Both papers claim that stability has been achieved by expanding the electron and hole recombination zone[28-29]. Zhang et al. also emphasizes the importance of steric hindrance effect for the TADF stability[30]. They show that the additional carbonyl group critically increases the OLED device operational life time by one magnitude. Hiroki et al. insist that an efficient RISC (Reverse Intersystem Crossing) can increase the OLED device efficiency and stability[31]. Most of the results have been focused on finding OLED device life time and new TADF structure relationship by connecting the two properties without any analysis of the excited states dynamics. Although the device operational properties shows the direct results on the OLED stability, it is necessary to understand the chemical and physical orientation of the TADF instability in molecular level to understand and utilize the molecular systems better. The excited state dynamics, molecular orientation and intermolecular interaction effects on the devices operational life-time is still vague. Therefore, I present the origin of TADF degradation using various spectroscopic methods in this dissertation. I investigated the molecular properties of several TADF isomers using carbazole, benzonitrile and triazine by applying various spectroscopic methods such as fs-transient, time-resolved upconversion

fluorescence in different concentration. Different intermolecular interaction of the isomers in varying concentrations shows the different excited state dynamics such as fluorescence spectrum, excited state dynamics and transient absorption. Surprisingly, these different excitation dynamics affect the molecular degradation via UV-exposure. In this dissertation, the study of the different excitation dynamics and their effect on the TADF stability has been proposed.

1-4.   Ultra-fast optical investigation of the organic electronic materials

As mentioned before, organic photovoltaic and OLED are the most important application in the area of organic electronics materials. The most crucial issues facing the field is getting higher efficiency and increasing device operational life-time to extend its application to the real world and compete with the conventional inorganic electronic devices[2, 3]. The main difference between the inorganic and organic electronics might be their structural orientation. Additionally, one has to keep in mind that the solid-state properties of the materials are very different: inorganic semiconductors are typically covalently bound and crystallize in simple structures such as the cubic lattice; organic semiconductors on the contrary are characterized by dipole–dipole bonds (van der Waals bonds) and crystallize, if they do at all, in rather complicated crystal classes such as monoclinic or triclinic crystals[1]. Therefore, their semiconducting and other properties differ strongly and they are consequently used for rather different applications. Inorganic molecules has very regular and periodic lattice structure. However, organic molecular structural arrangement is very random. This structural difference may lead the inhomogeneous excited- and ground- state energy level distribution[1, 32, 33]. This inhomogeneity affect the exciton diffusion properties of the

organic molecular systems aggregates. Short exciton diffusion length below 10nm critically affect the absorption and electronic mobility of the organic molecular system.
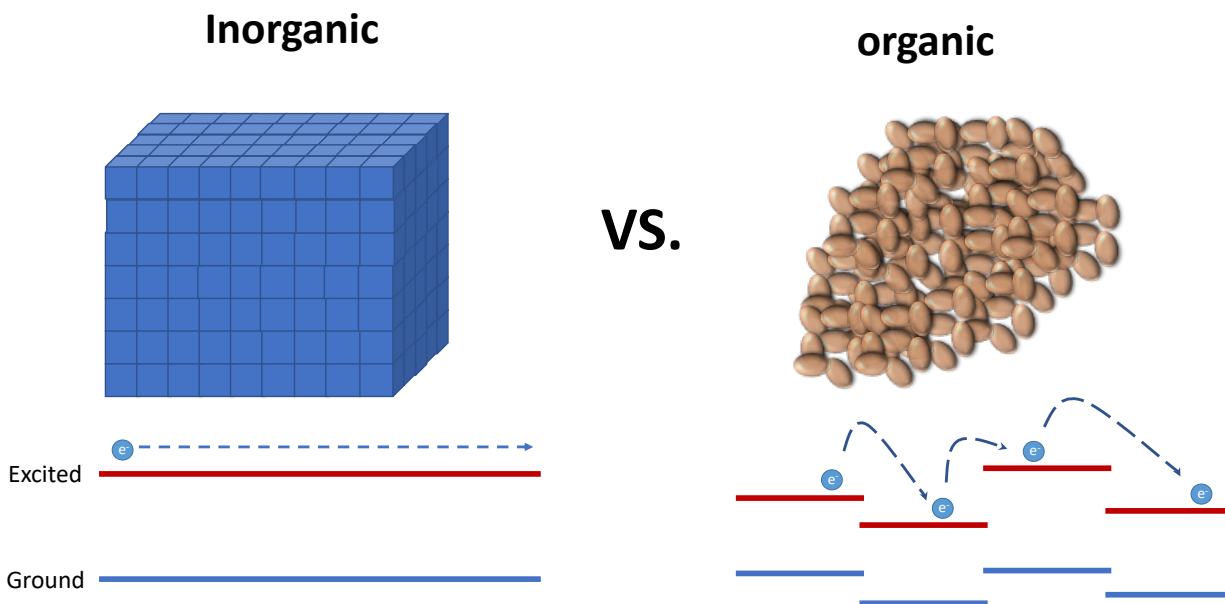
Figure 1-1. *Structural difference between inorganic and organic solid-state phase.*

Both properties highly affect the organic electronics properties and stability due to its non-uniform excited state distribution due to its structural inhomogeneity[32,33]. It is hence very important to investigate the exciton properties of the solid-state organic molecular in local level. In this dissertation, the important exciton properties of molecules such as coherent energy transport, dephasing and exciton life time will be discussed. The formation of the solid state and the effects of coupling is also discussed. In particular, I will present the influence of the morphology and differentiate between organic single crystals and polycrystalline or amorphous layers. Finally, we discuss the optical properties of organic materials and in particular the importance of the Coulomb-bound exciton. For this purpose, various spectroscopic methods has been used such as Two-photon

absorption, up-conversion fluorescence analysis, time-correlated single photon counting and time-resolved NSOM microscopy. Following chapter II simply introduces the methods.

1-5.   Dissertation Outline.

In this dissertation I mainly aimed to find answers about the importance of the localized molecular interaction for organic electronics devices' efficiency and stability. How critically does the heterogeneity in solid state of the organic molecules affect the coupling properties of the materials? Localized interaction is important to the device operational stability? The main purpose of that interrogation is to understand and utilize the organic molecular system better. I strongly believe that the inhomogeneous localized molecular interaction is one of the most important features limiting the organic molecular systems' potential. Using different sets of experiments, I studied several important issues to answer these questions. The remainder of this dissertation has been distributed as follows. In chapter II, various spectroscopic methods have been introduced to investigate of the excited state dynamics and local interaction. Basic theory of non-linear spectroscopy such as two-photon absorption, fluorescence upconversion has been explained. Transient-absorption and two-photon NSOM interferometric methods have also been introduced to understand the chapter III and VI. The work discussed in chapter III is published in *the Journal of Physical Chemistry C and* the work in chapter IV is published in *the Journal of Physical Chemistry C.* Chapter III and IV shows an importance of the localized intermolecular interaction using NSOM interferometric methods. NSOM microscopy allows us to understand the temporal and spatial heterogeneity of molecular aggregation by combining high-spatial and temporal

resolution. I believe that this method may allow us to understand the important intermolecular interaction of the organic molecular system in complex solid state, hence, utilizing these materials better. Chapters V and VI (These works will be used for patent applications in Korea) show the OLED materials stability measurement and analysis. OLED still has device operational stability problem. In the chapter V fast OLED materials stability evaluation without device fabrication using NSOM fluorescence microscopy is discussed. The origin of the TADF OLED molecules deformation also has been illustrated using ultra-fast spectroscopic methods. In Chapter VII, I summarize the insights gained from the investigations of organic electronic materials using NSOM microscopy and other ultra-fast spectroscopic methods.

1-6.   References

1.   Riede, M.; Lüssem, B.; Leo, K. Organic Semicondoctors, *Comprehensive Semiconductor Science and Technology*, **2011**, 4, 448-507.

2.   Polman, A.; Knight, M.; Garnett, E.C.; Ehrler, B.; Sinke, W.C. Photovoltaic Materials: Present Efficiencies and Future Challenges. *Science*, **2016**, 352, aad4424.

3.   Kaltenbrunner, M. et al. An Ultralightweight Design for Imperceptible Plastic Electronics. *Nature*, **2013**, 499, 458– 465.

4.   Tang., C. Two-layer organic photovoltaic cell. *Appl. Phys. Lett.*, **2013**, 48, 183-185.

5.   Tang, C.; VanSlyke, S. Organic electroluminescent diodes. *Appl. Phys. Lett.*, **1987**, 51, 913-915.

6.   Yuan, J. et al. Single-Junction Organic Solar Cell with over 15% Efficiency Using Fused-

        Ring Acceptor with Electron-Deficient Core. *Joule*, **2019**, 3, 1140–1151.

7.   Cui, Y. et al. Over 16% efficiency organic photovoltaic cells enabled by a chlorinated

        acceptor with increased open-circuit voltages. *Nat. Commun.,* **2019**, 10, 2515.

8.   Kim, S. et al. Organic Light-Emitting Diodes with 30% External Quantum Efficiency

        Based on a Horizontally Oriented Emitter. *Adv. Funct. Mater.*, **2013**, 23, 3896–3900.

9.   Goodson, T., Solar Fuels: Materials, Physics, and Applications; CRC Press, Boca Raton,

        Florida, 2017.

10.   Hedley, G.; Ruseckas, A.; Samuel, I. Light Harvesting for Organic Photovoltaics. *Chem.*

        Rev. **2017**, 117, 796−837.

11.   Menke, S. M.; Holmes, R. J. Exciton Diffusion in Organic Photovoltaic Cells. *Energy*

        Environ. Sci. **2014**, 7, 499– 512.

12.   Yu, G.; Gao, J.; Hummelen, J.;Wudl, F.; Heeger, A. Polymer photovoltaic cells:

        enhanced efficiencies via a network of internal donor-acceptor heterojunctions, *Science*,

        1995, 270, 1789-1791.

13.   Park, S. et al. Bulk heterojunction solar cells with internal quantum efficiency

        approaching 100%. *Nat. Photonics*, **2009**, 3, 297-303.

14.   Gray, H.; Winkler, J. Long-range electron transfer. *Proc. Natl. Acad. Sci. USA*, **2005**,

        102, 3534–3539.

15.   Scholes, G. Using Coherence to Enhance Function in Chemical and Biophysical Systems.

        Nature, **2017**, 543, 647– 656.

16.   Haedler, A. Long-Range Energy Transport in Single Supramolecular Nanofibers at Room

        Temperature. *Nature*, **2015**, 523, 196– 200.

17.   Winiger, C.; Li, S.; Kumar, G.; Langenegger, S.; Haner, R. Long-Distance Electronic Energy Transfer in Light Harvesting Supramolecular Polymers. *Angew. Chem., Int. Ed.*, **2014**, 53, 13609– 13613.

18.   Riedl, T.; Görrn, P.; Kowalsky, W. Transparent Electronics for See-Through AMOLED Displays. *J. Dis. Technol., 2009,* 5, 501-508.

19.   Baldo, M. et al. Highly efficient phosphorescent emission from organic electroluminescent devices. *Nature,* **1998**, 395, 151-154.

20.   Baldo, M.; Lamansky, S.; Burrows, P.; Thompson, M.; Forrest, S. Very high-efficiency green organic light-emitting devices based on electrophosphorescence. *Appl. Phys. Lett.*, **1999**, 75, 4-6.

21.   Adachi, C.; Baldo, M.; Thompson, M.; Forrest, S. Nearly 100% internal phosphorescence efficiency in an organic light-emitting device. *J. Appl. Phys.*, **2001**, 90, 5048-5051.

22.   Chan, C.; Tanaka, M.; Nakanotani, H.; Adachi, C. Efficient and stable sky-blue delayed fluorescence organic light-emitting diodes with CIE_y below 0.4. *Nat. Commun.,* **2018**, 9, 5036.

23.   Yang, Z. et al. Recent advances in organic thermally activated delayed fluorescence materials. *Chem. Soc. Rev.*, **2017**,46, 915-1016.

24.   Uoyama, H.; Goushi, K.; Shizu, K.; Nomura, H.; Adachi, C. Highly efficient organic light-emitting diodes from delayed fluorescence. *Nature*, **2012**, 492, 234-238.

25.   Hamze, R. et al. Eliminating nonradiative decay in Cu(I) emitters: >99% quantum efficiency and microsecond lifetime. *Science*, **2019**, 363, 601–606.

26.   Xiang, S. et al. To improve the efficiency of thermally activated delayed fluorescence OLEDs by controlling the horizontal orientation through optimizing stereoscopic and linear structures of indolocarbazole isomers. *J. Mater. Chem. C*, **2018**,6, 5812-5820.

27.   Hosokai, T. et al. Evidence and mechanism of efficient thermally activated delayed fluorescence promoted by delocalized excited states. *Science Advances*, **2017**, 3, e1603282.

28.   Nakanotani, H. et al. Promising operational stability of high-efficiency organic light-emitting diodes based on thermally activated delayed fluorescence. *Scientific Reports*, **2013**, 3, 2127.

29.   Cui, L. et al. Long-lived efficient delayed fluorescence organic light-emitting diodes using n-type hosts. *Nat. Commun.*, **2017**, 8, 2250.

30.   Zhang, D.; Cai, M.; Zhang, Y.; Zhang, D.; Duan, L. Sterically shielded blue thermally activated delayed fluorescence emitters with improved efficiency and stability. *Mater. Horiz.*, **2016**, 3, 145-151.

31.   Noda, H.; Nakanotani, H.; Adachi, C. Excited state engineering for efficient reverse intersystem crossing. *Science Advances*, **2018**, 4, eaao6910.

32.   Vogelsang, J.; Adachi, T.; Brazard, J.; Vanden Bout, D.; Barbara, P. Self-assembly of highly ordered conjugated polymer aggregates with long-range energy transfer. *Nat. Mater.*, **2011**, 10, 942–946.

33.   Noriega, R. et al. A general relationship between disorder, aggregation and charge transport in conjugated polymers. *Nat. Mater.*, **2013**, 12, 1038-1044.

CHAPTER II

Ultra-fast and localized spectroscopic methods to investigate the organic conjugated

molecular systems.

2-1.   Introduction

The Importance of the ultra-fast spectroscopy has been found from its etymology. The word

Spectroscopy comes from the Latin "spectron" meaning spirit and the Greek "σκοπιεν" meaning

to see. While we are not able to see the molecules, light is used to investigate the materials.

Different spectroscopies give you different perspectives on the materials. These noncontact light

matter interaction give us a bunch of signals from the materials. Important steady state information

such as resonance frequencies, spectral amplitudes and lineshapes has been generated from

traditional steady state spectroscopy from fluorescence and absorption spectrum. While this

general information is important to understand the basic properties of organic systems, it is difficult

to interrogate the excited states dynamics of the systems. It is well known that the excited state

exciton dynamics are critical to the organic electronics efficiency and stability[1, 2]. To understand

and utilize organic electronic materials better, it is essential to investigate the excited dynamics

rather than just focus on the conventional methods. However, excited state dynamics is generally

very fast chemical process with timescales ranging from fs to ps. It is hence needed to invoke a measurement process in that same time scale. Multiple light-matter interactions from ultra-fast non-linear spectroscopy can be used to correlate different spectral features in the fast time domain. Spectroscopic methods can be used to analyze molecular structure, vibration relaxation, interaction and exciton transfer for understanding the molecular dynamics which is critical to the organic electronic materials such as light-harvesting systems and OLED[3-5]. This is why ultra-fast spectroscopy using fs-laser is critical for the organic electronic systems.

Additionally, complex system such as aggregate and conjugated polymer has many different molecular orientation and the spectra from the molecules become congested or ensembles. Therefore, the signals form the conventional far-field based microscopy is in vague by a number of molecular orientation in solid state[4]. It is hence essential to develop better spectroscopic methods to discriminate the heterogeneity of the molecular aggregate. For this purpose, near-field microscopy methods have been introduced, allowing for better spatial resolution below optical diffraction limit. More importantly, combination of ultra-fast nonlinear spectroscopy and near field scanning microscopy (NSOM) may allow detect the heterogeneity of the transition dephasing time and intermolecular coupling in organic molecular aggregates which is crucial for understanding of the contribution of coherent effects in organic electronic systems. We can hence resonantly drive one spectroscopic feature and see how another is influenced. In this chapter, basic theory and feature of the spectroscopic methods has been introduced to better understand the chapters following.

2-2.   Two-photon Absorption

Two photon absorption is a process when two different photons are absorbed simultaneously on a molecular system or atom, then excited to a higher state where the energy is two folds of the excitation photon. The molecular systems absorption is not the same, proportional to the photon intensity, which is general feature of the non-linear optical behavior. Hence, the absorption coefficient of the molecular system becomes quadratic feature. Electron displacement in an organic
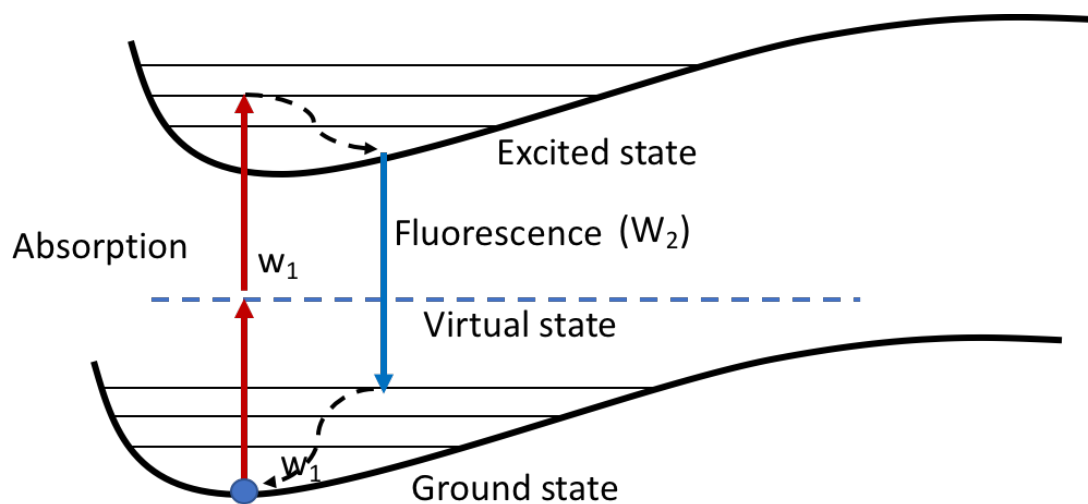
Figure 2-1. Graphical explanation of the two-photon absorption.

material due to light exposure in non-linear optics has been simplified as using anharmonic oscillator model. The polarizability of a material P (t) can be described as a power series in electric field strength as equation 2-1

$$P(t) = \chi_1 E(t) + \chi_2 E^2(t) + \chi_3 E^3(t) + \cdots \qquad (2\text{-}1)$$

where χ_n is called n[th] order molecular susceptibilities. It is noticeable that polarization of the molecular systems of higher order susceptibilities is proportional to the power of the excitation electronic wave. Using this feature higher resolution for microscope and micro-fabrication, higher penetration depth for bio materials which is low absorption coefficient in IR (Infrared Rays) and low Rayleigh scattering is achievable. This specific feature is why non-linear optical (NLO) behavior is important and popular in scientific applications such as fluorescence microscopy, micro-fabrication and optical storage. In spectroscopic application, two-photon absorption also shows its superior advantage which not shown in single-photon spectroscopy. Simultaneous absorption allows high lying excited states and forbidden states as combination of the multiple photon which is difficult to access in single photon scheme. The synthesis of information from these different spectroscopies provides a greatly clarified view of the excited state properties of a molecule[6]. For example, by combining vibronic analyses from the spectra of one- and two-photon transitions into the same electronic absorption band, it is possible to achieve a nearly complete assignment of vibrations in the excited state[6]. Thus, my research has concentrated on using non-linear optical techniques for investing the organic electronic materials.

2-3.   Fluorescence Upconversion.

Fluorescence of organic chromophores is sensitive to environmental changes. Hence, fluorescence measurement of organic molecules is widely used for interrogating important molecular properties such as conformation changes, solvent relaxation, charge transfer characteristics and vibration relaxations[7,8]. Most fluorescence decays occur between sub-ps and ns. Higher temporal resolution

and fluorescence sensitivity is critical to investigate molecular systems better. Many spectroscopy techniques have been introduced in fluorescence decay dynamics measurement for the purpose. Time Correlated Single-Photon Counting (TCSPC) and streak camera using photoelectrical effect sensitive to weak signal are the most popular and simple methods[9, 10]. However, it is very difficult and expensive to achieve sub-picosecond temporal resolution using these methods because of the temporal limitation of the electrical process. It is hence needed to develop methods based on optical fluorescence measurement using ultra-fast laser and NLO.
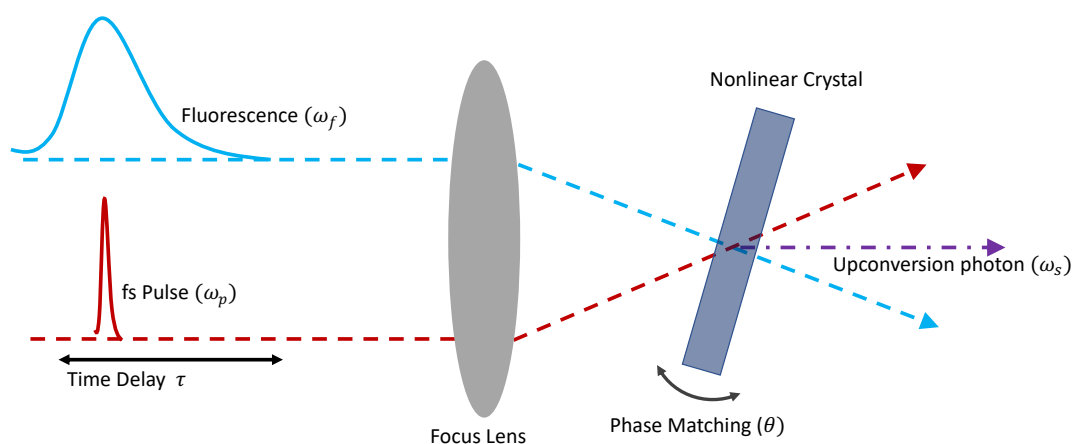
Figure 2-2. Schematic diagram of the fluorescence upconversion.

Fluorescence upconversion may be the solution to the problem. Combination of the fs-laser and sum-frequency (2nd order non-linear effect) allows the higher temporal resolution and sensitivity[11, 12]. Additionally, this methods has been used for broad spectrum range from UV to Near-IR[12-15] and various chemical process such as solvation dynamics, coherent vibration relaxation and charge transfer properties and solvation relaxation in both solution and solid phase[4, 16-18]. It is also noticeable that the sum frequency is very sensitive to the light polarization. Upconversion is effectively used for the fluorescence anisotropy measurement. Hence we can sensitively verify the

energy migration, molecular rotation and conformational change. Figure 2-2. shows the schematic diagram of the fluorescence upconversion. As shown in the figure, upconversion is actually a cross-correlation of the fluorescence and a laser pulse in different time. Fluorescence excited by the light has been monitored by sum-frequency photons from the fs-laser pulse inside the nonlinear crystal with phase-matching conditions. Sum frequency photons are only generated during the pulse width of the fs-pulse laser. We can hence get very high temporal resolution around the fs-laser pulse width. One thing we should consider is the phase matching conditions. To get the higher signal wavelength and wave vector of the upconversion systems have to meet the condition

$$\omega_s = \omega_f + \omega_p \tag{2-2}$$

$$k_s = k_f + k_p \tag{2-3}$$

where wavevector k is the $2\pi n/\lambda$. To meet these conditions, it is necessary rotate the nonlinear crystal very carefully.

2-4. Transient Absorption Spectroscopy.

Transient Absorption (TA) is a well-known technique for investigating the excited state behavior of molecular systems. The method involves using two pulses in different time domains so called pump-probe.
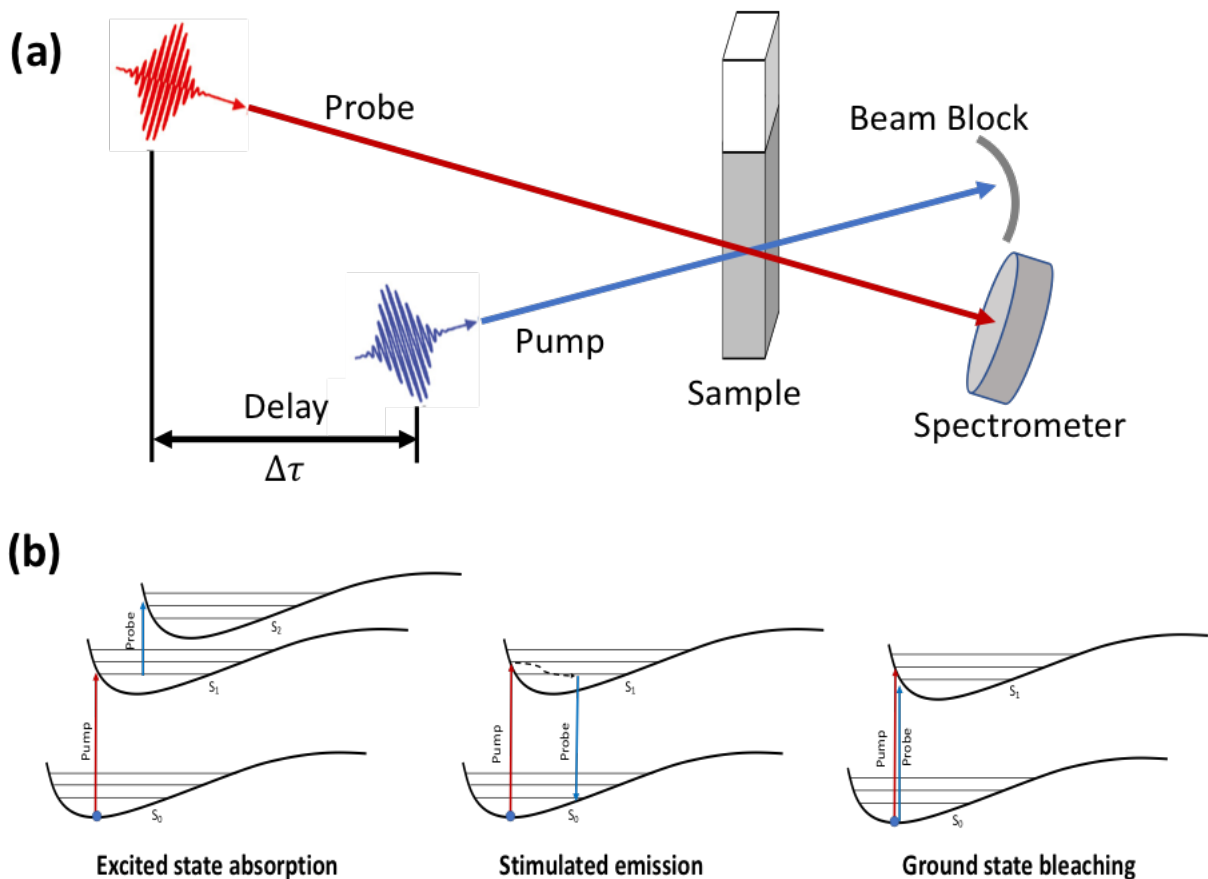
Figure 2-3. *(a) Schematic diagram of the TA spectroscopy and (b) different mechansim of the TA signal.*

First pulse excites the molecules via single photon excitation at a wavelength lower than the absorption maximum of the materials, then white super continuum second pulse is exposed to the molecule to investigate the interaction of the excited state by the first pulse. One can interrogate the excited state dynamic by measuring the variation of the second excited white super continuum probe in wavelength and time. A schematic diagram of TA the has been shown in Figure 2-3. TA signal can be obtained by three different processes, so called, excited state absorption (ESA), Stimulated emission (SE) and ground state bleaching (GSB)[19]. Optically allowed transition from

the excited state to higher excited state may exist in certain wavelength regions due to the absorption of the white probe pulse at these wavelengths when pump pulse is exposed to the sample before the probe pulse. In this case absorption spectrum difference ΔA becomes positive in the wavelength if the probe pulse is relatively weaker than the pump pulse that the excited-state population is less affected by the white probe pulse. This process is known as excited state absorption (ESA). The second process for TA is stimulated emission (SE). Assuming a two-level system, the Einstein coefficients A_{12}(Ground to exited state) and A_{21}(Excited state to ground state) are the same. Thus, stimulated emission can occur if the white probe pulses spur the transition from the excited state and ground state of the excited population by pump pulse. While the photon in stimulated emission is emitted in the exact same direction as the probe photon, weak probe pulse does not affect the signal critically. Hence, stimulated emission in TA will lead to a negative ΔA. Final process is the ground state bleaching. Let us consider that the excited population is not fully saturated via the pump pulse. In this case ground state absorption is favored rather than excited state absorption from the white probe pulse. In this case, ΔA in ground state absorption wavelength becomes negative. One can easily interrogate and resolve the excited state dynamics by monitoring the these kinetics. However, it is noteworthy that the three processes are mostly not independent processes for most molecules. We need to be careful when interpreting TA signals.

2-5. NSOM microscopy

Ultrafast laser technologies opens a new world of the NLO spectroscopy in chemistry. Owing to the vectorial nature and short pulse width of broad band fs-laser and combination of the linear and nonlinear spectroscopy, real-time dynamics of organic molecules has been unveiled[20]. We now have more knowledge and information about the electronic charge transfer, vibration relaxation, conformation change and other fast processes taking place in the organic molecules. However, it is still challenging to get a higher spatial resolution beyond the optical diffraction limit (<200nm) for discriminating the molecular heterogeneity depending on its orientation inside the solid state phase of molecular aggregates. This poor resolution is not enough to understand the multiple desired phenomena in condensed matter physics as determined by nanometer scale such as electronic, phonon scattering lengths[4, 20]. It is hence essential to develop new methods interrogating the molecular interaction with better spatial resolution to achieve and understand better the applications of the organic electronics devices. SEM (Scanning Electronic Microscopy), STM (Scanning Tunneling Microscopy) and AFM (Atomic Force Micrscopy) allow the spatial resolution beyond the optical diffraction limit. However, applying these methods is not appropriate to utilize the huge benefit of ultra-fast optical spectroscopy at the same time. It is hence necessary to find out the optical microscopy that fully appropriate the nature of the NLO spectroscopy. In this regime, NSOM (Near Field Optical microscopy) is one of the best solution for that purpose. NSOM exploiting near-field electro-magnetic field is a microscopy technique having higher spatial resolution than the conventional optical microscopy using far-field. According to Abbe's theory[21] of image formation, the highest spatial resolution of the optical component are limited

22
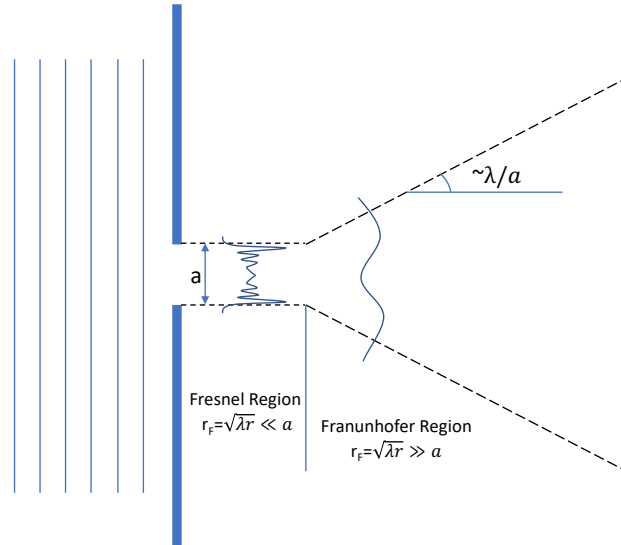
Figure 2-4. *Fresnel and Fraunhofer diffraction via aperture.*

by its aperture size. The minimum resolution using light has been expressed as following

$$d = 0.61 \frac{\lambda_0}{N.A.} \tag{2-4}$$

where, λ_0 is the vacuum wavelength and N.A. is the numerical aperture. Based on the minimum visible range light wavelength (400nm) and the equation, 200nm is the ideal spatial resolution of the optical microscope. However, this equation is only effective in the Franunhofer diffraction region, so called far-field[20]. As seen in the figure 2-4, optical diffraction after a size of aperture, can be divided as Fresnel region and Fraunhofer region depending on the distance from the aperture. NSOM uses the light field of the Fresnel Region, so called near-field. These fields carry the high frequency spatial information that is equal to high spatial resolution based on the information theory. NSOM therefore yields a higher spatial resolution
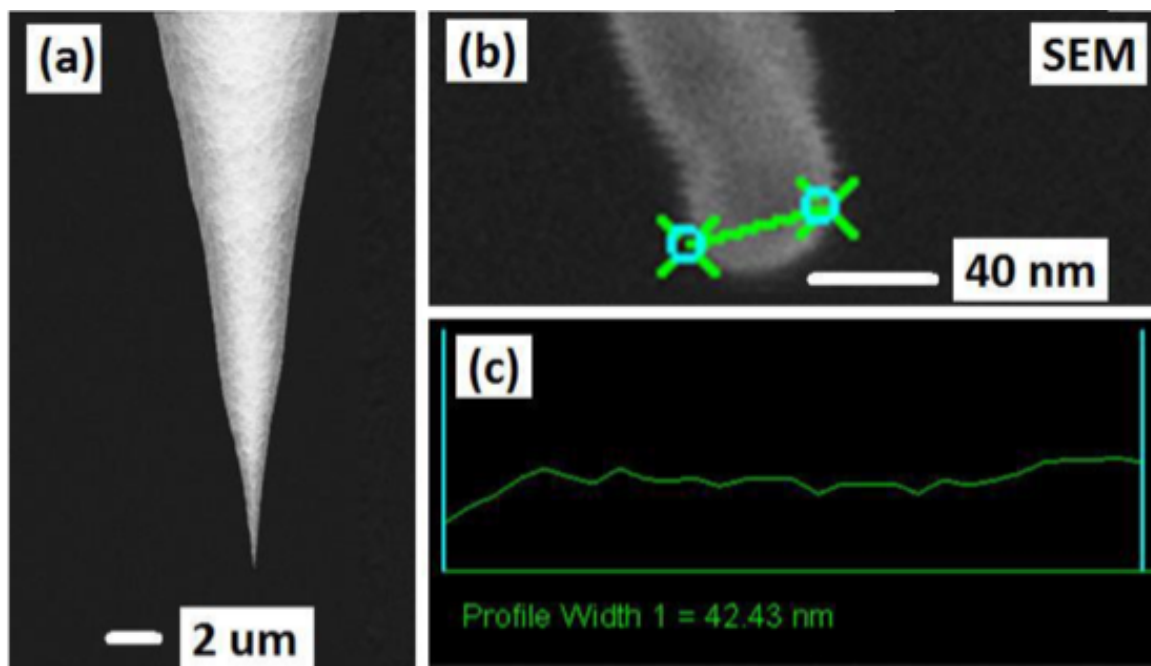
Figure 2-5. SEM image of a sample NSOM probe used with ~40 nm tip diameter (a) SEM image of ~10 um x ~18 um field of view (b) zoomed in SEM image of the NSOM tip (c) SEM profile.

beyond the optical diffraction limit through a careful distance control from the object within the Fresnel region. Figure 2.5 shows the traditional NSOM tip. The NSOM tip size is ~40nm. This tiny aperture size allows the near field formation at the end of the tip. Using this tip we can get a superior spatial resolution as seen in Figure 2.6 in well-known fluorescence reference materials like Rhodamine B.
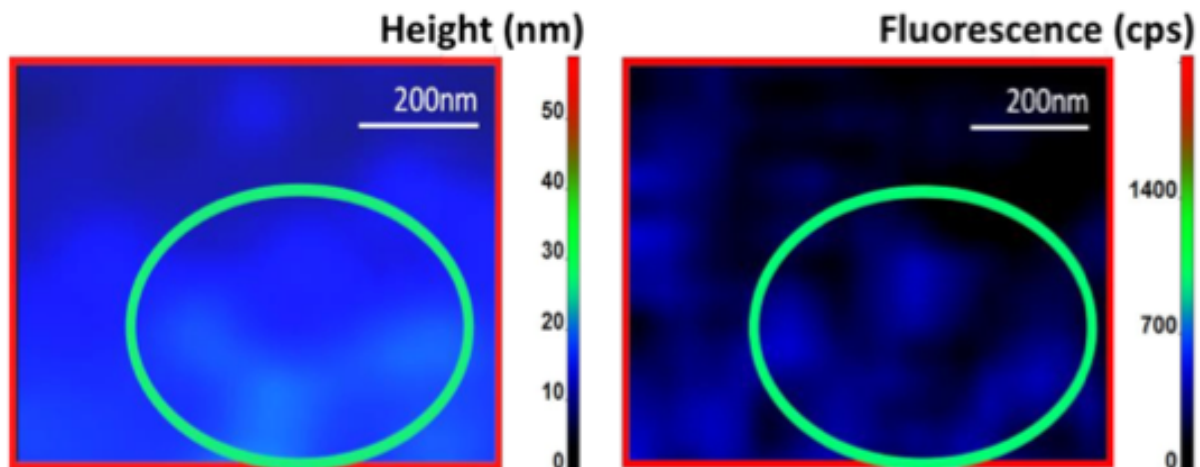
Figure 2-6. *NSOM scanning for rhodamine B. Rhodamine B topology (left) and fluorescence (right).*

2-6. Time-Resolved NSOM microscopy.

While NSOM guarantees a superior spatial resolution, we only get the fluorescence intensity information using NSOM only. Fluorescence gives some important information, but is not sufficient to investigate the localized energy transfer and heterogeneity of the molecular aggregate, and more importantly excited state dynamics of organic systems in coherent regime. We hence combine the wave-packet interferometric spectroscopy and NSOM. The two photon NSOM interferometric time resolved spectroscopy has been developed to investigate the intermolecular coupling strength and dephasing of molecular systems. The excited state dynamics have been investigated with the near-field optical scanning microscope excited in two-photon mode by a sequence of phase-locked femtosecond pulses. The phase-locked pulse pair excitation technique provides interferometric femtosecond time resolution with the capability of detecting coherent

effects and a ~40 nm spatial resolution in two-photon excitation regime. The transition dephasing time, which is crucial for understanding of the contribution of coherent effects in organic photovoltaic structures, can also be measured with this method. Figure 2-7 illustrates the representative feature of how the two-pulse two photon NSOM interferometric system works to measure the molecular coherent excitation dynamics.
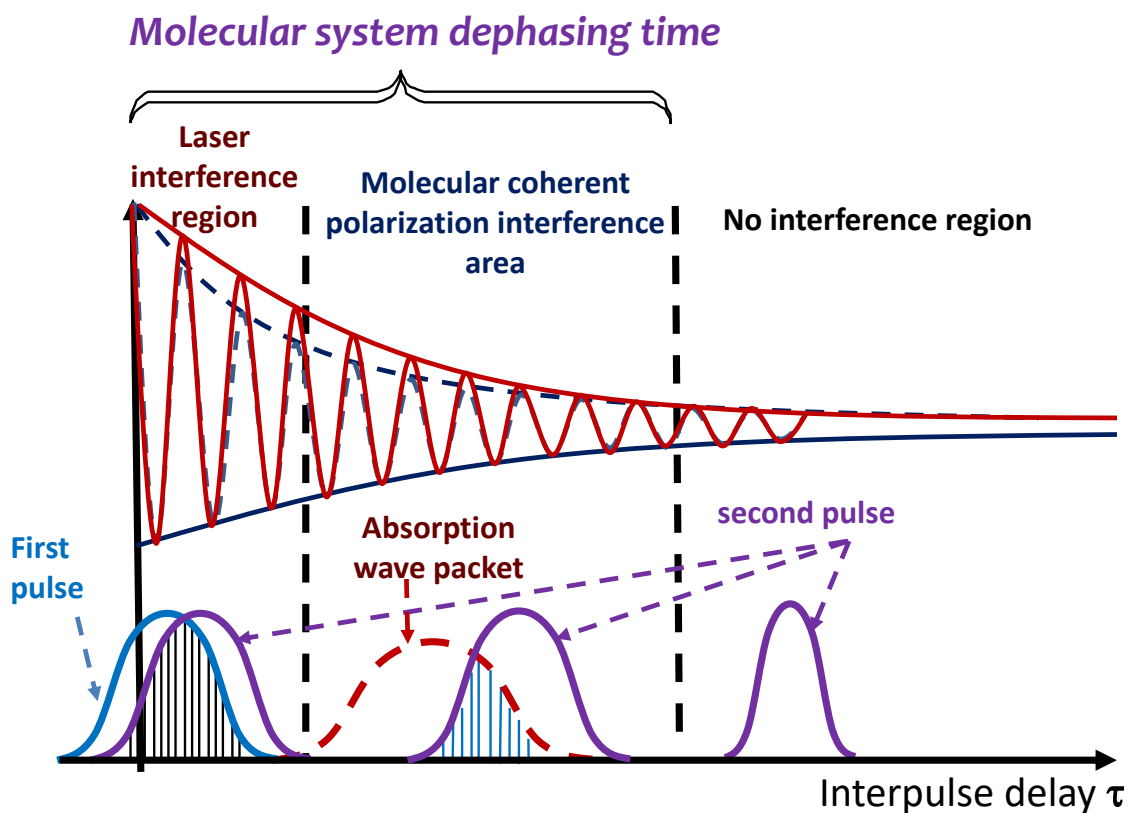
Figure 2-7. *Representative feature of coherent excitation transport via two photon excitation interferometry. Dashed line indicate excitation laser autocorrelation. Solid line shows the coherent excitation transition*

The two excitation fs-pulse pulses generates coherent excited state or wavepacket which is a coherent superposition of electronic states of a molecular transition dipole aligned with the light polarization[22-24]. The wave function $\Psi(t)$ of the molecular system after pulse excitation can be expressed[22] by

$$\Psi(t) = |g\rangle > + \sum_n c_n(t)|e_n\rangle \tag{2.5}$$

Where g is the ground state, $c_n(t)$ is the time dependent amplitude of the excited state e_n.

And two-photon absorption in the excited state amplitude $c_n(t)$ of each pulse is :

$$C_n(t) = \frac{i}{\hbar}\sum_j \frac{u_{nj}u_{jg}}{\hbar(\omega_j - \omega_L + i\Gamma_{jg})} \times \hat{E}^2(\omega_n) \tag{2.6}$$

Where u_{nj} and u_{jg} are transition dipole moment between the ground state and excited state j and g, ω_j and ω_n is the transition frequencies from the ground to the excited state, ω_L is the excitation laser frequency, Γ_{jg} is the homogeneous linewidth of the j_{th} state and $\hat{E}^2$ is the Fourier transform of the excitation pulse. In adjusting the pulse pair with the interpulse delay of τ the electric field $E(t) = A(t)e^{-i\omega_L t} + A(t-\tau)e^{-i\omega_L(t-\tau)}$ where A(t) is the slow varying pulse amplitude for excitation. The excited state population has evolved as a function of the interpulse delay τ. [22, 24].

We measured the coherent excited state population dynamics as measuring the fluorescence of the molecular system. The region can be divided into three parts : laser interference, molecular coherent polarization interference and no interference region as a function of the interpulse delay as shown in figure 2-7. If the interpulse delay is below the excitation pulse width, the collective excitation population is highly affected by the laser itself[25] than the molecular absorption wave

packet. We hence say that this region is a laser interference region. Beyond the region, excited state interference between molecular absorption wave packet from the first pulse and second laser pulse becomes dominant and gives a significant coherent excitation dynamics evolution corresponding with the exciton coupling and electronic dephasing[4, 22, 26]. At the longer interpulse delay time the excitation wavepacket diminished through electronic dephasing and lost its coherence. One is not able to see the interference feature. In this region, no electronic coherent dynamics has been expected although there is still vibronic coherence. However, we assume that these vibronic coherence is very weak and not considered in this paper. We measure the excitation wavepacket envelope and interference by measuring the fluorescence. The interference and envelope gives some specific information of the molecular systems such as excited state coupling to the external components and energy transfer to the other molecule[4, 22, 26].

2-7.   References

1.   Riede, M.; Lüssem, B.; Leo, K. Organic Semicondoctors, *Comprehensive Semiconductor Science and Technology*, **2011**, 4, 448-507.

2.   Wang, P. et al. Stable and Efficient Organic Dye-Sensitized Solar Cell Based on Ionic Liquid Electrolyte. *Joule*, **2018**, 2, 2145-2153.

3.   Fleming, G. Chemical applications of ultrafast spectroscopy. Oxford University Press, 1986.

4.   Varnavski, O.; Kim, T.; Cai, Z.; Yu, L.; Goodson, T. Inhomogeneity of the Ultrafast Excited State Dynamics in Organic Photovoltaic Materials Measured at Nanoscale. *J. Phys. Chem. C*, **2018**, 122, 22201−22209.

5.   Yamakita, Y. et. al. Femtosecond electronic relaxation and real-time vibrational dynamics in 2′-hydroxychalcone. *Phys. Chem. Chem. Phys.*, 2019,21, 5344-5358.

6.   Friedrich, D. Two-Photon Molecular spectroscopy. *J. Chem. Educ.,***1982**, 52, 472-481.

7.   Lakowicz, J. Principles of Fluorescence Spectroscopy, 3rd Ed, Springer Science+Business Media, LLC, NY. 2006.

8.   Saha, R.; Verma, P.; Rakshit. S.; Saha, S.; Mayor, S.; Pal. S. Light driven ultrafast electron transfer in oxidative redding of Green Fluorescent Proteins. *Sci. Rep.* **2013**, 3, 1–7.

9.   Duncan, R.; Bergmann, A.; Cousin. A.; Apps, D.; Shipston, M. Multi-dimensional time-correlated single photon counting (TCSPC) fluorescence lifetime imaging microscopy (FLIM) to detect FRET in cells. *J. Microsc.* **2004**, 215, 1–12.

10.   Saha, S.; Mandal, P.; Samanta, A. Solvation dynamics of Nile Red in a room temperature ionic liquid using streak camera. *Phys. Chem. Chem. Phys.*, **2004**, 6, 3106–3110.

11.   Sajadi, M.; Quick, M.; Ernsting, N. Femtosecond broadband fluorescence spectroscopy by down- and up- conversion in b-barium borate crystals. *Appl. Phys. Lett.*, 2**013**, 103, 173514.

12.   Jimenez, R.; Fleming, G.; Kumar, P.; Maroncelli, M. Femtosecond solvation dynamics of water. *Nature*, **1994**, 369, 471–473.

13.   Chosrowjan, H.; Taniguchi, S.; Tanaka, F. Ultrafast fluorescence upconversion technique and its applications to proteins. *FEBS J.*, **2015**, 282, 3003–3015.

14.   Zhang, L.; Kao, Y.; Qiu, W.; Wang, L.; Zhong, D. Femtosecond studies of tryptophanfluorescence dynamics in proteins: local solvation and electronic quenching. *J. Phys. Chem. Lett. B* , **2006**, 110, 18097–18103.

15.   Tomi, T. et. al. Energy and electron transfer in the photosynthetic reaction center complex of Acidiphilium rubrum containing Zn-bacteriochlorophyll a studied by femtosecond up-conversion spectroscopy. Biochemica et Biophysica Acta (BBA) –. *Bioenergetics*, **2007**, 1767, 22–30.

16.   Jarzeba, W.; Walker, C.; Johnson, A.; Barbara, P. Nonexponential solvation dynamics of simple liquids and mixtures. *Chem. Phys.*, **1991**, 152, 57–68.

17.   Rubtsov, I.; Yoshihara, K. Vibrational coherence in electron donor-acceptor complexes. *J. Phys. Chem. A* , **1999**, 103, 10202–10212.

18.   Mataga, N. et. al. First unequivocal observation of the whole bell-shaped energy gap low in intramolecular charge separation from S2 excited state of directly linked porphyrin-imide dyads and its solvent-polarity dependencies. *J. Am. Chem. Soc.*, **2001**, 123, 12422–12423.

19.   Berera, R.; Grondelle, R.; Kennis, Ultrafast transient absorption spectroscopy: principles and application to photosynthetic systems. *J. Photosynth Res.,* **2009**, 101, 105–118.

20.   Dunn, R. Near-Field Scanning Optical Microscopy. *Chem. Rev.,* **1999**, 99, 2891-2928.

21.   Abbe, E. Beiträge zur theorie des mikroskops und der mikroskopischen wahrnehmung. *Arch. Mikrosk. Anat.*, 1**873**, 9, 413−468.

22.   Sato, S.; Nishimura, Y.; Sakata, Y.; Yamazaki, I. Coherent Control of Oscillatory Excitation Transfer in Dithia-1,5[3,3]anthracenophane by a Phase-Locked Femtosecond Pulse Pair. *J. Phys. Chem. A*, **2003**, 107, 10019-10025.

23.   Blanchet, V.; Nicole, C.; Bouchene, M-A.; Girard, B. Temporal Coherent Control in Two-Photon Transitions: From Optical Interferences to Quantum Interferences. *Phys. Rev. Lett.* **1997**, 78, 2716-2719.

25.   Dudovich, N.; Dayan, B.; Faeder, S.; Silberberg, Y. Transform-Limited Pulses Are Not Optimal for Resonant Multiphoton Transitions. *Phys. Rev. Lett.*, **2001**, 86, 47-50.

26.   Naganuma, K.; Mogi, K.; Yamada, H. General method for ultrashort light pulse chirp measurement. *IEEE J. Quantum Electron.*, **1989**, 25, 1225-1233.

27.   Scherer, N. et. al. Fluorescence-detected wave packet interferometry: Time resolved molecular spectroscopy with sequences of femtosecond phase-locked pulses. *J. Chem. Phys.,* **1991**, 95, 1487.

CHAPTER III

Inhomogeneity of the Ultrafast Excited State Dynamics in Organic Photovoltaic Materials

Measured at Nanoscale

3-1.   Introduction

New organic electronic devices, such as photovoltaics are of great interest in many different

areas of research and technology[1,2]. Although there has been great progress in the area of organic

photovoltaics, many challenges remain which limit our ability to achieve the potential of various

organic materials[1,3,4]. Solid state organic light conversion devices are known to intrinsically

possess structural and electronic inhomogeneity which limits their performance[1,4]. A better

understanding of the excitation transport properties on a local level opens a path to solving the

problem of the mismatch between the light absorption and the exciton transport length in organic

photovoltaic cells and thus enhancement of their efficiency[5]. One of the long-standing questions

in this regard concerns the contributions of coherent and incoherent energy transport in organic

photovoltaic devices and their role in achieving long excitation transport lengths in organic

systems.[6-11] In order to get a deeper insight into the local transport dynamics in these systems there

is a need to probe transport processes in the condensed phase and to follow the energy transport

dynamics with fast time resolution and high spatial resolution. There have been a number of reports illustrating the importance of incoherent (distance dependent) energy transport in organic photovoltaics utilizing spectroscopic techniques in solution and in the solid state[4]. However, the case for coherent energy transport has not been thoroughly investigated in the solid state. Perhaps the reason this challenge exists stems from the very fast (~100fs) time scale and relatively small (<10nm) length scales a coherent energy transport mechanism may be operable in certain organic photovoltaic systems[6]. Various approaches combining ultrafast pump-probe methods with confocal[12] and near field microscopy[13-15] have been demonstrated. Pioneering work of Hell and coauthors with stimulated emission depletion (STED)[16] combines microscopy with a nonlinear pump-dump scheme. STED has been used to increase the spatial resolution of the fluorescence microscopy but the time-resolution obtained with this method remains in the range of ~100ps. Application of the third donut -shaped saturation pulse to the pump-probe microscopy can provide resolution enhancement beyond the optical diffraction limit[17] but distortions of the time profile by the third pulse in the solid state are possible. Another interesting approach for the visualization of the exciton transport has been suggested[18] and further developed for ultrafast pump-probe microscopy with spatial and time resolution 50nm and 300fs, respectively.[19] This method also allows for the spatial resolution below the diffraction limit in a confocal arrangement. However, it requires relatively high light intensity to keep the noise at a low level[19] thus limiting the applicability of this method for the organic systems. While the contribution of coherent energy transport in solid state organic structures has been recognized by many authors[7-11], none of the above time-resolved microscopy approaches were able to directly detect coherent effects. Near-field scanning optical microscopy (NSOM) has been shown to be a powerful method to probe the optical properties of the material in small domains that can be affected by the spatial

inhomogeneity. The spatial resolution of NSOM can be below 50nm[20] and, in combination with femtosecond excitation techniques, a time resolution of ~100fs can be achieved[13-15]. However, the technical complexity of the standard pump-probe NSOM combination along with the stability of the sample system under the relatively high excitation power makes it challenging to realize the method's potential capabilities. The scientific information obtained with this approach in organic systems remains very limited[15,21]

In this chapter the excitation energy transport properties in a photovoltaic material consisting of novel non-fullerene dimeric perylene diimide acceptor (DPDI) with PTB-7 donor (molecular structures are provided in Fig. 3-1.) has been introduced. The energy transfer dynamics have been investigated with the near-field scanning optical microscope excited in two-photon mode by a sequence of phase-locked femtosecond pulses (Near Field Two Photon Interferometry (NFTPI) method), Fig. 3-1. The phase-locked pulse pair excitation technique provides interferometric femtosecond time resolution with the capability to detect coherent effects and ~40nm spatial resolution in two-photon excitation regime. Here we have observed coherent transients in the near field microscope, including NSOM signal oscillations associated with the excitation energy transport in the organic structure. To the best of my knowledge, this is the first direct measurement of the coherent transport associated with the long range excitation energy transport in a solid state organic material at room temperature with both high time and spatial resolution by near-field optical microscopy.
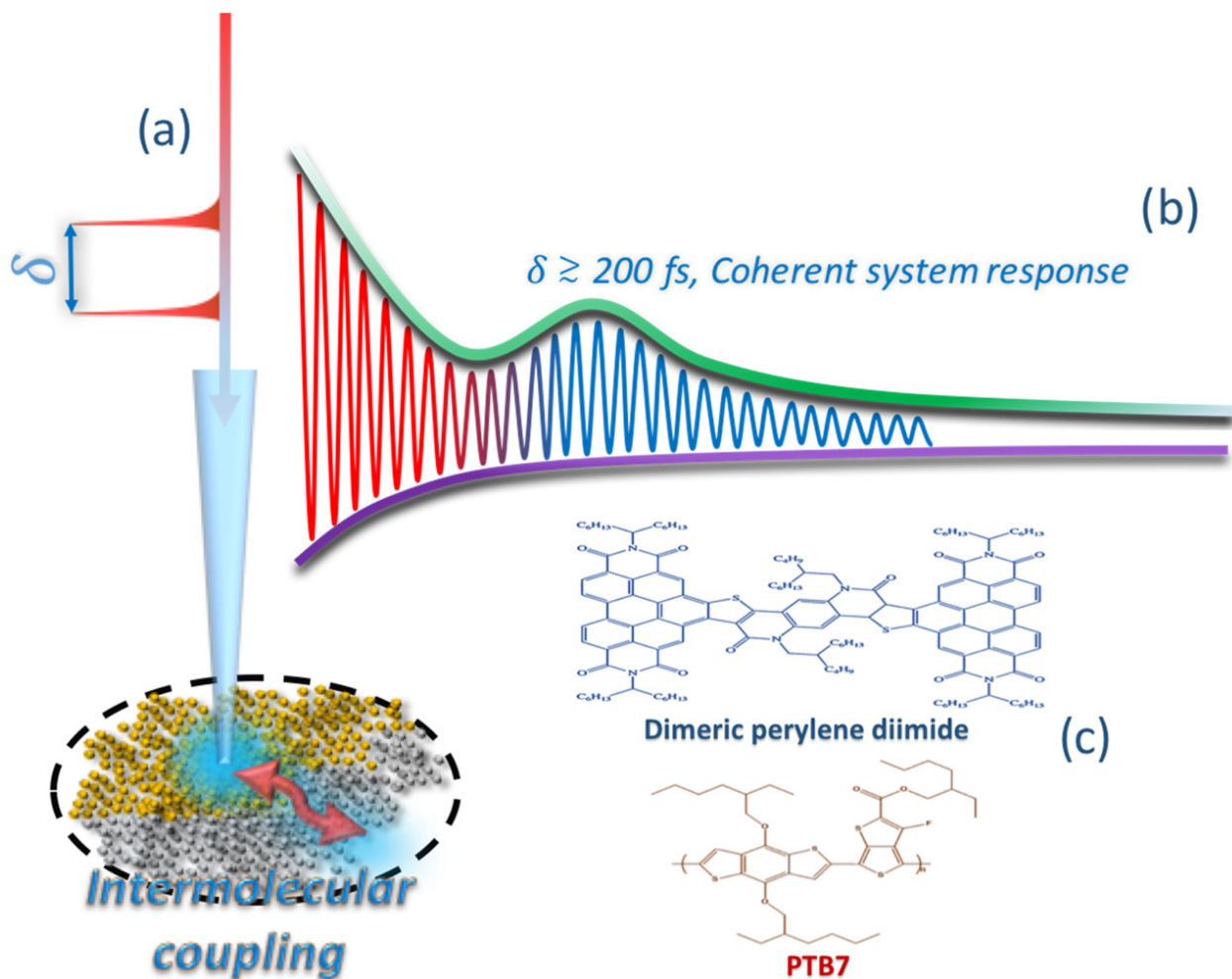
Figure 3-1. *Schematic representation of near field scanning optical microscope utilizing an ultrafast pulse sequence two-photon excitation. (a) Schematic of two-photon, pulse pair driven NSOM. Ultrashort pulse sequence (< 125 fs pulse width) with inter-pulse delay τ has been introduced to the NSOM fiber. (b) The system's time and spatial resolution allowed for the detection of the specific modulation of the interferometric two-photon excited fluorescence signal for the photovoltaic organic material between 125 ~ 500 fs pulse-to-pulse delay which is larger than the pulse width used for the excitation. (c) Structures of a DPDI and PTB-7 investigated in this work.*

3-2. Experimental section

A dimeric perylene diimide molecular system (DPDI) investigated in this work has been developed as an efficient non-fullerene electron acceptor for the bulk heterojunction (BHJ) organic solar cells.[22] The synthesis and characterization of DPDI have been described elsewhere.[22] This class of molecule is an attractive alternative to the fullerenes as electron acceptors, which are typically used in BHJ cells.[23] They possess electron affinity comparable to that of fullerenes, are inexpensive to synthesize, and strongly absorb the visible light which is advantageous for the BHJ cell applications.[24] The molecular structure of DPDI is shown in Figure 3-1c. It has the absorption and fluorescence peaks in benzene-hexane mixture (2:3 ratio) solution at 461nm and 547nm, respectively (spectroscopic information is provided in Figure 3-2.).
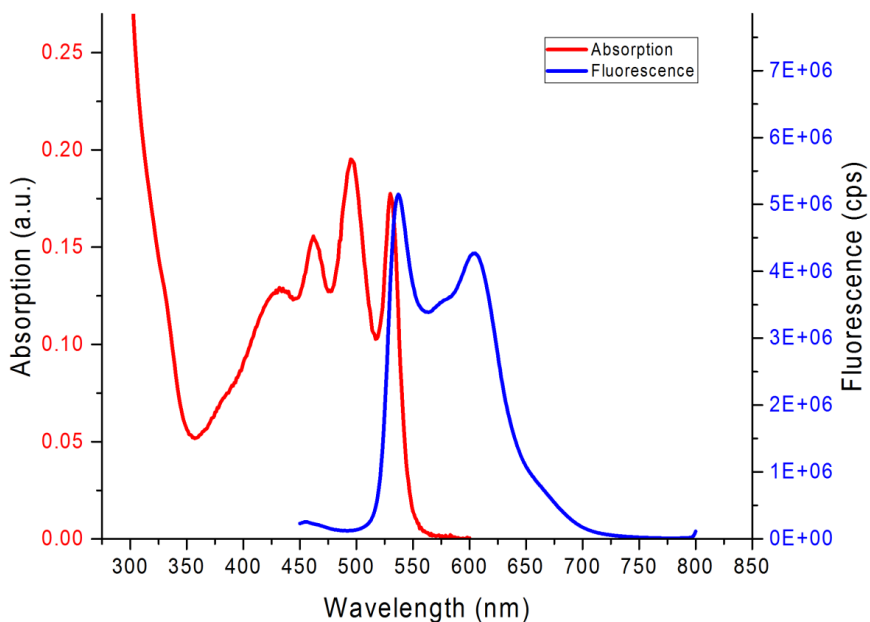
Figure 3-2. *Normalized absorption and emission spectra of compounds in 2:3 ratio of benzene-hexane mixture.*

Solution of the perylene diimide dimer in benzene-hexane mixture (2:3 ratio) was drop cast on a glass substrate. The resulting samples were vacuum dried under ~10 inHg at 30°C for ~24 hours. The dried and cooled (to room temperature, under vacuum) samples were then used for NSOM experiments. The absorption and fluorescence spectra of DPDI in solutions at different concentrations of DPDI and in the thin films (overaged over the area 0.3 cm^2 for the absorption and over the area 10^{-4} cm^2 for the fluorescence) have been measured (Fig. 1 in ref 22). The absorption spectrum in the thin film was found to be shifted to the red by ~6 nm in comparison with that in solution. The fluorescence spectrum in the thin film showed a spectral broadening with a substantial increase of the red shoulder (Table 1, Fig. 1 in ref 22). These spectral changes from the DPDI solution to the solid state film point to the aggregate formation in the thin film.[22] It is also worth noting that the different fluorescence spectra has been recorded at different excitation spots (~100um in diameter) in the thin DPDI film. This indicates heterogeneity of the DPDI aggregates at different locations. We have also performed the measurements on a polymer blend containing the well-known donor polymer Poly[[4,8-bis[(2-ethylhexyl)oxy]benzo[1,2-b:4,5-b']dithiophene-2,6-diyl][3-fluoro-2-[(2-ethylhexyl)carbonyl]thieno[3,4-b]thiophenediyl]] (PTB-7)[25] and DPDI acceptor forming a composition used in BHJ photovoltaic cells. The structure of PTB 7 is shown on Fig. 3-1c. PTB7 is one of the most efficient donor materials for organic solar cells.[25] The synthesis procedure for PTB7 has been described elsewhere.[26] This donor material has relatively low band gap and rigid polymer backbone.[25, 26] Solution of the PTB-7 and DPDI acceptor blend has been made by mixing two solutions with same volume, each solution was made by using the same substance weight and the same volume of chloroform. The sample was dried in vacuum at 30°C after drop casting on a thin glass substrate.

The NSOM excitation system used in this work provides the phase- locked femtosecond pulse pairs with the accurate control of the inter-pulse separation in the pair. Interesting approach based on the fluorescence detection after four-pulse excitation sequence has been reported[27]. This method utilizes the interpulse phase modulation decoupled from the interpulse envelope delays in 2D spectroscopy configuration (Phase-modulation 2D fluorescence spectroscopy : PM-2D FS)[25,26]. While this approach provide additional information on excitonic coupling[26] its application to the near-field microscopy of organic materials is very challenging due to its complexity and higher excitation power. However, the theoretical instrumentation developed for PM-2D FS may be helpful for deeper modelling of the two-photon two pulse microscopy described in this work. Our method utilizes two wedged BBO crystals with the mutually orthogonal optical axis orientation installed on the translation stage to produce a pair of femtosecond pulses from a single input pulse.[27]
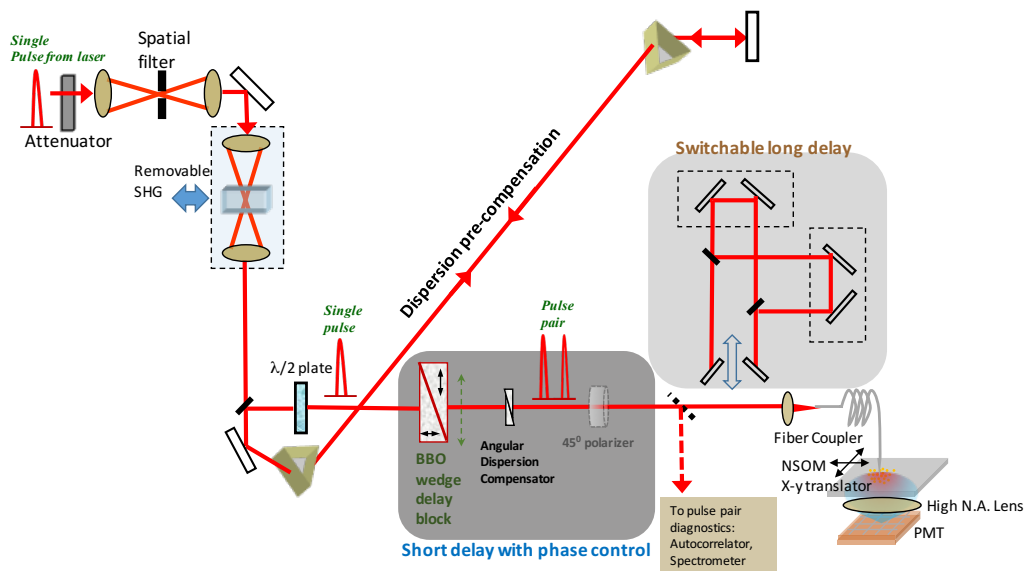
Figure 3-3. *Schematic diagram of two photon NSOM excitation. A switchable long time scale inter- pulse variable delay line provides pulse pairs with relatively long inter-pulse delays up to 200ps (without inter-pulse phase control) is shown in the grey box.*

A detailed description and optical diagram of the system has been illustrated in Fig. 3-3. A femtosecond pulse of duration 124 fs at the wavelength 810nm (peak of the laser spectrum) is introduced to the system in the first stage. A variable attenuator is installed to adjust the intensity of the laser pulse to the microscope appropriately. Spatial mode profile of the light after the attenuator is rectified by passing the light through a spatial filter located just after the attenuator. The switchable second harmonic generator is installed for one photon microscope excitation mode but this was not used in this work. Two wedged BBO crystals arrangement is the main functional part of the two-photon, two pulse NSOM excitation system[27]. The birefringent crystal wedges mounted on the delay stage provide a very accurate inter-pulse separation control with the increment of 0.015fs. These two wedged α-BBO crystals with mutually orthogonal optical axis orientations (FOCtek Photonics, Inc.) are used to produce the variable delay between two collinear orthogonally polarized pulses.[8] The rectangular BBO- block with the optical axis aligned vertically is installed in front of the BBO wedge to pre-compensate the constant interpulse delay introduced by the wedges having non-zero thickness at the apex. The $\lambda/2$ waveplate prepares the light beam polarized a 45º with respect to the horizontal plane, two polarization components of which (horizontal and vertical) experience different time delays in the 2-wedge BBO block installed on the motorized delay stage (MFA-PPD, Newport). The output polarizer oriented at 45º with respect to the horizontal (vertical) plane prepares two collinear pulses of equal amplitude having the same polarization (45º with respect to horizontal plane) with the mutual inter-pulse delay dictated by the amount of particularly oriented birefringent α-BBO crystal in the light path. Both pulses travel the same optical path allowing mutual phase locking with high stability. The delay system is capable of maintaining the phase difference between two pulses accurately and precisely. Interferometric
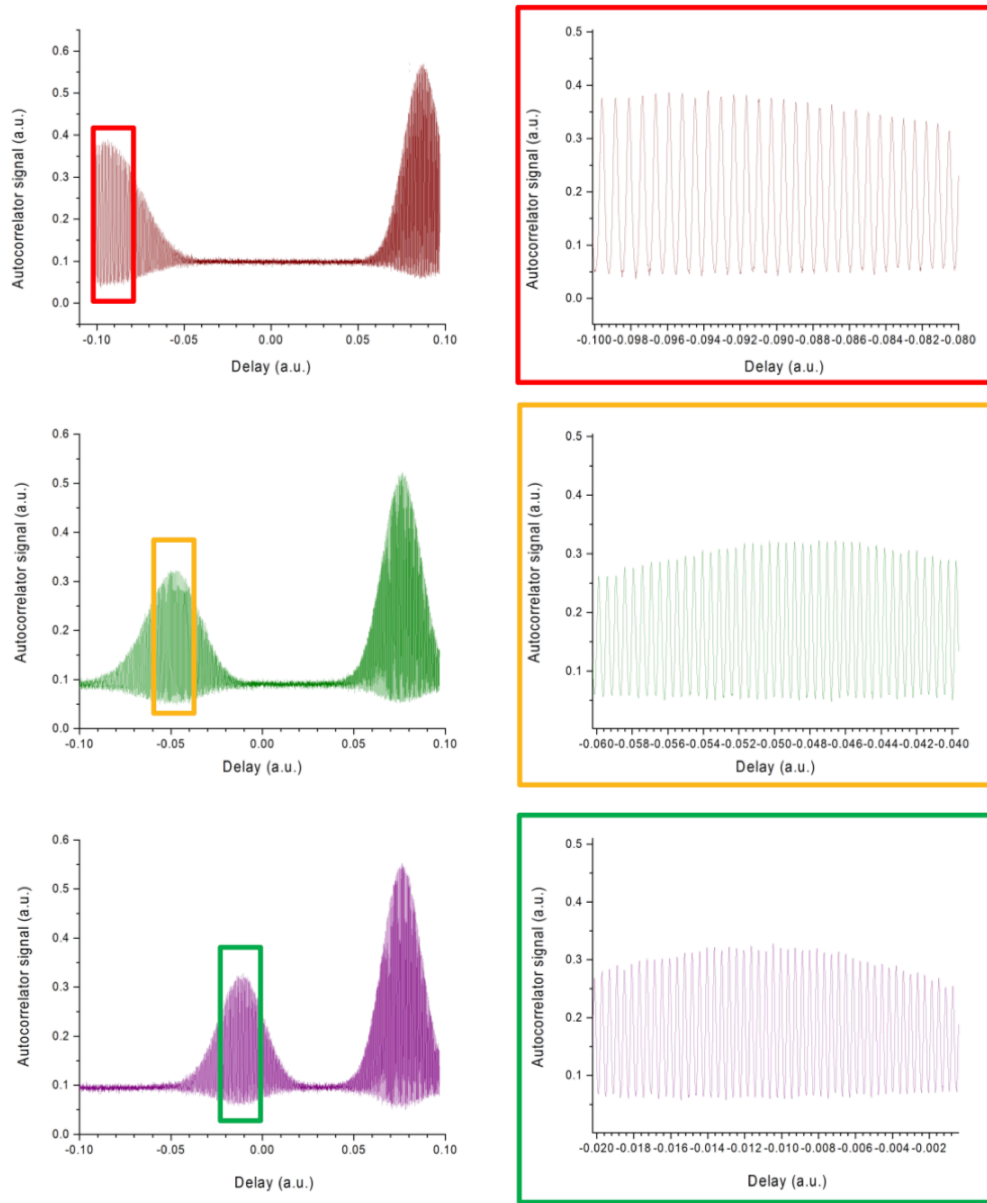
Figure 3-4. *Autocorrelation traces at different delays introduced by the BBO wedge system. Only two pulses from the autocorrelation triplet are shown. Delay line positions in mm on the graphs are 15mm, 10mm, 5mm from top to bottom.*

autocorrelator traces of the pulse pair created by the birefringent delay line at different delays show the robust phase control between two pulses (See Fig. 3-4).

Measurements were performed using Ti:Sapphire (Spectra Physics Mai Tai) providing 810nm 124fs (full width half maximum) pulses at 80 MHz. In the interpulse delay unit the birefringent BBO wedges had an apex angle 6.[20] and maximum thickness of 3.3mm. They were mounted on translation stages driven by the actuators (MFA-PPD, Newport) with the resolution of 0.1um. The wedge system provides an accurate inter-pulse separation control with the increment of 0.015fs and the repeatability of 0.198fs. Interferometric autocorrelator traces of the pulse pair created by the birefringent delay line at different delays show the robust phase control between two pulses (See Fig. 3-3). Before entering the first BBO wedge, two orthogonally polarized pulses passed the 1.0 mm-thick rectangular BBO block with the optical axis aligned vertically to pre-compensate the constant interpulse delay introduced by the wedges having non-zero thickness (~0.5 mm) at the apex.   The interpulse delay was calibrated using pulse pair traces from second order interferometric autocorrelator (Avesta Ltd., AA 10D). Autocorrelation trace of the pulse pair forms the three-peak picture symmetrical around the central peak. Only two peaks are shown on Fig. 3-4 to obtain better interference fringes resolution. With the scan speed used in these measurements the interference fringes are well resolved as shown in the insets. Interferometric pulse pair autocorrelation measurements (with a small correction for the nonlinearity of the scan speed) were used for the time calibration of the delay line. We have coupled the pulse sequence with the NSOM microscope (CDP, MoScan Near- Field Multiscope) which utilizes non-metallized fiber probe.[9] Our previous measurements on individual gold nanoclusters carried out with this NSOM utilizing the same fiber tip for the near field sample illumination using two-photon excitation have demonstrated the lateral point resolution below 40nm for this system.[10] By removing the fluorescence filter we were able to measure the excitation power after the tip as a function of the delay line position. No systematic drift of the excitation power has been detected (Fig. 3-5).
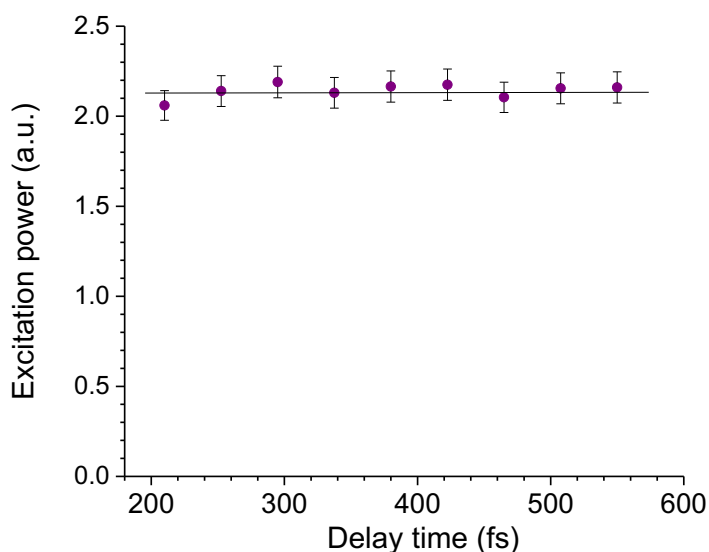
Figure 3-5. The pulse pair excitation power measured in NSOM transmission mode using blank substrate as a function of the delay line position.

The pulse sequence was coupled with the NSOM microscope (CDP, MoScan Near-Field Multiscope) which utilizes non-metallized fiber probe.[20, 28] Pulse pair beam was coupled to a single mode fiber. The tapered end of this fiber served as the local excitation source for the NSOM setup (Mo Scan NSOM, CDP systems). The average power at the NSOM fiber coupler was below 0.5mW to ensure negligible sample degradation. Raster scanning of the 1um x 1um to 10um x10um areas with the pixel size in the range 10-40nm at bin times in the range 20-40 ms was performed. The fluorescence of the sample was collected using a far-field inverted objective and transferred through a fiber optic cable to a filter set in front of the photomultiplier tube. Technical details of the NSOM system used in this contribution can be found in refs [20, 28]. Our previous measurements on individual gold nanoclusters carried out with this NSOM utilizing the same fiber tip for the near field sample illumination in two-photon regime have demonstrated the lateral point

resolution below 40nm for this system[20]. This sub optical diffraction limit at the NSOM microscope has also been verified for small DPDI aggregate as well as for rhodamine B drop cast sample (See Fig. 2-6). Investigation of the local exciton ultrafast dynamics in the aggregates of the DPDI molecules and in the DPDI/PTB7 blend has been carried out using two-photon, two pulse excitation regime of the NSOM described above.

3-3. Results and Discussion

The two-photon excited fluorescence signal from the NSOM as a function of the inter-pulse delay of the excitation pulse pair holding the microscope tip at a fixed position on the solid phase molecular sample has been measured from the newly developed NSOM interferometric system. Two-photon excitation regime with the excitation at 810nm has been applied. The use of a nonlinear two-photon regime allows the second order interferometry to provide information regarding the evolution of both electronic population and coherences[29]. To minimize the sample degradation and shorten the time of the experiment we used the following interpulse delay scanning protocol. We performed a series of short delay time scans with fine interpulse delay increment of 0.21fs and a scan length of 7fs. Each short scan started at a particular time delay delay point Ts. Starting delay line positions Ts for short scans varied stepwise with the increment ~20fs (in the experiment shown in Fig. 3-6) and ~40fs (for the data shown in Fig. 3-9). The experiments has been performed with increasing Ts (forth scan) followed by the scan with decreasing Ts to make sure that the fluorescence profile is reproducible and there is no sample degradation effects
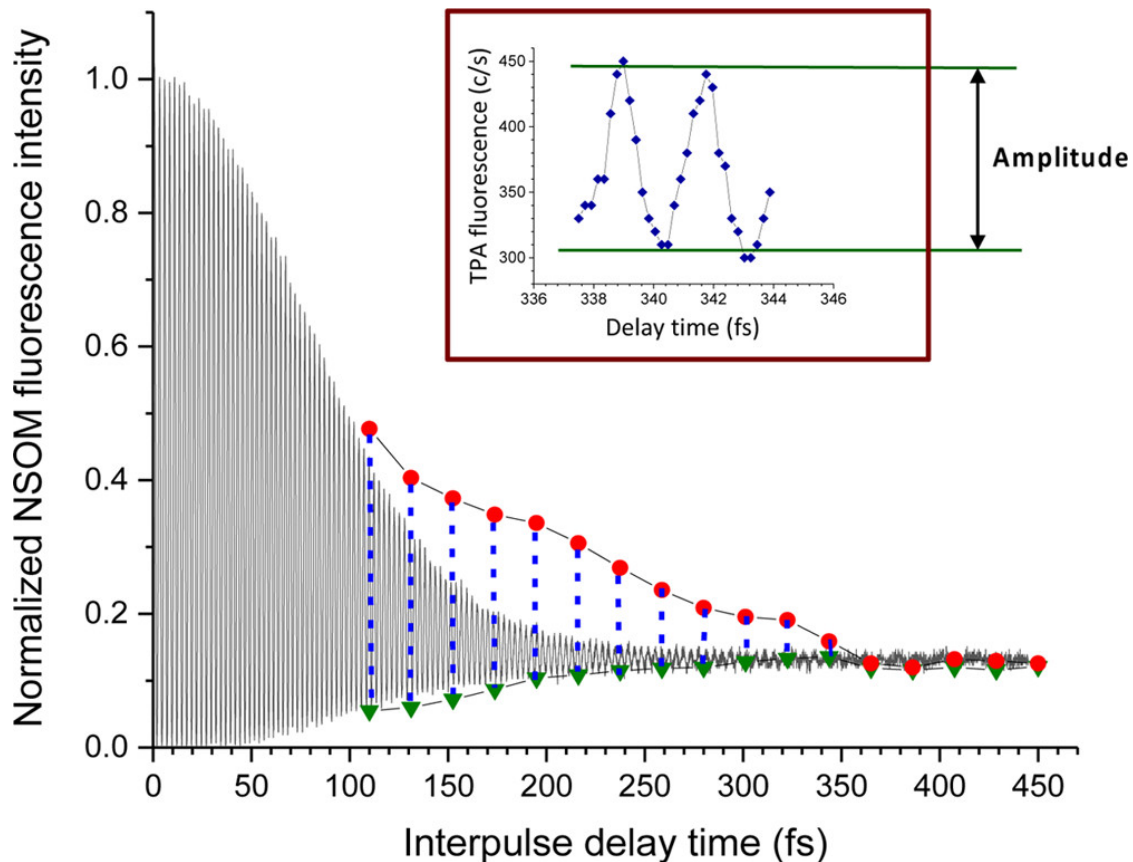
Figure 3-6. *The oscillations of the normalized NSOM two-photon excited fluorescence as a function of the interpulse delay. The oscillation amplitude was obtained by changing the interpulse delay by half of wavelength from max (filled red circles) to min (filled green triangles) at each long delay time point. Dash blue lines are guides for eyes connecting the maximum and minimum of fluorescence intensity when the delay is shifted by half a wavelength (1.35 fs) at each delay. The excitation pulse autocorrelation function is shown as a reference (solid grey line) for the comparison of the modulation depth as a function of the excitation laser interpulse delay. The NSOM fluorescence intensity and the signal from the autocorrelator are normalized 0.125 at long delays >450fs. The details of the normalization procedure are provided in the text. NSOM fluorescence intensity as a function of the interpulse delay on short time scale near the delay of 340 fs is shown in the inset. Fast fluorescence oscillation is clearly observable as a function of the interpulse delay.*
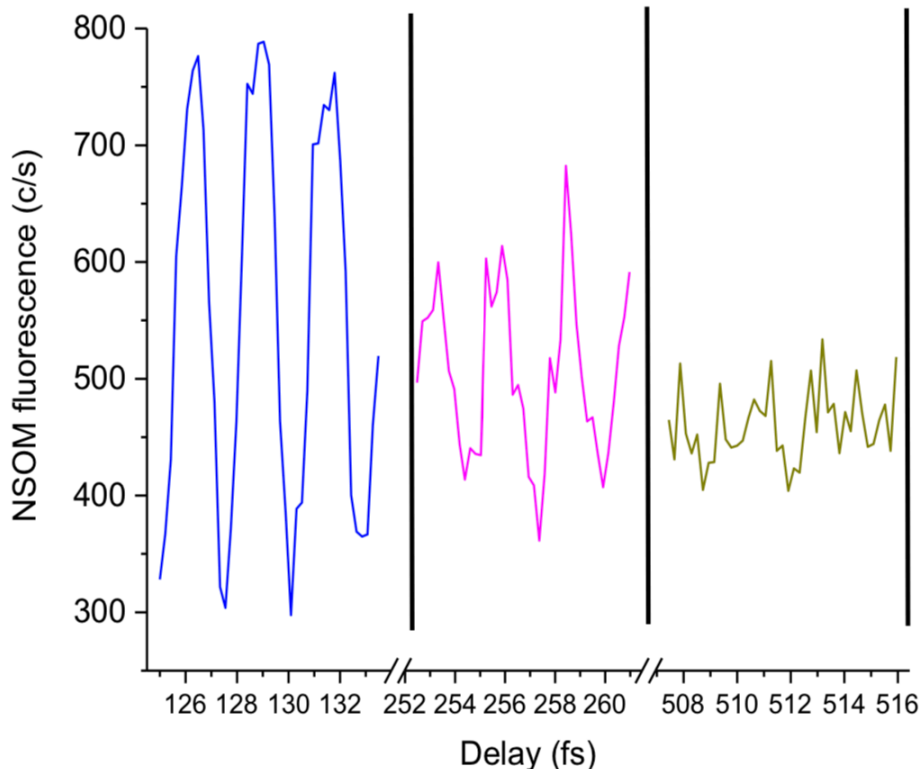
Figure 3-7. Fast oscillations of the NSOM fluorescence intensity as a function of the inter-pulse delay.

contributed to the result. Within short scans the fluorescence signal from the microscope showed a clear periodic modulation with the main period of 2.7 fs in the short scans with starting delay times Ts near the optical pulse overlap area (optical interference) and more complex periodical regime containing also additional short period of 1.35 fs for the short scans performed outside the optical pulse overlap area (quantum interference)[30]. Representative signal profiles are shown in Figure 3-7. Similar trends have been previously reported for the ionization signal of the atomic beam after two-photon phase locked pulse pair excitation in macroscopic experiment[30]. The fast oscillation of the TPA fluorescence in the transition area between two regimes is also shown in the

inset of Figure 3-6. The period of 2.7 fs corresponds to the optical period of the excitation light with wavelength 810nm while a shorter period corresponds to the molecular transition in the DPDI excited via two-photon absorption. In the first set of experiments we measured the maximum and minimum fluorescence at each starting delay time Ts. The entire scanning process has been executed from Ts = 110fs to Ts = 450fs with ~20fs stepwise increment for investigating the long delay area outside the pulse overlap. We set the delay line at each Ts position and found the maximum NSOM fluorescence in the interferometric pattern. Then we measured the change in the fluorescence intensity when the delay was changed by a half of the wavelength (1.35 fs) thus going from the maximum to the minimum of the fluorescence signal. Figure 3-6 shows the maxima (red filled circles) and minima (green triangles) of the NSOM fluorescence intensity from the DPDI aggregate as a function of the delay time Ts (fluorescence maximum (or minimum) intensity at the inset of Fig. 3-6 does not appreciably change within each short 7fs–scan starting at particular Ts). The NSOM fluorescence signal has been normalized to the signal at long delays >400fs multiplied by factor 8. It is known that the two-photon interferometric autocorrelation signal of the optical pulse has the amplitude 1/8 of that for its peak value at zero delay.[31] This normalization procedure allows us to do a direct comparison of the observed NSOM fluorescence oscillations as a function of the interpulse delay time with those obtained for the excitation pulse using two-photon interferometric autocorrelator as a reference with instantaneous response. The excitation pulse autocorrelation trace at positive delays obtained with two-photon interferometric aurtocorrelator (Avesta Ltd., AA 10D) and normalized to 0.125 at long delays >400fs is shown in Fig.3-6 (solid grey line). It is clearly seen from Fig. 3-6 that coherent oscillations last well beyond the pulse autocorrelation time profile and the amplitude of these oscillations remains substantial up to time
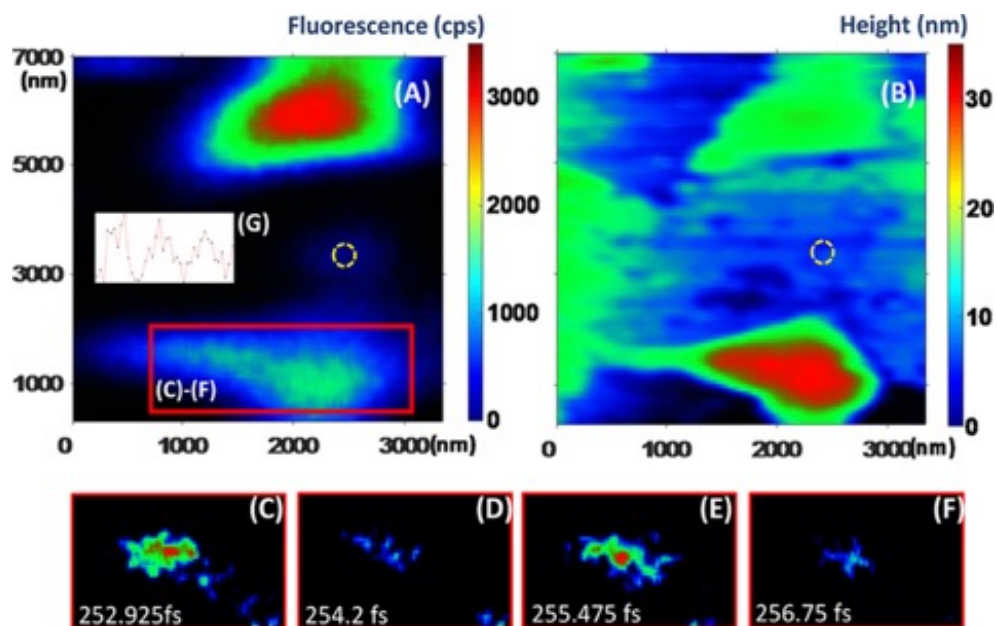
Figure 3-8. *Images of DPDI film obtained with the near-field microscope at different inter-pulse delays. (a) Two-photon excited NSOM scan of the aggregates of the perylene diimide dimer acceptor molecule, (b) corresponding topographic profile (AFM). (c-f) Periodic NSOM two-photon excited fluorescence intensity variation of NSOM image as a function of the inter-pulse delay under phase-locked pulse pair excitation of the sample aggregate. (g) Corresponding relative fluorescence intensity as a function of the interpulse delay (from 251.8 fs to 260.2 fs) when the probe is located at a particular position (X=2200, Y=1000). See Fig S10. for detailed quantitative information at this scan.*

delays of ~350fs. This signal is associated with the interference of the second pulse in the pair with the coherent polarization (wave packet) in the organic system created by the first pulse.[30,32] At longer delays the pulse autocorrelation trace showed just random noise while the material response from the DPDI still demonstrated clear fast modulation depicted in the inset of the delay ~ 340 fs. This experiment shows that even for interpulse delays substantially longer than the pulse duration, strong oscillations in the two-photon excited NSOM fluorescence persist. A slower modulation

of the coherent oscillations amplitude (envelope) as a function of the inter-pulse delay is also seen in Fig. 3-6.

In order to get a better insight of this coherent signal origin and its relation to the local molecular environment, we have performed the detailed investigation of the coherent excitation dynamics for different types of local molecular arrangements obtained with the NSOM. We have recorded the fluorescence intensity detected by the NSOM as a function of the interpulse separation time at several particular locations in the sample. The topographic image (AFM-scan) as well as the two-photon excited NSOM fluorescence intensity profile is shown in Fig. 3-8. By inspecting the NSOM fluorescence intensity as a function of the spatial location of the NSOM tip in Fig. 3-8a one can notice that the fluorescence intensity for the large and thick aggregate in the lower part of Fig. 3-8b (AFM profile) is smaller than that for the smaller and thinner aggregate in the upper part of the Fig. 3-8b. From the AFM profile Fig. 3-8b it is seen that the thickness of the lower aggregate is 2.5 times larger than that for upper (thinner) structure. At the same time the fluorescence intensity for the lower aggregate Fig. 3-8a is almost two times less than that for the upper (thinner) aggregate. Keeping in mind the small attenuation of the excitation beam due to a relatively weak two-photon absorption for 20-40nm thick structures the number of excited monomers is expected to be proportional to the aggregate's thickness. These observations clearly point to the fluorescence quenching in larger and thicker aggregates (by factor 5 in this particular case) in comparison with smaller and thinner aggregates. The enhanced fluorescence quenching in larger aggregates can be associated with the excitation transport to the defects and other quenching species in larger structure having larger amount of quenching centers than thinner structures with less quenching defects. Also, a relatively weak but detectable fluorescence is seen in the central part of the Figure 3-8a where the topographic profile in the positions near (X=2500, Y=3200,

Figure 3-8b) showed no significant features higher than 2 nanometers. This indicates that the weak fluorescence in this area is most probably emanating from isolated (non-aggregated) molecules at the region. We have compared the amplitude of the fast fluorescence oscillations of the two-photon excited fluorescence signal from the aggregates with that obtained in the area where the fluorescence emanating most probably from isolated molecules (Figure 3-8a, b). The two-photon fluorescence by two photon NSOM excitation at the lower aggregate in red rectangular frame clearly oscillates as a function of the inter-pulse delay on the femtosecond time scale as shown in Figure 3-8(c-f). The prominent oscillatory picture in fluorescence was observed for up to ~600 fs for the aggregates while the fluorescence oscillation from isolated molecules was not detected for the long delay (Figure 3-9). These results clearly showed longer lasting coherent transients of the large aggregates than that from isolated molecules. The long lasting coherent signal indicates a slower dephasing rate in the aggregates (Figure 3-9). The residual fit analysis of the slow envelope of the fast oscillating amplitude reveal a damped oscillatory signal in the large aggregates (Fig. 3-9 inset). The data has been obtained by subtracting the fluorescence oscillation amplitude from the exponential fitting of the oscillation amplitude itself. The slow modulation at the fast oscillation amplitude decayed with the characteristic time of ~300 fs and slow modulation periods of ~450fs based on the residual fitting analysis. These two parameters (period and decay time) were found to be dependent on the location of the NSOM tip on the aggregate (Fig. 3-10) with ~30% variation of the modulation period. For the isolated molecules or small aggregates the slow modulation is different from that observed in the aggregates: the amplitude decays near exponentially with no recurring features which were observed for the aggregates (Figure 3-9). Relatively slow dephasing for the aggregates can be related to the motional narrowing effect for the delocalized exciton in the aggregate.[33,34]
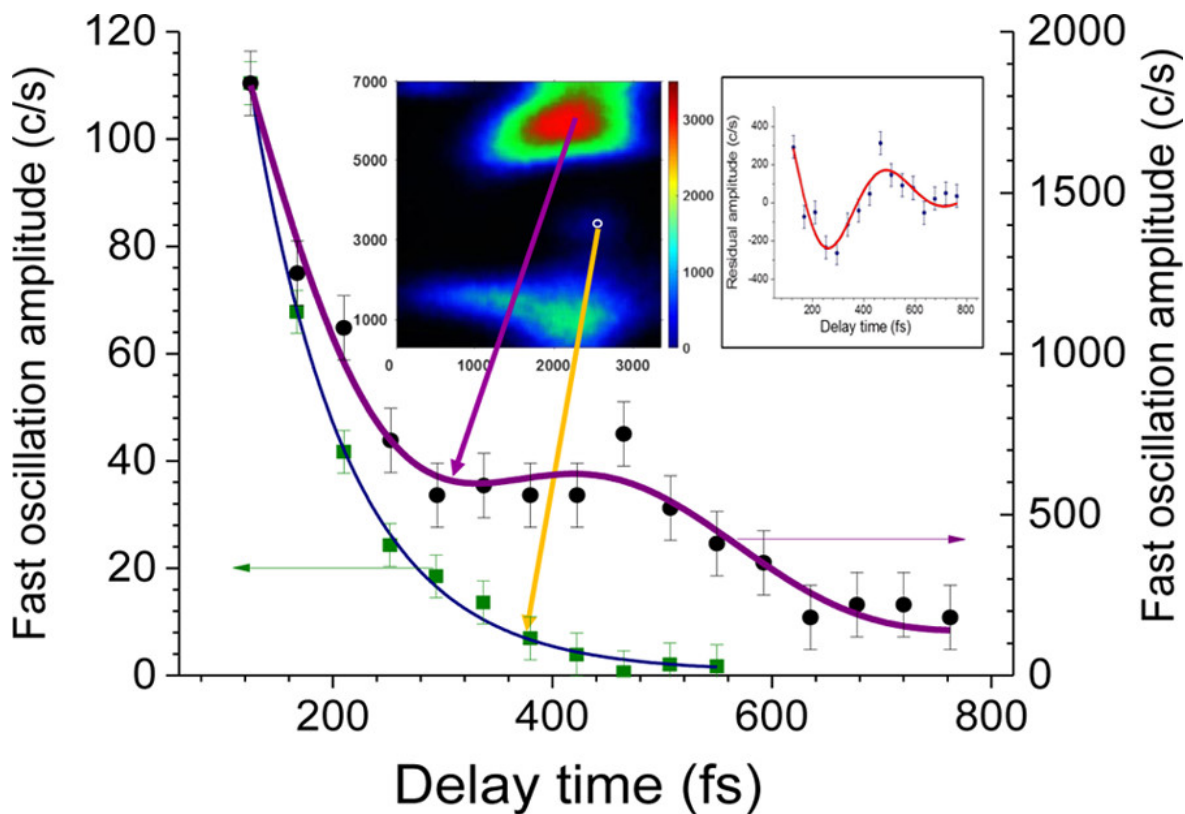
Figure 3-9. *The oscillation amplitude decay profiles measured for two different microscope tip positions (isolated molecules vs aggregate of DPDI) are shown. Near-field scanning fluorescence intensity profile is shown in the middle inset. The temporal evolution of the oscillation amplitude for the aggregate shows oscillations with the period 452 fs (black circles) while gradual near exponential decay has been detected for the isolated molecules (green squares). Best fits using sine –modulated exponential functions are depicted with the solid lines. The residual periodic signal after subtraction of the gradual exponential decay component for the aggregate is shown in the right inset. Schematic of the pulse pair two-photon excitation is shown in the top inset.*
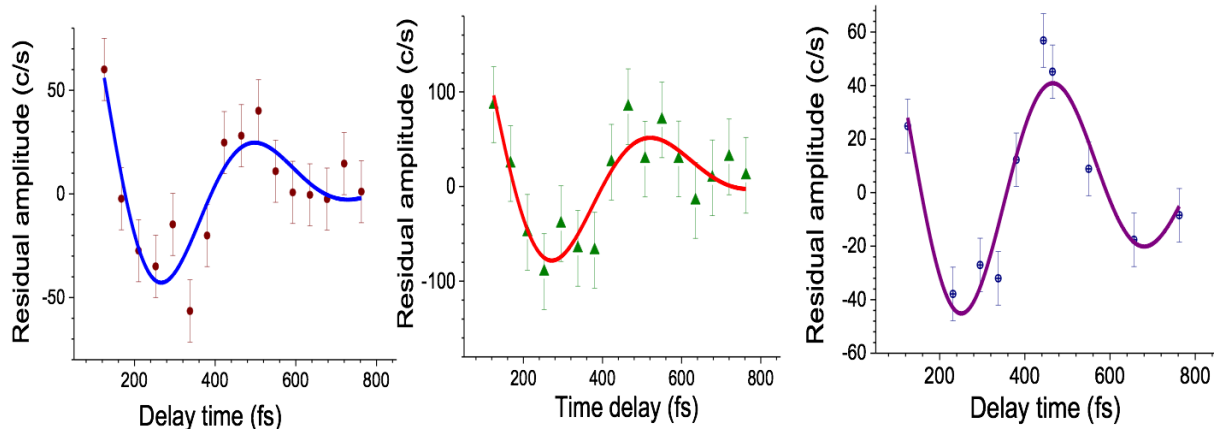
Figure 3-10. *The slow oscillating component of the interference envelope for different tip location on the perylene diimide dimer aggregate. Solid lines indicate best fits to the sine-damp function: y= Exp(−t/τ_d)Sin(Ωt + φ), where decay time τ_d, frequency Ω, and phase φ are variable parameters. The best fits show that the oscillating envelope periods shift from 382fs (left) to 520fs(right) in different tip position on DPDI aggregate.*

The optical interferences should vanish when the inter-pulse delay τ is longer than pulse duration τ_L whereas the wave packet interferences survive as long as τ is shorter than the characteristic time of the dephasing process. Within the weak field excitation regime the two-photon fluorescence signal associated with the excited state dynamics can be described utilizing the second order time-dependent perturbation theory[30]. The excited state time-dependent amplitude *c(t)* can be viewed as a sum of contributions from three different excitation paths P_1, P_2, P_3 [30]:

$$c(t, \tau) = P1(t) + P2(t, \tau) + P3(t, \tau) \tag{3-1}$$

where the wavefunction of the molecular system under two-photon excitation is

$\psi(t) = |g> +c(t)|e>$ the contribution P$_1$ is related to the absorption of two photons from the first pulse, P$_2$ is related to the absorption of two photons from the second pulse. P$_3$ corresponds to the combination of the absorption of one photon from the first pulse, the second photon from the second pulse and vice versa. The population of the excited state after the interaction (which is reflected in the fluorescence signal) can be expressed as $|c(\infty,\tau)|^2$ and contains contributions from each path and the interference terms between various paths. These interference terms between different excitation paths are responsible for the fast oscillation picture observed in the fluorescence τ-dependence. Outside the pulse overlap area and in the absence of sequential transition via intermediate level[35] the contribution associated with the path P$_3$ is negligible in the absence of the near resonant intermediate state (with is the case for the DPDI acceptor molecule used in this work). The contributions P$_1{}^n$ –P$_3{}^n$ for the population for the excited state n in a system with the multilevel excited state manifold can be calculated within the second order perturbation theory. Outside the pulse overlap area the quantum interference between paths leads to the excited state population N_f[32]:

$$N_f\ (\tau) = 2 \sum_n [\ 1 + cos\ (\omega_n\ \tau)\ ]\ |P_1^n|\ ^2 \qquad\qquad (3\text{-}2)$$

where P$_1{}^n$ is independent of τ. The fast oscillations (as a function of τ) are described by the first term. The slow modulation in this simple model appears when several excited states with different frequencies present in the summation. It could be due to vibrational levels or due to the energy transfer donor-acceptor coupling. In the time domain the slow modulation of the fast oscillations envelope can be connected to the vibrational wavepacket motion as well as to the population modulation associated with the excitation energy transfer in the aggregate.[36,37] In general, it is a

challenging task to distinguish between pure electronic and vibrational coherences in complex organic system[38]. Depending on the electron-exciton coupling parameter, electronic dephasing time, and interchromophore coupling strength[38, 39] a combination of different method should be used to investigate the vibration effects in the observed coherence. We made several observations pointing that the electronic nature of the detected wavepacket is associated with the intermolecular coupling and excitation energy transport rather than the vibrational coherences. Firstly, the modulation measured in the aggregates in our experiments corresponds to the wavenumber ~75cm^{-1}. Vibrational spectrum is a fingerprint of the molecule representing the set of bonds present in the material. Although it does depend on the environment, the line shifts are typically relatively small not exceeding few percentage point[40, 41]. If this peak is associated with the particular vibrational wavepacket motion, its position as a function of the interpulse delay is defined by the single frequency. However, we have observed a large variation of this period from 382fs to 520fs for different positions of the NSOM tip on the aggregate (Fig. 3-10). Additionally, for the derivatives of PDI the relative Raman line shifts were also found very small for different configurations[42, 43]. These indicate that the relatively large shift (~30%) of the frequency by the vibration-electronic coupling is less probable. Second, for the thin layer of the DPDI molecules located at the coordinates X=2500, Y=3200 in the Figure. 3-8a,b which is believed to contain isolated or weakly coupled DPDIs due to its very thin thickness (<2nm), the periodic modulation of the oscillation amplitude was completely lacking in our time window. This also indicates the intermolecular nature of the peak in the amplitude of coherent oscillations as a function of the interpulse delay as it disappears when the molecular organization and intermolecular interaction changes. This observation is an evidence that the molecular vibration effect is not dominant to the peak in the oscillation amplitude. Third, we have also measured the Raman spectrum in the film of DPDI. The

Raman spectrum does not provide any indications of the strong peak in the area near 75 cm^{-1} which could be responsible for the vibrational wavepacket observation at the interpulse delay near 450fs. Finally, the assertion is also supported by the following excitation dynamics measurement in a polymer blend contains the well-known donor polymer PTB-7[25] and DPDI acceptor. In the measurements the polymer blend dephasing time is much shorter than the pristine DPDI film due to strong coupling between DPDI and PTB-7. These facts, together with the absence of the slow modulation for the isolated molecules, show that the observed slow modulation is not due to intramolecular vibrational wavepacket evolution previously observed in the one-photon (linear), phase-locked pulse pair experiments but most probably associated with the intermolecular excitation states coupling in the aggregate.[32,36] Fast intermolecular coherent energy transfer is the rational explanation compatible with the whole set of data presented in this work.

As mentioned, we also measured the excitation dynamics in a polymer blend containning the well-known donor polymer PTB-7[25] and DPDI acceptor forming a composition used in BHJ photovoltaic cells. The blend film was prepared from chloroform solution with acceptor/donor mass ratio of 1:1 following the procedure similar to that used for preparation of neat DPDI sample (Supplementary Information). The NFTPI method described above was used to detect the two – photon excited fluorescence of the blend as a function of the interpulse delay. Figure 3-11 shows the fluorescence originating from the PTB-7/ DPDI blend. The average fluorescence intensity from DPDI was found substantially weaker in the blend in comparison with that from the neat DPDI film due to efficient quenching caused by the charge transfer between donor and acceptor components. For the DPDI aggregates in the blend we were able to observe the fast fluorescence oscillation with the period of excitation laser frequency. This is similar to those observed for the pristine DPDI film (See Fig. 3-12).
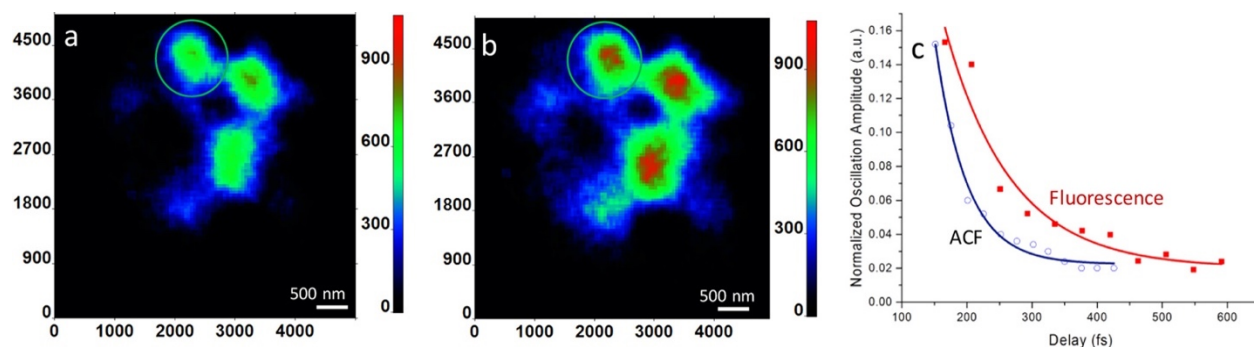
Figure 3-11. *PTB7 and DPDI blend sample fluorescence map and fluorescence oscillation amplitude decay profile as a function of inter-pulse delay. (a) destructive phase fluorescence image at the delay of 380.4fs. (b) constructive phase fluorescence image at the delay of 378.7fs. Scale bar on the right side of the figure (a) and (b) indicates fluorescence level of the map. (c) fluorescence oscillation amplitude (solid red squares) and the amplitude of the excitation autocorrelation function (ACF, open blue circles) as functions of the interpulse delay. Corresponding exponential fits are also shown (solid lines). Fluorescence oscillation amplitude on the figure (c) is measured at the point of X=2200 and Y= 4100 in the green circle of figure (a) and (b).*

As for the case of neat DPDI sample we observed the fluorescence intensity clearly oscillating as a function of the inter-pulse delay. However, the fluorescence oscillation amplitude monotonically decays and the decay time in the PTB-7/ DPDI blend is much faster than that of the neat DPDI sample. Analysis of the oscillation amplitude showed fast decay of the fast oscillating amplitude in the blend (<100fs) which is indicative of higher dephasing rate (Figure 3-11c). Interestingly, we have not observed any recurrent feature in the oscillation amplitude associated with the coherent energy transport similar to that observed for neat DPDI (See, Fig. 3-10) pointing out of the incoherent energy transport regime due to much higher dephasing rate in the blend in comparison
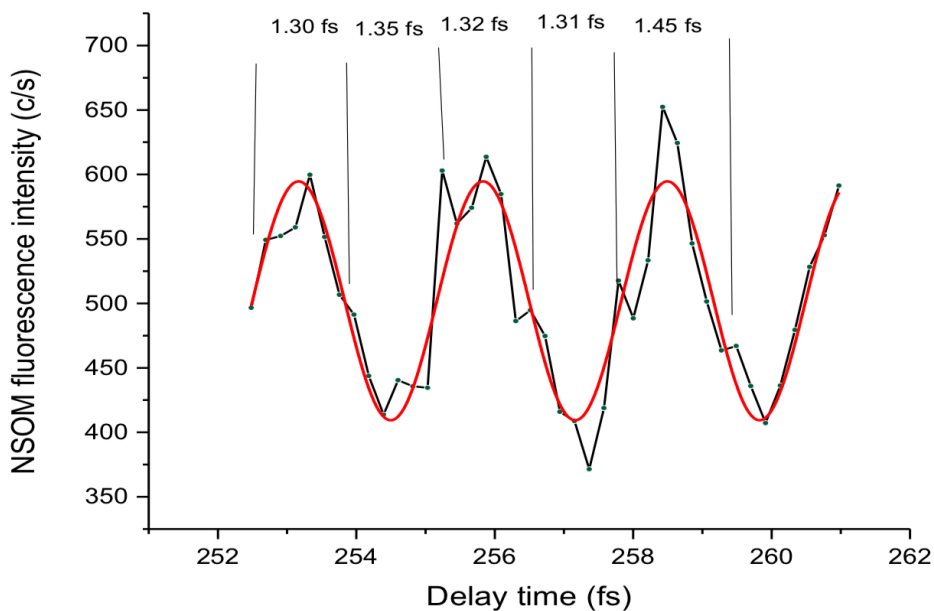
Figure 3-12. *Illustration of the appearance of the short period near 1.35fs beyond the main pulse overlap area. Best fit with the sine function (period 2.68fs) is shown as a reference.*

with the neat DPDI. This fast dephasing is indicative of stronger coupling of the acceptor system DPDI with the PTB7 donor which is expected in the blend. This strong coupling results in shortening of the dephasing time from ~230fs in the neat DPDI film to ~46fs in the PTB7/DPDI blend. This short electronic dephasing time should completely eliminate the coherent peak of electronic origin in accordance with our experiment. In addition, the vibrations generally dephase with >500fs dumping time[36,38] and should still be tangible in the blend if the additional peak in neat DPDI film originates from molecular vibration. However, there is no significant additional signal around the range in the blend (Fig. 3-11c). This observation also makes the assignment of the peak as the vibrational coherence less justified. In our experiments we have shown that the presence of the peak in coherent oscillations as a function of the interpulse delay correlated with the intermolecular coupling strength in the DPDI structure. We assign the periodic modulation of

the coherent signal to the coherent energy transport in the aggregate. Energy transfer period of 450 fs corresponds to the coupling strength in the aggregate ~38cm^{-1} in the dimer approximation. In spite of the fact that the energy transport mechanism in the particular blend was found to be incoherent there is still a potential in using coherent energy transport discovered in neat DPDI to be implemented in other organic photovoltaic blends by better managing of the donor and non-fullerene acceptor aggregates structures.

3-4. Conclusions

Using near field optical scanning microscope excited in two-photon mode by a sequence of phase-locked femtosecond pulses we were able to measure the coherence dynamics at the local level including that coherent energy transfer in DPDI acceptor film as well as obtaining dephasing time for the acceptor in the photovoltaic blend. Our experiments clearly show the feasibility of detecting the coherent contribution to the local excitation energy transport on the femtosecond time scale and measuring the dephasing time on a spatial scale of tens of nm in photovoltaic systems. The effect of local structural properties on the coherent transport contribution in multichromophoric systems can be probed with this approach. This work opens new avenues in investigation of functionalities of solar and energy conversion devices enhanced by the quantum coherence as well as the fast processes in other classical and quantum related phenomena in solid state.

3-5. References

1.   Polman, A.; Knight, M.; Garnett, E. C.; Ehrler, B.; Sinke, W. C. Photovoltaic Materials: Present Efficiencies and Future Challenges. *Science*, **2016**, 352, No. aad4424.

2.   Kaltenbrunner, M.; Sekitani, T.; Reeder, J.; Yokota, T.; Kuribara, K.; Tokuhara, T.; Drack, M.; Schwödiauer, R.; Graz, I.; Bauer-Gogonea, S.; et al. An Ultralightweight Design for Imperceptible Plastic Electronics. *Nature*, **2013**, 499, 458−465.

3.   Saliba, M.; Matsui, T.; Domanski, K.; Seo, J-Y.; Ummadisingu, A.; Zakeeruddin, S. M.; Correa-Baena, J-P.; Tress, W. R.; Abate, A.; Hagfeldt, A.; et al. Incorporation of Rubidium Cations into Perovskite Solar Cells Improves Photovoltaic Performance. *Science*, **2016**, 354, 206−209.

4.   Menke, S. M.; Holmes, R. J. Exciton Diffusion in Organic Photovoltaic Cells. *Energy Environ. Sci.,* **2014**, 7, 499−512.

5.   Goodson, T., III Solar Fuels: Materials, Physics, and Applications; *CRC Press, Boca Raton, Florida,* **2017**.

6.   Scholes, G. D.; Fleming, G. R.; Chen, L. X.; Aspuru-Guzik, A.; Buchleitner, A.; Coker, D. F.; Engel, G. S.; van Grondelle, R.; Ishizaki, A.; Jonas, D. M.; et al. Using Coherence to Enhance Function in Chemical and Biophysical Systems. *Nature,* **2017**, 543, 647−656.

7.   Haedler, A. T.; Kreger, K.; Issac, A.; Wittmann, B.; Kivala, M.; Hammer, N.; Köhler, J.; Schmidt, H. W.; Hildner, R. Long-Range Energy Transport in Single Supramolecular Nanofibers at Room Temperature. *Nature*, **2015**, 523, 196−200.

8.   Winiger, C. B.; Li, S.; Kumar, G. R.; Langenegger, S. M.; Haner, R. Long-Distance Electronic Energy Transfer in Light Harvesting Supramolecular Polymers. *Angew. Chem., Int. Ed.,* **2014**, 53, 13609− 13613.

9.   Wan, Y.; Stradomska, A.; Knoester, J.; Huang, L. Direct Imaging of Exciton Transport in Tubular Porphyrin Aggregates by Ultrafast Microscopy. *J. Am. Chem. Soc.,* **2017**, 139, 7287−7293.

10.   Escalante, M.; Lenferink, A.; Zhao, Y.; Tas, N.; Huskens, J.; Hunter, C. N.; Subramaniam, V.; Otto, C. Long-Range Energy Propagation in Nanometer Arrays of Light Harvesting Antenna Complexes. *Nano Lett.*, **2010**, 10, 1450−1457.

11.   Caram, J. R.; Doria, S.; Eisele, D. M.; Freyria, F. S.; Sinclair, T. S.; Rebentrost, P.; Lloyd, S.; Bawendi, M. G. Room-Temperature Micron- Scale Exciton Migration in a Stabilized Emissive Molecular Aggregate. *Nano Lett.,* **2016**, 16, 6808−6815.

12.   Virgili, T.; Grancini, G.; Molotokaite, E.; Suarez-Lopez, I.; Rajendran, S. K.; Liscio, A.; Palermo, V.; Lanzani, G.; Polliac, D.; Cerullo, G. Confocal Ultrafast pump−probe Spectroscopy: a New Technique to Explore Nanoscale Composites. *Nanoscale,* **2012**, 4, 2219−2226.

13.   Smith, S.; Orr, B. G.; Kopelman, R.; Norris, T. 100 Femtosecond/100 nm Near −Field Probe. *Ultramicroscopy*, **1995**, 57, 173−175.

14.   Guenther, T.; Emiliani, V.; Intonti, F.; Lienau, C.; Elsaesser, T.; et al. Femtosecond Near-Field Spectroscopy of a Single GaAs Quantum Wire. *Appl. Phys. Lett.,* **1999**, 75, 3500−3502.

15.   Karki, K.; Namboodiri, M.; Khan, T. Z.; Materny, A. Pump- Probe Scanning Near Field Optical Microscopy: Sub-Wavelength Resolution Chemical Imaging and Ultrafast Local Dynamics. *Appl. Phys. Lett.*, **2012**, 100, No. 153103.

16.   Dyba, M.; Hell, S. Focal Spots of Size $\lambda/23$ Open Up Far-Field Fluorescence Microscopy at 33 nm Axial Resolution. *Phys. Rev. Lett.,* **2002**, 88, No. 163901.

17.   Wang, P.; Slipchenko, M. N.; Mitchell, J.; Yang, C. E.; Potma, O.; Xu, X.; Cheng, J. Far-field Imaging of Non-Fluorescent Species with Subdiffraction Resolution. *Nat. Photonics,* **2013**, 7, 449−453.

18.   Akselrod, G. M.; Deotare, P. B.; Thompson, N. J.; Lee, J.; Tisdale, W. A.; Baldo, M. A.; Menon, V. M.; Bulovic, V. Visualisation of Exciton Transport in Ordered and Disordered Molecular Solids. *Nat. Commun.,* **2014**, 5, No. 3646.

19.   Guo, Z.; Wan, Y.; Yang, M.; Snaider, J.; Zhu, K.; Huang, L. Long- Range Hot Carrier Transport in Hybrid Perovskites Visualized by Ultrafast Microscopy. *Science*, **2017**, 356, 59−62.

20.   Abeyasinghe, N.; Kumar, S.; Sun, K.; Mansfield, J. F.; Jin, R.; Goodson, T., III Enhanced Emission from Single Isolated Gold Quantum Dots Investigated Using Two-Photon-Excited Fluorescence Near-Field Scanning Optical Microscopy. *J. Am. Chem. Soc.,* **2016**, 138, 16299−16307.

21.   Biagioni, P.; Celebrano, M.; Zavelani-Rossi, M.; Polli, D.; Labardi, M.; Lanzani, G.; Cerullo, G.; Finazzi, M.; Duò, L. High- Resolution Imaging of Local Oxidation in Polyfluorene Thin Film by Nonlinear Near-Field Microscopy. *Appl. Phys. Lett.,* **2007**, 91, No. 191118.

22.   Carlotti, B.; Cai, Z.; Kim, H.; Sharapov, V.; Madu, I. K.; Zhao, D.; Chen, W.; Zimmerman, P. M.; Yu, L.; Goodson, T., III Charge Transfer and Aggregation Effects on the Performance of Planar vs. Twisted Non- Fullerene Acceptor Isomers for Organic Solar Cells. *Chem. Mater.,* **2018**, 30, 4263−4276.

23.   Zhao, F.; Dai, S.; Wu, Y.; Zhang, Q.; Wang, J.; Jiang, L.; Ling, Q.; Wei, Z.; Ma, W.; You, W.; et al. Single-Junction Binary-Blend Nonfullerene Polymer Solar Cell with 12.1% Efficiency. *Adv. Mater.*, **2017**, 29, No. 1700144.

24.   Li, S.; Zhang, Z.; Shi, M.; Li, C-Z.; Chen, H. Molecular Electron Acceptors for Efficient Fullerene-free Organic Solar Cells. *Phys. Chem. Chem. Phys.*, **2017**, 19, 3440−3458.

25.   Liang, Y.; Xu, Z.; Xia, J.; Tsai, S-T.; Wu, Y.; Li, G.; Ray, C.; Yu, L. For the Bright Future-Bulk Heterojunction Polymer Solar Cells with power Conversion efficiency of 7.4%. *Adv. Mater.*, 2010, 22, E135− E138.

26.   Liang, Y.; Feng, D.; Wu, Y.; Tsai, S.-T.; Li, G.; Ray, C.; Yu, L. Highly Efficient Solar Cell Polymers Developed via Fine-Tuning of Structural and Electronic Properties. *J. Am. Chem. Soc.*, **2009**, 131, 7792−7799.

27.   Brida, D.; Manzoni, C.; Cerullo, G. Phase-Locked Pulses for Two-Dimensional Spectroscopy by a Birefringent Delay Line. *Opt. Lett.,* **2012**, 37, 3027−3029.

28.   Raymond, J. E.; Goodson, T., III Single-Particle Two-Photon Absorption Imaging and Enhancement Determination for Organic Nanoparticles. *J. Phys. Chem. Lett.,* **2011**, 2, 329−333.

29.   Liau, Y.-H.; Unterreiner, A. N.; Chang, Q.; Scherer, N. F. Ultrafast Dephasing of Single Nanoparticles Studied by Two-Pulse Second-Order Interferometry. *J. Phys. Chem. B*, **2001**, 105, 2135−2142.

30.   Blanchet, V.; Nicole, C.; Bouchene, M-A.; Girard, B. Temporal Coherent Control in Two-Photon Transitions: From Optical Interferences to Quantum Interferences. *Phys. Rev. Lett.,* **1997**, 78, 2716−2719.

31.   Naganuma, K.; Mogi, K.; Yamada, H. General Method for Ultrashort Light Pulse Chirp Measurement. *IEEE J. Quantum Electron.*, **1989**, 25, 1225−1233.

32.   Scherer, N. F.; Carlson, R. J.; Matro, A.; Du, M.; Ruggiero, A. J.; Romero-Rochin, V.; Cina, J. A.; Fleming, G. R.; Rice, S. A. Fluorescence-Detected Wave Packet Interferometry: Time Resolved Molecular Spectroscopy with Sequences of Femtosecond Phase- Locked Pulses. *J. Chem. Phys.*, **1991**, 95, 1487−1511.

33.   Knapp, E. W. Lineshapes of Molecular Aggregates. Exchange Narrowing and Intersite Correlation. *Chem. Phys.*, **1984**, 85, 73−82.

34.   Varnavski, O.; Sukhomlinova, L.; Twieg, R.; Goodson, T., III Ultrafast Exciton Dynamics in a Branched Molecule Investigated by Time-Resolved Fluorescence, Transient Absorption, and Three-Pulse Photon Echo Peak Shift Measurements. *J. Phys. Chem. B*, **2004**, 108, 10484−10492.

35.   Ariunbold, G. O.; Sautenkov, V. A.; Scully, M. O. Switching from a Sequential Transition to Quantum Beating in Atomic Rubidium Pumped by a Femtosecond Laser. *J. Opt. Soc. Am. B*, **2011**, 28, 462−467.

36.   Brinks, D.; Stefani, F. D.; Kulzer, F.; Hildner, R.; Taminiau, T. H.; Avlasevich, Y.; Müllen, K.; van Hulst, N. F. Visualizing and Controlling Vibrational Wave Packets of Single Molecules. *Nature,* **2010**, 465, 905− 909.

37.   Hildner, R.; Brinks, D.; Nieder, J. B.; Cogdell, R. J.; van Hulst, N. F. Quantum Coherent Energy Transfer over Varying Pathways in Single Light-Harvesting Complexes. *Science,* **2013**, 340, 1448−1451.

38.   Halpin, A.; Johnson, P. J. M.; Tempelaar, R.; Murphy, R. S.; Knoester, J.; Jansen, T. L. S.; Miller, R. J. D. Two-dimensional spectroscopy of a molecular dimer unveils the effects of vibronic coupling on exciton coherences. *Nat. Chem.,* **2014**, 6, 196−201.

39.   Duan, H.-D.; Nalbach, P.; Prokhorenko, V. I.; Mukamel, S.; Thorwart, M. On the origin of oscillations in two-dimensional spectra of excitonically-coupled molecular systems. *New J. Phys.*, **2015**, 17, No. 072002.

40.   Lueck, H. B.; Daniel, D. C.; McHale, J. L. Resonsnce Raman Study of Solvent Effects on a Series of Triarilmetane Dyes. *J. Raman Spectrosc.,* **1993**, 24, 363−370.

41.   Schmid, E. D.; Moschallski, M.; Peticolas, W. L. Solvent Effects on the Absorption and Raman Spectra of Atomic Nitro Compounds. *J. Phys. Chem.,* **1986**, 90, 2340−2346.

42.   Angelella, M.; Wang, C.; Tauber, M. J. Resonance Raman Spectra of a Perylene Bis(dicarboximide) Chromophore in Ground and Lowest Triplet States. *J. Phys. Chem. A,* **2013**, 117, 9196−9204.

43.   Brown, K. E.; Veldkamp, B. S.; Co, D. T.; Wasielewski, M. R. Vibrational Dynamics of a Perylene −Perylenediimide Donor-Acceptor Dyad Probed with Femtosecond Stimulated Raman Spectroscopy. *J. Phys. Chem. Lett.,* **2012**, 3, 2362−2366.

CHAPTER IV

Coherent Energy and Charge Transport Processes in Oligothiophene Dendrimers Probed in Solution and Solid State with time-resolved spectroscopy and microscopy methods.

4-1. Introduction

Organic conjugated macromolecules continue to attract great interest in the broader community related to optical and electronic applications.[1-4] Indeed, there are several advantages to light harvesting and emitting devices constructed with organic conjugated systems such as better transparency, flexibility, lightweight, as well as improved electron mobility and reduction in cost.[5-12] In particular, dendritic macromolecules have shown great improvements in the processing, purification, and understanding of the optical and electronic properties.[13-18] Dendrons and dendrimers macromolecules have demonstrated promising properties as organic semiconducting materials for electronic devices due to low band gap, broad absorption spectrum, and efficient charge transfer characteristics. Furthermore, conjugated dendrimers are expected to have both advantages of good processability of polymers and good reproducibility of small molecules.[13] Inspired by these promising characteristics of this class of macromolecules, a new family of oligothiophene dendrimers decorated with diketopyrrolopyrrole groups was investigated. In regard to their optical properties, there have been reports illustrating that some organic dendrimers show enhanced electronic coupling and very fast energy transfer dynamics.[15-22] It has been

suggested that the fast energy dynamics and strong intra-molecular coupling in these systems results in a possible coherent energy transfer process involving several of the contributing chromophores in the dendrimer macromolecule. While many of these experiments were done in solution, it became evident that the process of energy transfer in synthetic light harvesting materials in the solid-phase play a large role in the ultimate efficiency of a resulting device.[23-26] Previous investigations have utilized ultrafast time-resolved spectroscopic techniques to probe the energy dynamics in dendrimers.[27-31] These methods allow one to relate excited state ultrafast processes with the dynamics of electronic coupling in the organic structure.[17-32] It was found that strong electronic coupling between different chromophores (inter-molecular) and between different portions of the same dendrimer macromolecule (intra-molecular) can be explained by either a coherent or incoherent energy transfer mechanism.[23-26,32] Many of these reports were completed with solution phase measurements. In our work, for the first-time solution and solid -phase ultrafast dynamic investigations were carried out on these organic macromolecules. Three-pulse photon echo peak shift (3PEPS) and time-resolved nonlinear near-field scanning optical microscopy (NSOM), in addition to transient absorption and fluorescence up-conversion, have been utilized. 3PEPS spectroscopy is well known to be strongly sensitive to intra-molecular interactions in solution with very high time resolution (~50 fs)[32]; this method is capable of providing time scales and coupling strengths of dephasing processes that are coupled to electronic transitions.[32-48] On the other hand, time-resolved two-photon NSOM microscopy measurements illustrate both intra- and inter-molecular transfer processes (~100 fs) in the solid phase with a high spatial resolution (~40nm).[41] Different trends have been found from this comparison, showing a way to utilize coherent transport in this class of organic materials for light harvesting applications.

3T-p-DPP
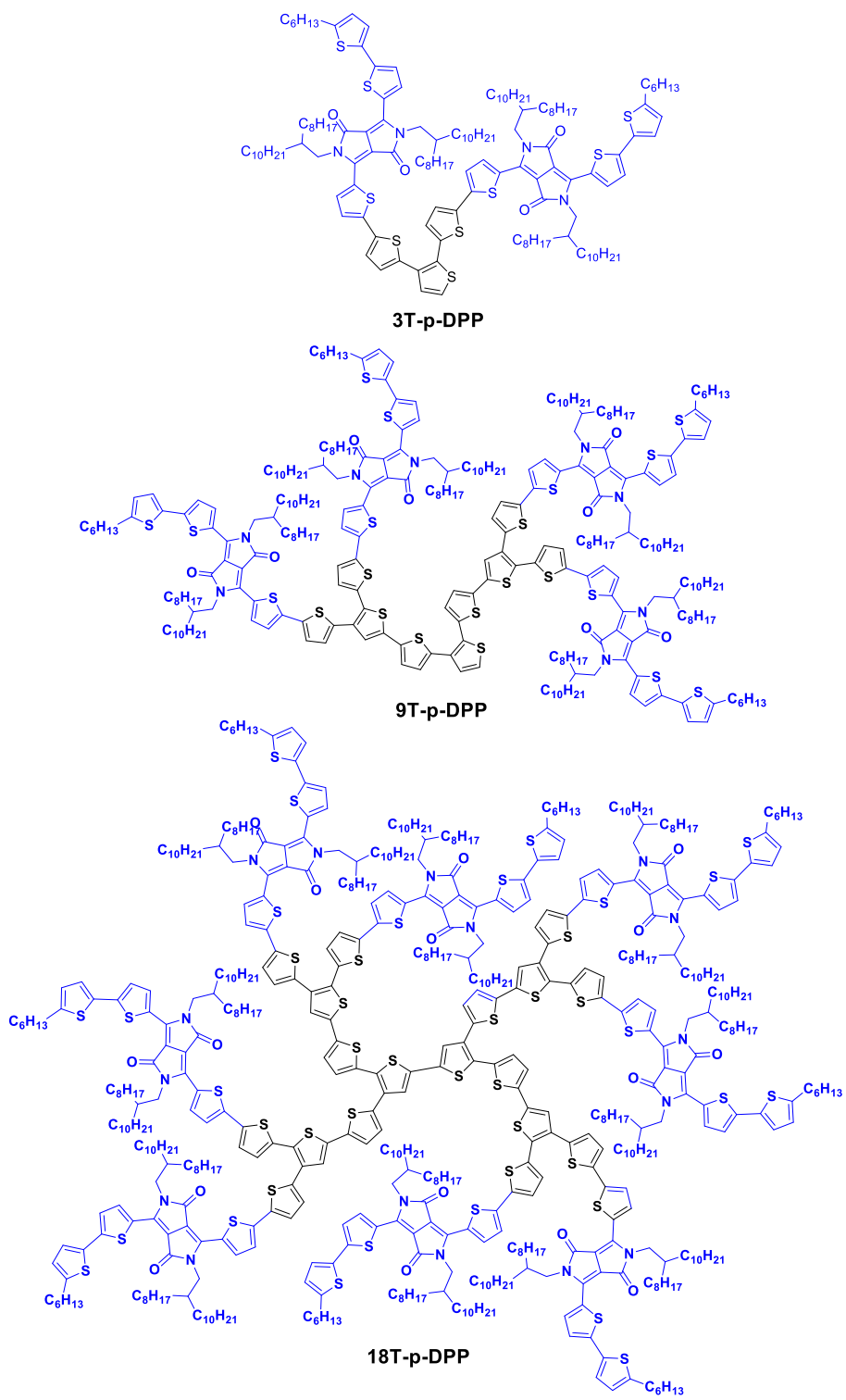
9T-p-DPP

18T-p-DPP

Figure 4-1. *Chemical Structures of 3T-p-DPP, 9T-p-DPP and 18T-p-DPP.*

66

4-2.   Experimental results

The investigated systems fall into a new family of dendritic oligothiophenes functionalized with diketopyrrolopryrrole groups (DOT-p-DPPs) synthesized by Ma et al.[13] (Figure 4-1). These macromolecules present oligothiophene units as the core electron donor and diketopyrrolopryrrole (DPP) groups as electron acceptors on the multi-branched portion. Figure 4-2. shows normalized UV-Vis absorption (a) and fluorescence emission spectra (b) for all the systems. Absorption spectra present dual-band features typical of DPP derivative molecules, one low-energy band centered at 600 nm and a high-energy absorption band centered at 400 nm. The low-energy can be ascribed to the absorption of the diketopyrrolopryrrole unit. The high-energy band corresponds to the $\pi \rightarrow \pi^*$ transition and it can be associated with the oligothiophene core portion of the systems. In the case of 3T-p-DPP a fluorescence efficiency of 40% was found, while for 9T-p-DPP system the fluorescence quantum yield decreases to 15%, and, for the higher generation system (18T-p-DPP) to a value of 2%. The fluorescence quenching could suggest the occurrence of intramolecular charge transfer processes occurring in the systems between the electron donor portion and the electron acceptor unit[50-57]. Nevertheless, fluorescence spectra show only a slightly bathochromic behavior passing from 3T-p-DPP to 18T-p-DPP, and in all cases, emission spectra are comparable with the fluorescence spectra of T-DPP sub-unit[50].
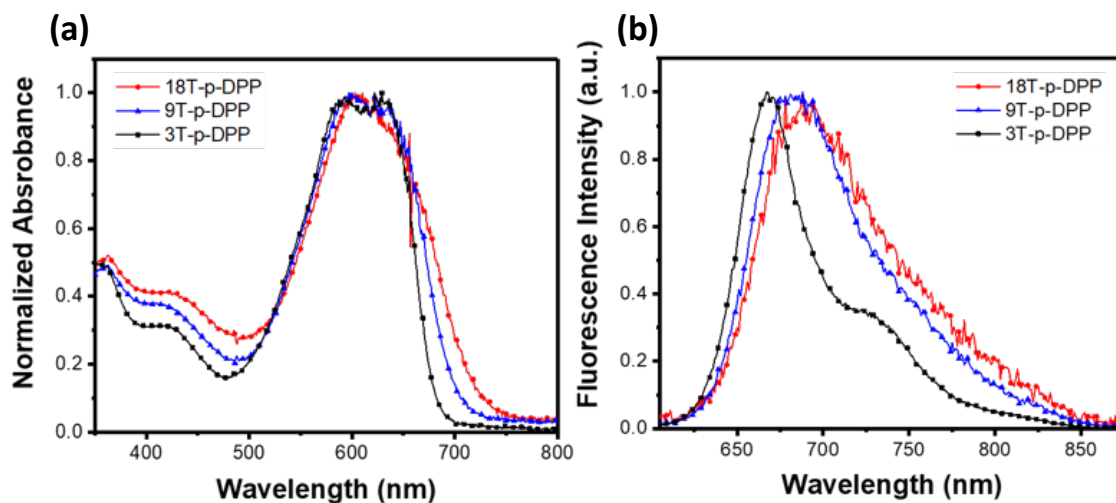
Figure 4-2. *Normalized UV-vis absorption* **(a)** *and fluorescence* **(b)** *spectra of T-p-DPPs in dichloromethane solution.*

Time-resolved absorption anisotropy measurements were carried out using a polarized degenerate transient absorption experiment at 410 nm. The experimental anisotropy decays were calculated from the decays curves of the polarized parallel, $I_{par}(t)$, and polarized perpendicular, $I_{perp}(t)$, intensity with respect to the pump polarization (Figure 4-3.). The anisotropy decays were best modeled by a bi-exponential decay with an ultrafast component and a residual component in all cases, which suggest the presence of a fast energy redistribution between dipoles oriented in different directions.

	λ_{abs}/nm	λ_{em}/nm	ϕ_F
3T-p-DPP	615	668	0.39
9T-p-DPP	600	683	0.15
18T-p-DPP	603	688	0.02

Table 4-1. *Absorption and Emission properties of DPP-functionalized dendritic oligothiophenes.*
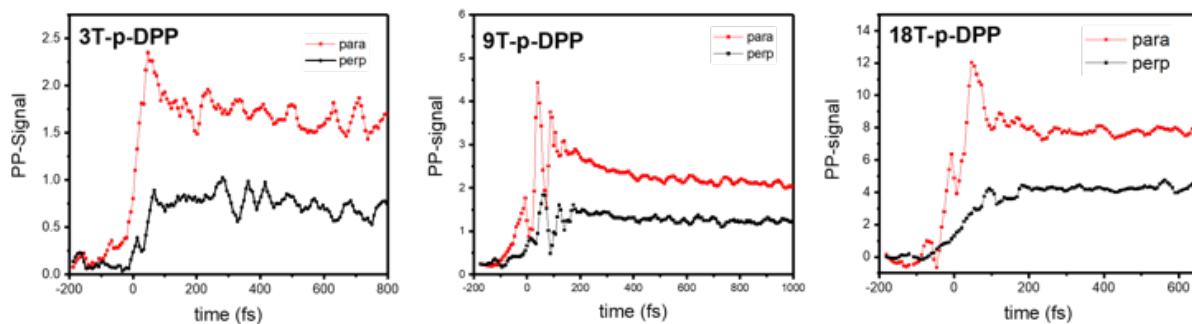
Figure 4-3. *Transient absorption components polarized parallel and perpendicular with respect to the pump of dendritic samppples. Pump and Probe wavelength = 410 nm.*

When molecules are excited by polarized light, in fact, the transition dipole moment is going to be oriented initially in the same direction of the light polarization, then, during relaxation process, a change of anisotropy will be observed if processes involving a change in the orientation of transition occur.
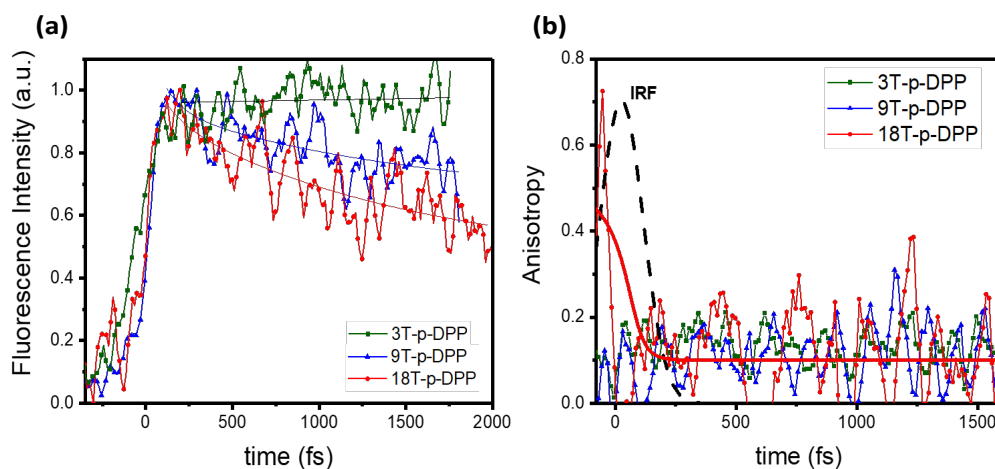
Figure 4-4. *a) Magic Angle fluorescence dynamics components and best fit for 3T-p-DPP, 9T-p-DPP and 18T-p-DPP. Excitation wavelength 400 nm. Emission wavelength 650 nm (3T-p-DPP, 9T-p-DPP) and 680 nm (18T-p-DPP). b) Fluorescence Anisotropy decay in a short time scale for 3T-p-DPP, 9T-p-DPP and 18T-p-DPP, thick line is the result of a best fitting model.*

69

Comparing the different macromolecules, the dendron 3T-p-DPP presents a slower anisotropy decay compared to the dendrimer 18T-p-DPP and the dendron 9T-p-DPP. Furthermore, an initial anisotropy higher than 0.4 was observed for all the investigated systems probably due to excited state absorption contribution, which lead to higher anisotropy. After these ultrafast decays, the anisotropy assumes a significantly slower decay described by a long decay component (rest), which contributes the residual anisotropy value. Anisotropy decay was also investigated using the femtosecond fluorescence up-conversion technique. Figure 4-4. shows the isotropic ($I_{par}+2I_{perp}$) fluorescence decay profile in case of 3T-p-DPP, 9T-p-DPP and 18T-p-DPP together with exponential fitting functions. Experimental results and model fittings of the anisotropy decay are shown in Figure 4-4. together with the Instrument Response Function (IRF). Comparing these findings with the fluorescence dynamics of the single subunit T-DPP[50], the faster dynamic observed in 18T-p-DPP is probably due to a charge transfer process occurring from the oligothiophene core unit to the T-DPP subunit. In order to better understand the nature of the intramolecular interaction between the electron donor and electron acceptor portion in these dendrimers systems in solution, a 3-pulse Photon Echo Peak Shift (3PEPS) experiment has been performed. 3PEPS spectroscopy is well known to be strongly sensitive to these interactions, and provides, under certain conditions, direct insight into the energy gap correlation function[34-40,47,48]. Figure 4-5. shows photon echo signals in both phase-matching directions for 18T-p-DPP 9T-p-DPP and 3T-p-DPP at T=0 (population period). Peak shift values were determined by fitting Gaussian to the two 3PE signals and taking half the distance in time between the maxima of these fits. Comparing the three systems, a difference in the initial peak shift value is observed: 18T-p-DPP presents a peak shift of about 10 fs, while the initial peak shift for 3T-p-DPP and 9T-p-DPP appear to be very small. A non-zero initial peak shift is inversely related to the system-bath
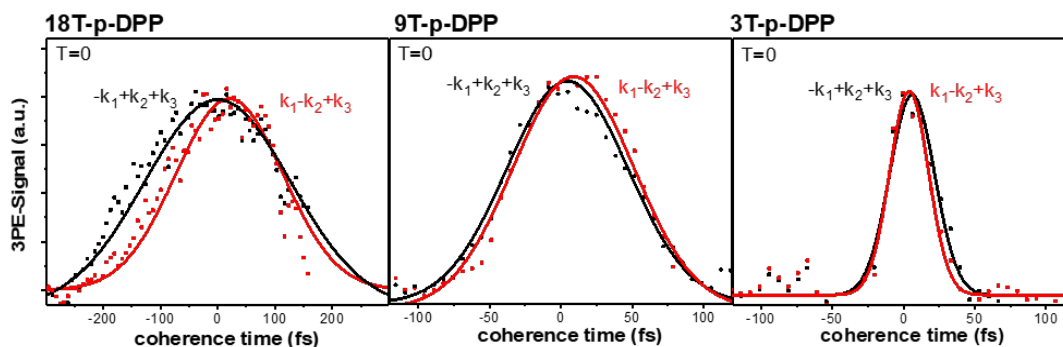
Figure 4-5. *Echo signals in both phase matching directions $k_1-k_2+k_3$ (red) and $-k_1+k_2+k_3$ (black) for 18T-p-DPP, 9T-p-DPP and 3T-p-DPP macromolecule at T=0 (population period).*

coupling. The higher initial peak shift observed in case of the dendrimer 18T-p-DPP, may suggest a higher inhomogeneity. In fact, initial peak shift value is inversely related to the system-bath coupling.[34-40,45-48] Furthermore, larger FWHM of the photon echo signal (18T-p-DPP > 9T-p-DPP >3T-p-DPP) indicates a decrease of the effective system-bath electronic coupling.[42] For the investigated systems, no echo signal was observed at longer population period T. The absence of echo signal at a population period longer than the pulse duration (T>50 fs) is probably due to excitation beam utilized to perform the measurements (410 nm) which involve an S_0-S_2 transition; thus, internal conversion $S_2 \rightarrow S_1$ may occur before the third pulse arrives. A two-pulse two-photon interferometric NSOM experiment has been utilized to evaluate intra- and inter-molecular coupling and coherent dynamics of the dendritic systems in the solid state[41]. Figure 2-7. in chapter 2 invited again illustrates the representative feature of the two-pulse two-photon NSOM interferometric system. Three different regions can be identified as a function of the interpulse delay: the laser interference region, the molecular coherent polarization interference region, and no-interference region. The pulse interference gives some specific information on the molecular systems such as excited state coupling to the external components and energy transfer to the other

71

molecule[41,58,62]. Figure 4-6a shows the long scan of the 3T-p-DPP, and short scan data at a specific interpulse delay position. As expected, the fluorescence modulation amplitude monotonically decreased with increasing the interpulse delay due to the electronic dephasing of the molecular system. In order to estimate the dephasing rate of the 3T-p-DPP system, we calculated the expected dephasing rate by convoluting the autocorrelation function (ACF) at various dephasing rates. Figure 4-6a shows that the 3T-p-DPP dephasing rate is well adjusted with the 35fs dephasing rate. Inset of Figure 4-6a shows the interferometric fluorescence modulation as a function of the interpulse delay of the NSOM interferometry system at the specific delay region. Clear fluorescence oscillation at the delay due to the interference between the two absorption wavepackets can be observed. The best fitting results of the measurement shows the prominent fluorescence modulation of 2.7 fs period due to the coherent excitation polarization at the delay. This period is in accordance with the excitation laser wavelength of 810 nm. The same feature is also verified by the NSOM image in Figure 4-6b. The NSOM images illustrate the topology and fluorescence intensity at delay A and B (inset of Figure 4-6a). Delay position A is constructive and position B is a destructive delay position. At the different delay positions, we can see clear fluorescence difference due to the interference of the absorption wavepackets. However, if the interpulse delay increases beyond ~400 fs, we could not see the clear fluorescence modulation as the polarization at the excited state by the fs-laser pulse lost its coherence due to electronic dephasing. Figure 4-6c shows the coherent fluorescence amplitude modulation as a function of the interpulse delay. The fluorescence oscillation amplitude monotonically decays and each dendritic system has shown clearly different decay rates due to electronic dephasing[63]. The fluorescence oscillation amplitude decay time for the 3T-p-DPP, 9T-p-DPP, and 18T-p-DPP are
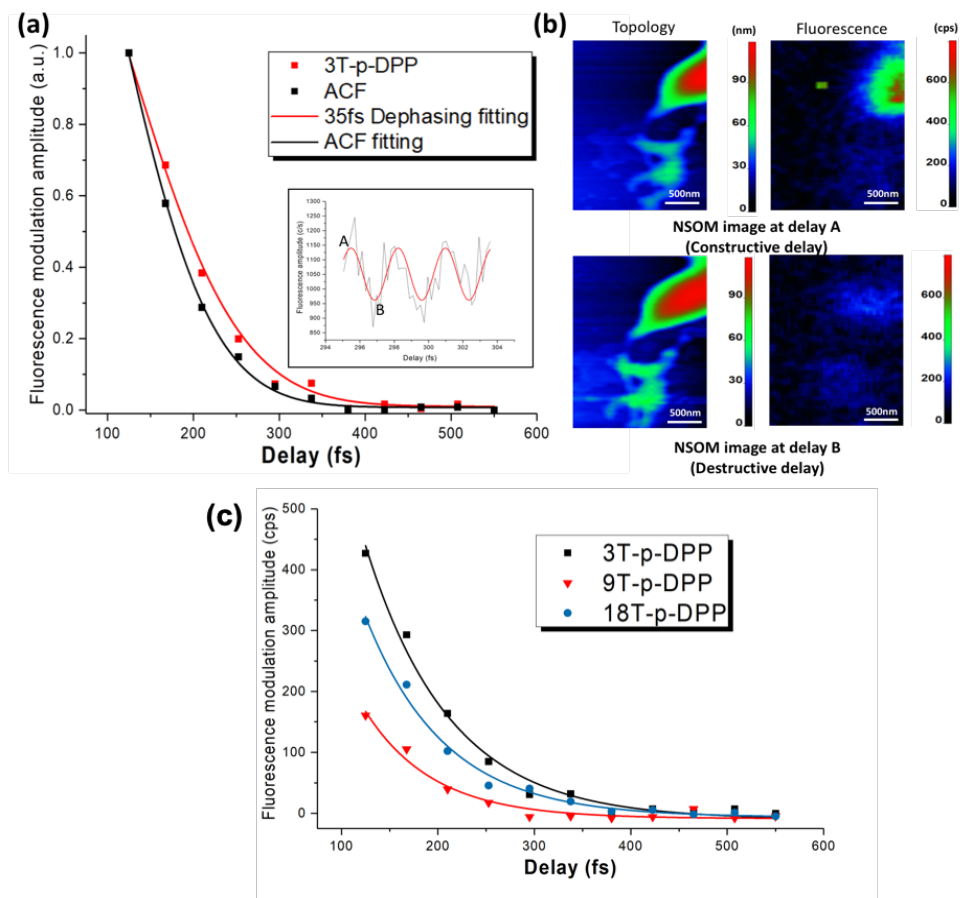
Figure 4-6. **(a)** *Fluorescence modulation amplitude of the 3T-p-DPP as a function of the interpulse delay. Inset indicates the fluorescence modulation amplitude from 295 fs to 304 fs interpulse delay. ACF shows the two-photon autocorrelation function of the excitation laser for the two photon NSOM interferometry system.* **(b)** *Two-photon interferometric NSOM image at different interpulse delay position of the inset. Constructive interference and destructive interference has been shown at the delay A and B in the inset, respectively.* **(c)** *Fluorescence modulation amplitude of the dendritic systems in this work. Solid lines indicate the different dephasing decay curve by single decay exponential fitting. Solid lines indicate the best fitting results to the exponential decay function: $y= y0+A_1Exp(-t/\tau_d)$, where decay time τ_d, maximum fluorescence modulation amplitude A_1 and average fluorescence background noise level y_0 are variable parameters.*

87fs, 71fs, and 82fs, respectively. It is intriguing that the 9T-p-DPP has the fastest dephasing rate among the three molecules. Efficient and fast charge transfer rate leads to fast electronic dephasing of the molecular systems[63]. In this regards, the fastest dephasing rate of 9T-p-DPP can be attributed to its efficient intermolecular charge transfer characteristic.

4-3.   Discussion

In this chapter, the combination of time-resolved spectroscopy in solution-phase and interferometric near field microscopy in solid-phase allows us to compare coherent transport in solution and in organic films. In the solution phase, larger peak shift was observed for the dendrimer with respect to the dendron systems, which may be attributed with higher transition dipole moment and longer dephasing time[16-22,27-39] with respect to the other two dendron systems. Interestingly, even though 18T-p-DPP and 9T-p-DPP present the same electron donor/electron acceptor groups ratio, 18T-p-DPP has shown a faster anisotropy decay time compared to 9T-p-DPP, suggesting that intra-molecular coupling effects may contribute to this faster depolarization time. In order to analyze the nature of molecular coupling, we have utilized a simple phenomenological model developed by Leegwater[64] for the dendrimer system 18T-p-DPP. Details on this theoretical model are provided in the supporting information. Figure 4-7. shows that a coherence process must be taken into account to support the faster decay time component of the anisotropy observed from experimental measurements. Based on these findings, an estimation of the interaction strength can be found for the dendrimer macromolecule. For all the calculated curves, a decay time of 50 fs gives an interaction strength around 700 cm^{-1}. From these experimental and modeling findings, coherent domains due to the strong coupling between

chromophores may be identified in case of the higher generation dendrimer system. A qualitative conclusion in regards to the excitation energy transfer in solution phase is that energy is transferred coherently between slightly delocalized states at early times, and then more slowly through a hopping mechanism (incoherent dynamic) between more localized states. Furthermore, in order to rationalize solid phase results obtained using NSOM methods, larger homogeneous linewidths were considered. Assuming the same interaction strength within macromolecules,
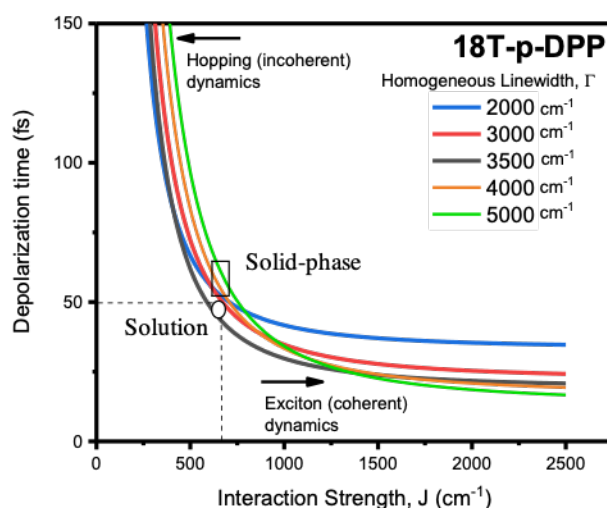
Figure 4-7. *Theoretical dependence of depolarization time on the interaction strength J for the symmetric dendrimer system 18T-p-DPP. The dash line shows the depolarization time obtained from transient anisotropy experiment.*

it can be inferred that, as we pass from solution to solid phase coherence dynamics is gradually lost in case of the dendrimer 18T-p-DPP. Interestingly, this trend parallels with the analysis of NSOM data. The symmetric dendrimer system, 18T-p-DPP, has shown more localized interactions among a smaller number of chromophores. On the other hand, in case of the dendron structure, 9T-p-DPP, NSOM results support a more efficient inter-molecular charge transport. The

different photo-behavior shown by these systems can be rationalized considering the molecular structure and the symmetry of the system. The larger and higher generation of the 18T-p-DPP leads to more molecular orientation and organization. This might be detrimental to confirm the strong molecular coupling of the molecular system. In general, dendrimers systems gave superior results compared to dendrons as well as higher generations to smaller ones.[65-69] However, from these findings, we have demonstrated how excited state electronic properties change drastically upon going from solution to the solid phase. Stronger coherent transport properties and longer charge delocalization length have been observed for the smaller dendritic system in the solid-phase. On the other hand, in the solution-phase stronger coherent dynamics and faster depolarization were found in case of the bigger dendrimer macromolecule. These differences observed in the solution and in the solid-phase can be rationalized in terms of intra- and inter-molecular couplings properties. The dendron structure has shown more promising properties due to two couplings contributions. The first is due to a strong intra-molecular coupling occurring between the electron donor core portion and the electron acceptor branches. The second contribution is due to the strong ability to delocalize the charge via inter-molecular couplings among macromolecules. On the other hand, the bigger dendrimer in the solution-phase has shown localized intra-molecular interactions among smaller portions of the macromolecule. This different behavior may be due to the less availability of the core portion to the surroundings in case of the dendrimer with respect to the dendron macromolecule.

4-4.   Conclusion

In summary, the time-resolved spectroscopy and microscopy investigation presented in this work have provided information on coherent transport properties of dendritic macromolecules in

solution and in organic films. Through this comparison, we believe that dendron structures could lead to longer exciton mobility properties due to stronger intra-and inter-molecular couplings occurring in the solid-phase with respect to dendrimer structure. The importance of combining liquid and solid phase spectroscopy results has been shown. This combination of powerful spectroscopic methods could give an efficient way to improve the potential of this class of organic macromolecules for light harvesting applications.

4-5.   References

1.   Zhao, Y.; Zhao, X.; Zang, Y.; Di, C.; Diao, Y.; and Mei. J. Conjugation-Break Spacers in Semiconducting Polymers: Impact on Polymer Processability and Charge Transport Properties. *Macromolecules,* **2015**, *48* (7), 2048-2053

2.   Biniek, L.; Schroeder, B. C.; Nielsen, C. B.; McCulloch, I. Recent Advances In High Mobility Donor−Acceptor Semiconducting Polymers. *J. Mater. Chem.,* **2012**, *22*, 14803−14813.

3.   Marrocchi, A.; Seri, M.; Kim, C.; Facchetti, A.; Taticchi, A.; Marks, T. J. Low-Dimensional Arylacetylenes for Solution-Processable Organic Field-Effect Transistors. *Chem. Mater.,* **2009**, *21*, 2592−2594.

4.   Silvestri, F.; Marrocchi, A.; Seri, M.; Kim, C.; Marks, T. J.; Facchetti, A.; Taticchi, A. Solution-Processable Low-Molecular Weight Extended Arylacetylenes: Versatile p-Type Semiconductors for FieldEffect Transistors and Bulk Heterojunction Solar Cells. *J. Am. Chem. Soc.*, **2010**, *132*, 6108−6123.

5.   Facchetti, A.; π-Conjugated Polymers for Organic Electronics and Photovoltaic Cell Applications. *Chem. Mater.*, **2011**, *23*, 3, 733–758.

6.   Polman, A.; Knight, M.; Garnett, E. C.; Ehrler, B.; Sinke, W. C. Photovoltaic Materials: Present Efficiencies and Future Challenges. *Science,* **2016**, *352*, 4424.

7.   Goodson, T., III *Solar Fuels: Materials, Physics, and Applications*; CRC Press, Boca Raton, Florida, **2017**

8.   Saliba, M.; Matsui, T.; Domanski, K.; Seo, J-Y.; Ummadisingu, A.; Zakeeruddin, S. M.; Correa-Baena, J-P.; Tress, W. R.; Abate, A.; Hagfeldt, A. Incorporation of Rubidium Cations into Perovskite Solar Cells Improves Photovoltaic Performance. *Science,* **2016**, *354*, 206−209.

9.   Menke, S. M.; Holmes, R. J. Exciton Diffusion in Organic Photovoltaic Cells. *Energy Environ. Sci.* **2014**, *7*, 499−512.

10.   Kaltenbrunner, M.; Sekitani, T.; Reeder, J.; Yokota, T.; Kuribara, K.; Tokuhara, T.; Drack, M.; Schwödiauer, R.; Graz, I.; Bauer-Gogonea, S. An Ultralightweight Design for Imperceptible Plastic Electronics. *Nature,* **2013**, *499*, 458−465.

11.   Scharber, M. C.; Sariciftci, N.C. Efficiency of bulk-heterojunction organic solar cells. *Progress in Polymer Science,* **2013**, *38*, 12, 1929-1940.

12.   Liang, Y.; Xu, Z.; Xia, J.; Tsai, S.; Wu, Y.; Li, G.; Ray, C.; Yu, L. For the Bright Future— Bulk Heterojunction Polymer Solar Cells with Power Conversion Efficiency of 7.4%. *Adv. Mater.*, **2010**, *22*, E135–E138.

13.   Gao, W.; Luo, Q.; Wang, J.; Lin, Y.; Tang, C.; Dou, J.; Tan, H.; Zheng, Q.; Ma, C-Q.; Cui, Z. Peripherally diketopyrrolopyrrole-functionalized dendritic oligothiophenes – synthesis, molecular structure, properties and applications. *Polym. Chem*., **2017**, *8*, 1460.

14.   (a) Kozlov, O.; Luponosov, Y.; Solodukhin, A.; Flament, B.; Olivier, Y.; Lazzaroni, R.; Cornil, J.; Ponomarenko, S.; and Pshenichnikov, M. Ultrafast Exciton-to-Polaron Conversion in Densely Packed Small Organic Semiconducting Molecules. *Adv. Optical Mater.,* **2017**, *5*, 1700024 (b) Li, W.; Roelofs, C.; Wienk, M.; and Janssen, R. Enhancing the Photocurrent in Diketopyrrolopyrrole-Based Polymer Solar Cells via Energy Level Control. *J. Am. Chem. Soc.,* **2012**, *134*, 13787−13795

15.   Ma, C.-Q.; Pisula, W.; Weber, C.; Feng, X. L.; Müllen, K. and Bäuerle, P. Dendritic Oligothiophenes Terminated with Tris(alkyloxy)phenylethynyl Tails: Synthesis, Physical Properties, and Self-Assembly. *Chem. – Eur. J*., **2011**, *17*, 1507–1518

16.   Adronov, A.; Frechet, J. M. Light-harvesting dendrimers. *J. Chem. Soc., Chem. Commun.,* **2000**, *18*, 1701

17.   Ramakrishna, G.; Bhaskar, A.; Bauerle, P.; and Goodson, T. III Oligothiophene Dendrimers as New Building Blocks for Optical Applications. *J. Phys. Chem. A* **2008**, *112*, 2018-2026

18.   Ranasinghe, M.I.; Varnavski, O.; Pawlas, J.; Hauck, S.I.; Louie, J.; Hartwig, J.F.; and Goodson, T. III Femtosecond Excitation Energy Transport in Triarylamine Dendrimers. *J. Am. Chem Soc*., **2002**, *124*, 6520-6521

19.   Goodson, T. III; Varnavski, O.; and Wang, Y.; Optical properties and applications of dendrimer–metal nanocomposites. *International Reviews in Physical Chemistry*, **2004**, *23* (1), 109-150

20.   Goodson, T. III; Optical Excitations in Organic Dendrimers Investigated by Time-Resolved and Nonlinear Optical Spectroscopy. *Acc. Chem. Res*., **2005**, *38*, 99-107

21.   Varnavski, O.; Yan, X.; Mongin, O.; Blanchard-Desce, M.; Goodson, T. III Strongly Interacting Organic Conjugated Dendrimers with Enhanced Two-Photon Absorption. *J. Phys. Chem. C,* **2007**, *111*, 149-162

22.   Varnavski O, Goodson T III Femtosecond fluorescence dynamics and molecular interactions in a water-soluble nonlinear optical polymeric dye. *Chem. Phys. Lett.,* **2000**, *320* 688–696

23.   Collini, E.; Wong, C. Y.; Wilk, K. E.; Curmi, P. M. G.; Brumer, P.; Scholes, G. D. Coherently wired light-harvesting in photosynthetic marine algae at ambient temperature. *Nature,* **2010**, *463*, 644.

24.   Brédas, J.; Sargent, E. and Scholes, G. Photovoltaic concepts inspired by coherence effects in photosynthetic systems. *Nat. Mater.,* **2017,** *16,* 35-44

25.   Collini, E. Spectroscopic signatures of quantum-coherent energy. *Chem. Soc., Rev*., **2013**, *42*, 4932-4947

26.   Park, H.; Heldman, N.; Rebentrost, P.; Abbondanza, L.; Iagatti, A.; Alessi, A.; Patrizi, P.; Salvalaggio, M.; Bussotti, L.; Mohseni, M.; Caruso, F.; Johnsen, H.; Fusco, R.; Foggi, P.; Scudo, P.; Lloyd, S. and Belcher, A. Enhanced energy transport in genetically engineered excitonic networks. *Nat. Mater.,* **2016**, *15(2)*

27.   Varnavski, O.; Leanov, A.; Liu, L.; Takacs, J.; Goodson, T. III Femtosecond luminescence dynamics in a nonlinear optical organic dendrimer. *Phys. Rev. B,* **2000**, *61*, 12732

28.   Varnavski, O.; Samuel, I.D.W.; Pålsson, L.-O.; Beavington, R.; Burn, P. L.; Goodson, T. III Investigations of excitation energy transfer and intramolecular interactions in a nitrogen corded distrylbenzene dendrimer system. *J. Chem. Phys.,* **2002**, *116*, 20,

29.   Varnavski, O.; Menkir, G.; Goodson, T. III; and Burn, P.L. Ultrafast polarized fluorescence dynamics in an organic dendrimer. *Appl. Phys. Lett*., **2000**, *77*, 8, 21

30.   Wang, Y.; Xie, X.; and Goodson, T. III Enhanced Third-Order Nonlinear Optical Properties in Dendrimer−Metal Nanocomposites. *Nano Lett.*, **2005**, *5*, 12

31.   Badaeva, E.; Harpham, M.R.; Guda, R.; Suzer, O.; Ma, C-Q. Bauerle, P.; Goodson, T. III, and Tretiak, S. Excited-State Structure of Oligothiophene Dendrimers: Computational and Experimental Study. *J. Phys. Chem. B*, **2010**, *114*, 15808–15817

32.   Donehue, J. E.; Varnavski, O.; Cemborski, R.; Iyoda, M.; Goodson, T. III Probing Coherence in Synyhrtic Cyclic Light-Harvesting Pigments. *J. Am. Chen. Soc.,* **2011**, *133*, 4819-4828.

33.   Guillermo C. Bazan, G.; Oldham, W.; Lachicotte, R.; Tretiak, S.; Chernyak, V. and Mukamel, S. Stilbenoid Dimers: Dissection of a Paracyclophane Chromophore. *J. Am. Chem. Soc.,* **1998**, *120*, 9188-9204

34.   Engel, G. S.; Calhoun, T. R.; Read, E. L.; Ahn, T. K.; Mancal, T.; Cheng, Y. C.; Blankenship, R. E.; Fleming, G. R. Evidence for wavelike energy transfer through quantum coherence in photosynthetic systems. *Nature,* **2007**, *446*, 782.

35.   Grondelle, R.; Novoderezhkin, V. I. Photosynthesis: Quantum design for a light trap. *Nature,* **2010**, *463*, 614-5

36.   Lee, H.; Cheng, Y. C.; Fleming, G. R. Coherence dynamics in photosynthesis: protein protection of excitonic coherence. *Science,* **2007**, *316*, 1462.

37.   Cheng, Y. C.; Silbey, R. Coherence in the B800 Ring of Purple Bacteria LH2. *J. Phys. Rev. Lett*., **2006**, *96*, 028103.

38.   Scholes, G. D. Quantum-Coherent Electronic Energy Transfer: Did Nature Think of It First? *J. Phys. Chem. Lett.,* **2010**, *1*, 2

39.   Lang, M.J.; Jordanides, X.J.; Song, X.; and Fleming, G. R. Aqueous solvation dynamics studied by photon echo spectroscopy. *J. Chem. Phys.*, **1999**, *110*, 12

40.   Goodson, T. III; Time-resolved spectroscopy of organic dendrimers and branched chromophores. *Annu. Rev. Phys. Chem*. **2005**, *56*, 581–603

41.   Varnavski, O.; Kim, T.; Cai, Z.; Yu, L.; and Goodson, T. III Inhomogeneity of the Ultrafast Excited State Dynamics in Organic Photovoltaic Materials Measured at Nanoscale. *J. Phys. Chem. C,* **2018**, *122*, 38, 22201-22209

42.   Christensson, N.; Dietzek, B.; Yartsev, A.; Pullerits, T**.** Probing the strength of the system-bath interaction by three-pulse photon echoes. *J. Chem. Phys.,* **2009***, 130*, 024510

43.   Abeyasinghe, N.: Kumar, S.; Sun, K.; Mansfield, J. F.; Jin, R. and Goodson III, T. Enhanced Emission from Single Isolated Gold Quantum Dots Investigated Using Two-Photon-Excited Fluorescence Near-Field Scanning Optical Microscopy. *J. Am. Chem. Soc.,* **2016**, *138*, 50, 16299-16307

44.   Lahankar, S.; West, R.; Varnavski, O.; Xie, X.; Goodson, T.; Sukhomlinova, L.; and Twieg, R. Electronic interactions in a branched chromophore investigated by nonlinear optical and time-resolved spectroscopy. *J. Chem. Phys.,* **2004***, 120*, 337

45.   Ramakrishna, G.; Goodson, T., III. Excited-State Deactivation of Branched Two-Photon Absorbing Chromophores: A Femtosecond Transient Absorption Investigation. *J. Phys. Chem. A,* **2007**, *111*, 993− 1000.

46.   Varnavski, O.; Goodson, T. III Ultrafast Exciton Dynamics in a Branched Molecule Investigated by Time-Resolved Fluorescence, Transient Absorption and Three-Pulse Photon Echo Peak Shift Measurements. *J. Phys, Chem. B,* **2004**, *108*

47.   Nagasawa, Y.; Yu, J-Y.; Fleming, G. R. Solute–solvent interaction dynamics studied by photon echo spectroscopies in polymer glasses. *J. Chem. Phys.,* **1998**, *109*, 6175

48.   Oh, M.; Salvador, M. R.; Wong, C. Y.; and Scholes, G. C. Three-Pulse Photon-Echo Peak Shift Spectroscopy and Its Application for the Study of Solvation and Nanoscale Excitons. *Chem. Phys. Chem.* **2011**, *12*, 88 − 100

49.   Hwang, I; and Scholes, D. G. Electronic Energy Transfer and Quantum-Coherence in π-Conjugated Polymers. *Chem. Mater*., **2011**, *23*, 610-620

40.   Dhar, J.; Venkatramaiah, N.; Anitha, A.; and Patil, S. Photophysical, electrochemical and solid state properties of diketopyrrolopyrrole based moluecular materials: importance of the donor group. *J. Mater. Chem*., **2014**, *2*, 3457

51.   Wu, Z.; Fan, B.; Xue, F.; Adachi, C.; Ouyang, J. Organic Molecules Based on Dithienyl-2,1,3-Benzothiadiazole as New Donor Materials for Solution-Processed Organic Photovoltaic Cells. *Sol. Energy Mater. Sol. Cells,* **2010**, *94*, 2230−2237.

52.   Gautam, P.; Misra, R.; Siddiqui, S. A.; Sharma, G. D. Unsymmetrical Donor−Acceptor−Acceptor−π−Donor Type Benzothiadiazole-Based Small Molecule for a Solution Processed Bulk Heterojunction Organic Solar Cell. *ACS Appl. Mater. Interfaces,* **2015**, *7*, 10283−10292

53.   Albota, M.; Beljonne, D.; Bredas, J.; Ehrlich, J. E.; Fu, J.; Heikal, A. A.; Hess, S. E.; Kogej, T.; Levin, M. D.; Marder, S. R. Design of Organic Molecules with Large Two-Photon Absorption Cross Sections. *Science,* **1998**, *281*, 1653−1656.

54.   Carlotti, B.; Cai, Z.; Kim, H.; Sharapov, V.; Madu, I. K.; Zhao, D.; Chen, W.; Zimmerman, P. M.; Yu, L.; Goodson, T. III, Charge Transfer and Aggregation Effects on the Performance of Planar vs Twisted Nonfullerene Acceptor Isomers for Organic Solar Cells. *Chem. Mater.,* **2018**, *30*, 4263−4276

55.   Ricci, F.; Carlotti, B.; Keller, B.; Bonaccorso, C.; Fortuna, C.G.; Goodson, T. III; Elisei, F.; Spalletti, A. Enhancement of Two-Photon Absorption Parallels Intramolecular Charge-Transfer Efficiency in Quadrupolar versus Dipolar Cationic Chromophores. *J. Phys. Chem. C,* **2017**, *121*, 3987−4001

56.   Ricci, F.; Elisei, F.; Foggi, P.; Marrocchi, A.; Spalletti, A.; Carlotti, B. Photobehaviour and Non−Linear Optical properties of push−pull, symmetrical and highly fluorescent benzothiadiazole derivatives. *J. Phys. Chem. C*, **2016**, *120*, 23726−23739.

57.   Terenziani, F.; Katan, C.; Badaeva, E.; Tretiak, S.; BlanchardDesce, M. Enhanced Two-Photon Absorption of Organic Chromophores: Experimental and Theoretical Assessments. *Adv. Mater.,* **2008**, *20*, 4641−4678.

58.   Sato, S.; Nishimura,Y.; Sakata, Y.; and, Yamazaki, I. Coherent Control of Oscillatory Excitation Transfer in Dithia-1,5[3,3]anthracenophane by a Phase-Locked Femtosecond Pulse Pair. *J. Phys. Chem. A,* **2003**, *107* (47) 10019-10025

59.   Dudovich, N.; Dayan, B.; Faeder, S.; and Silberberg, Y. Transform-Limited Pulses Are Not Optimal for Resonant Multiphoton Transitions. *Phys. Rev. Lett.,* **2001**, *86*, 47

60.   Blanchet, V.; Nicole, C.; Bouchene, M.; and Girard, B. Temporal Coherent Control in Two-Photon Transitions: From Optical Interferences to Quantum Interferences. *Phys. Rev. Lett.,* **1997**, 78, 2716

61.   Naganuma, K.; Mogi, K.; Yamada, H. General method for ultrashort light pulse chirp measurement. *IEEE J. Quantum Electron.,* **1989**, *25* (6), 1225–1233

62.   Scherer, N.; Carlson, R.; Matro, A.; Du, M.; Ruggiero, A.; Romero-Rochin, v.; Cina, J.; Fleming, G.; and Rice, S. Fluorescence-detected wave packet interferometry: Time resolved molecular spectroscopy with sequences of femtosecond phase-locked pulses. *J. Chem. Phys.,* **1991,** *95*, 1487

63.   Parson, W. Vibrational Relaxations and Dephasing in Electron-Transfer Reactions. *J. Phys. Chem. B,* **2016**, *120*, 11412-11418

64.   Leegwater, J.A. Coherent versus Incoherent Energy Transfer and Trapping in Photosynthetic Antenna Complexes. *J. Phys. Chem.,* **1996**, *100*, 14403

65.   Ahn, T-S.; Nantalaksakul, A.; Dasari, R.R; Al-Kaysi, R. O.; Mu1ller, A. M.; Thayumanavan, S. and Bardeen, C. J. Energy and Charge Transfer Dynamics in Fully Decorated Benzyl Ether Dendrimers and Their Disubstituted Analogues. *J. Phys. Chem. B,* **2006**, *110*, 24331-339

66.   Szarko, J.M.; Rolczynski, B.S.; Lou, S.J.; Xu, T.; Strzalka. J.; Marks, T.J.; Yu, L.; and Chen, L.X. Photovoltaic Function and Exciton/Charge Transfer Dynamics in a Highly Efficient Semiconducting Copolymer. *Adv. Funct. Mater*., **2014**, *24*, 10–26

67.   Varnavski, O.; Ispasoiu, R. G; Balogh, L.; Tomalia, D.; Goodson, T. III Ultrafast time-resolved photoluminescence from novel metal–dendrimer nanocomposites. *J. Chem. Phys.,* **2001**, *114*, 5

68.   Varnavski, O.; Ostrowski, J.; Sukhomlinova, L.; J. Twieg, R.; Bazan, G.; and Goodson, T. III Coherent Effects in Energy Transport in Model Dendritic Structures Investigated by Ultrafast Fluorescence Anisotropy Spectroscopy. *J. Am. Chem. Soc.,* **2002**, *124*, *8,* 1736-1743

69.   Ma, C-Q.; Fonrodona, M.; Schikora, M.; Wienk, M.; Janssen, R. and Bauerle, P. Solution-Processed Bulk-Heterojunction Solar Cells Based on Monodisperse Dendritic Oligothiophenes. *Adv. Funct. Mater.,* **2008**, *18*, 3323–3331

CHAPTER V

Effective and fast OLED device stability estimation using NSOM two-photon fluorescence microscopy.

5-1.   Introduction

OLED display has been rapidly replacing the conventional LCD (Liquid crystal display) market. However, it is still challenging to get a better device operational lifetime competitive with the LCD display because of its self-light-emitting mechanism[1-3]. Most properties for display of OLED are superior to the LCD.

Figure 5-1. *An example of burn-in in OLED devices.*
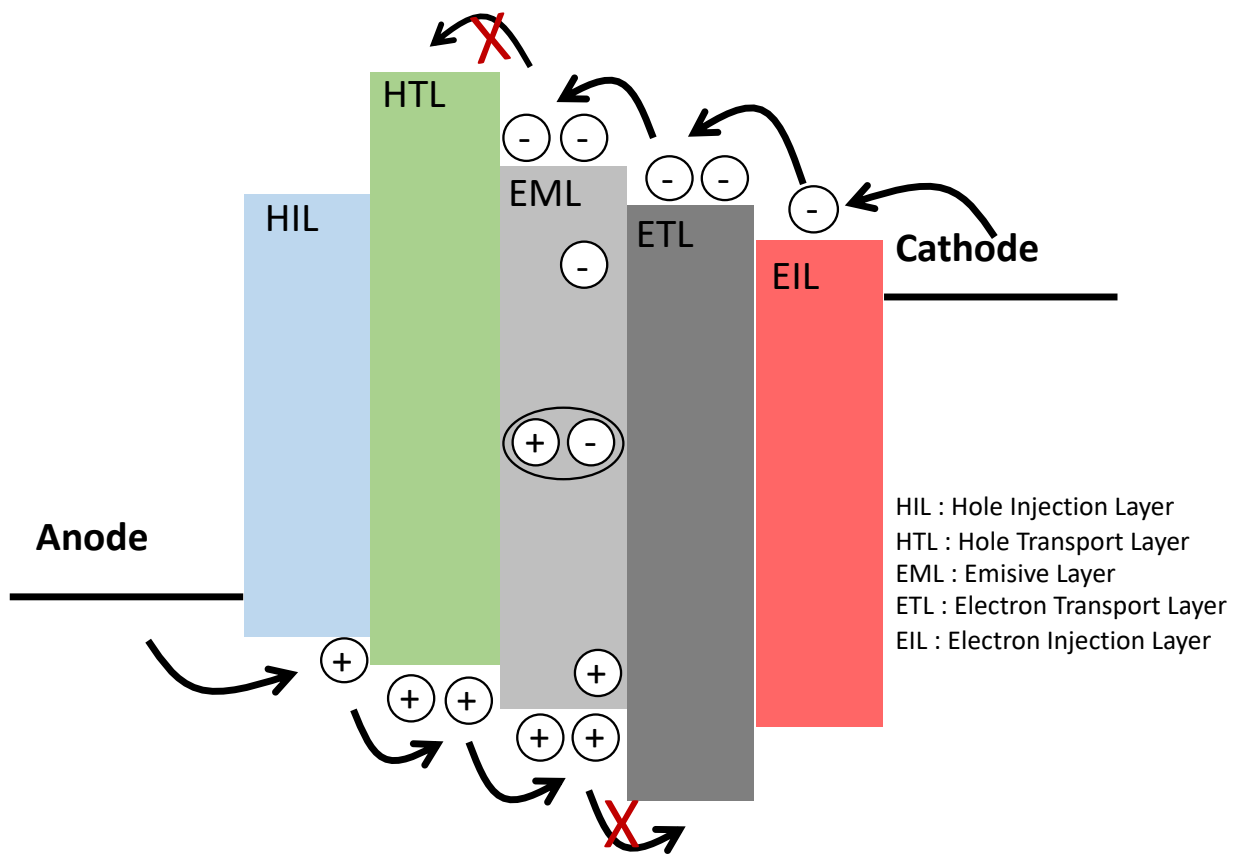
***Figure 5-2**. Traditional OLED structure and emission mechanism.*

However, the poor device stability in comparison with LCD is prohibiting the rapid expansion of the OLED display market. As seen in the figure 5-1, OLED shows critical burn-in problem not seen in LCD. To solve this problem large number of materials have been introduced and developed such as heavy metal, polymer and oligomer based phosphorescence and TADF (Thermally Activated Delayed Fluorescence) OLED materials[3-5]. However, it is difficult to evaluate the device operation life time of the materials in short. Because of its structural complexity having multiple layers seen in figure 5-2 the device fabrication needs huge time and long test-time is required to estimate the operational life time. These feature may disturb the fast evaluation of the OLED

materials. It is hence necessary to develop new methods for the fast device life-time estimation of the newly developed OLED materials. The OLED structure consists of multiple layers of thin films in the order of a few hundred angstrom stacked between two anode and cathode electrodes. During the device operation, hole and electron injected from the two electrodes are recombined to form the exciton, then, emit the light from radiative decay[6] in emissive layer of ~10nm layer. This operation process instinctively indicates that the OLED device efficiency and stability may be critically affected by the localized excited state dynamics of the materials. It is also important to evaluate how critically localized excitation dynamics effect the OLED device efficiency and stability. To interrogate this question in this chapter NSOM microscopy for localized fluorescence measurement has been introduced. Surprisingly, NSOM microscopy efficiently estimates the real device operational life time of the OLED device. NSOM measurement has been utilized to obtain fluorescence decay of newly developed TADF OLED materials from LG Chem doped inside of PMMA film. TADF OLED is expected to replace the current dominant phosphorescence or fluorescence OLED materials as expected owing to their high efficiency and stability[5, 7-10]. Because the OLED materials uses triplet species without using metal-ligand bonding which is critical to the molecular stability by using unique donor-acceptor structure[5, 7-10]. It is presented that the fluorescence decay during the NSOM fluorescence measurement is highly correlated with the real device operational life time for the TADF materials.

5-2.   Experimental Results and Discussion.
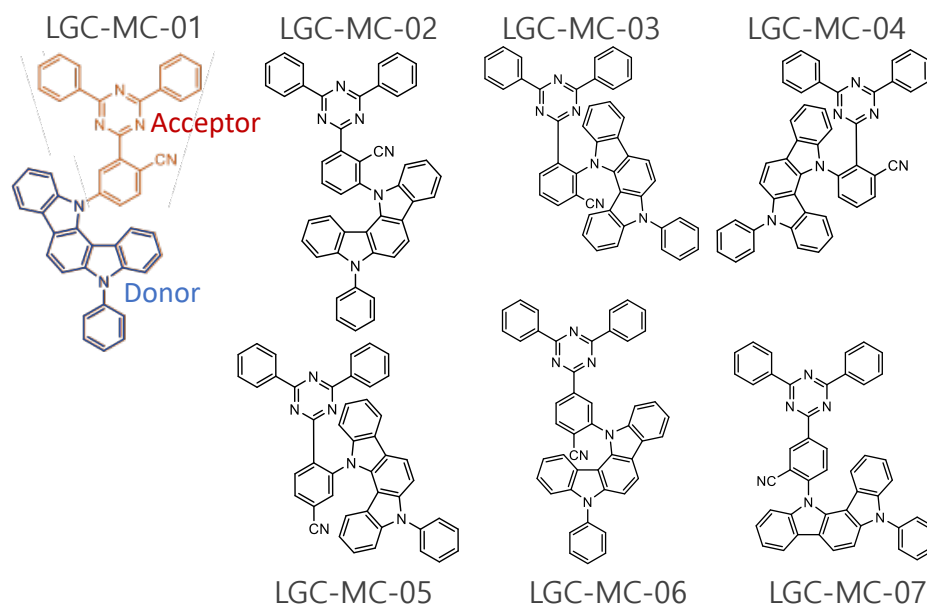
Figure 5-3. Structure of the TADF OLED materials.

The steady state analysis of the materials has been probed using UV-Vis and two photon absorption. The focus of our investigation is to probe the steady state difference of the isomer-molecules in Fiugre 5-3. Among them we selected a series of samples (LGC-MC- 01, 05 and 07) to evaluate the material properties better and determine which set of the samples has a significant difference in Q.E. and LT90 properties, which would enable us to clarify the molecular orientation effect based on the device data (Table 5-1) from LG Chem. The three chromophores studied showed distinct steady state properties in chloroform. Their UV-Vis results (Fig. 5-4.) show almost ideal absorption spectra but differing the charge transfer absorption band between 375~450nm. Interestingly, the absorption value has been correlated with the device Q.E.
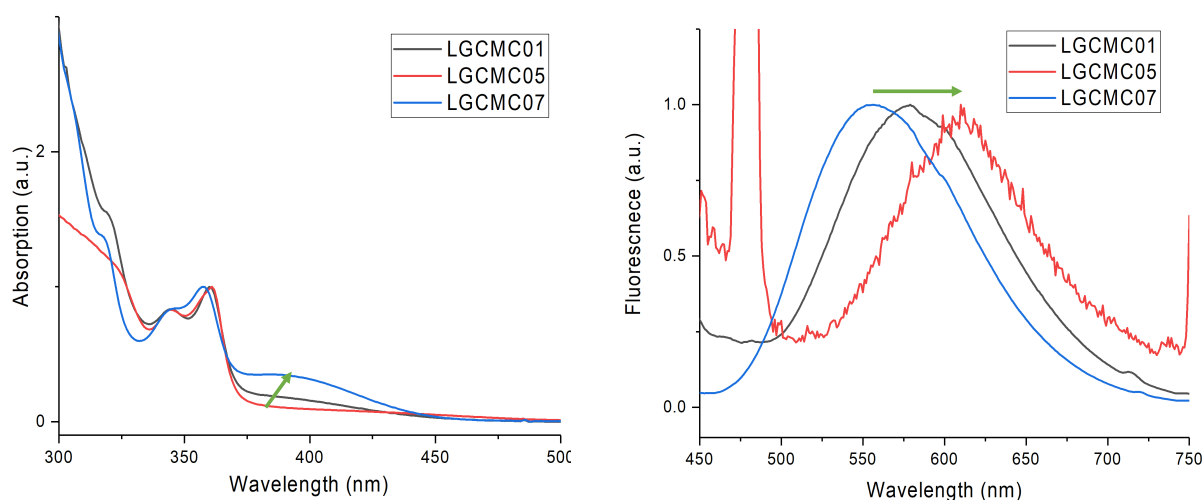
Figure 5-4. *Steady state absorption and emission spectra of LGC-MC- 01,05 and 07 in chloroform.*

This results indicates that charge transfer characteristics in TADF is an important parameter for characterization. Photoluminescence spectra and intensity of the materials in the same exposure and solvent condition has also displayed the different peak wavelength and fluorescence intensity. This also shows that the donor and acceptor moiety orientation of the TADF materials is very critical to the emission properties. Extinction coefficient measurements were performed following Beer and Lambert's law, and LGC-MC-01 showed the highest potential

Samples	Absorptivity ($10^4 M^{-1} cm^{-1}$)	Quantum Yield	TPA cross-section (GM)
LGC-MC-01	1.32 @ Absorption Peak	0.0090	6.48
LGC-MC-05	1.07 @ Absorption Peak	0.0014	631.4
LGC-MC-07	1.24 @ Absorption Peak	0.076	6.54

Table 5-1. *Absorptivity, Quantum Yield and TPA cross-section of the LGC-MC-01, 05 and 07.*
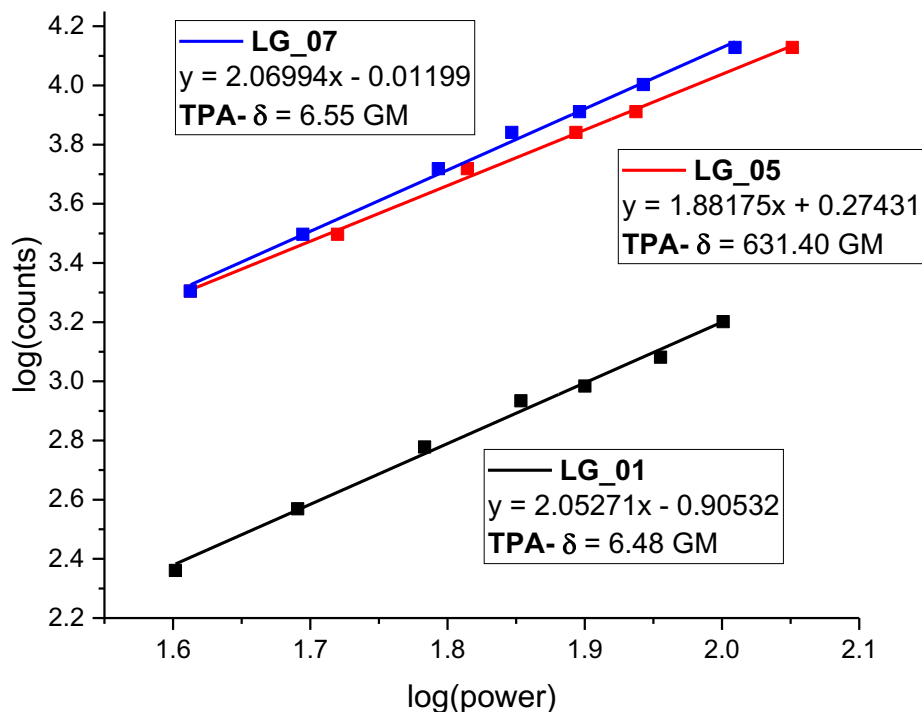
Figure 5-5. *TPA absorption measurement of LGC-MC-01, 05 and 07.*

for photon absorptivity. Fluorescence quantum yield measurements were performed with two reference chromophores that were cross-referenced, and with concentrations of about 10^{-5} M. Their fluorescence quantum yield values were different by about one order of magnitude in comparison as shown in the Table 5-1. LGC-MC-07 displayed the highest quantum yield of only about 7.6%. It can be said that these chromophores are not the best emitters of singlet photons, however the study of the mechanisms at which they give up their excitation energy would be interesting to figure out. The three studied chromophores showed TPA (Two-Photon Absorption) capabilities at 790 nm excitation. LGC-MC-05, the sample with the lowest quantum yield, yielded the highest TPA cross-section. For the other two chromophores (LGC-MC-01 and LGC-MC-07),
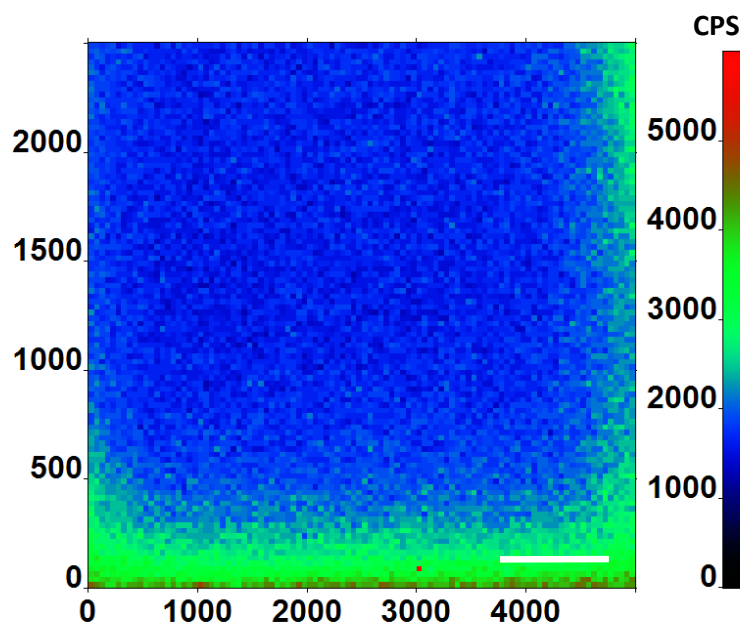
Figure 5-6. *NSOM fluorescence measurement of the LGC-MC-01 OLED molecular doped PMMA film. Solid bar indicate 1um scale.*

despite their fluorescence quantum yield values being different by an order of magnitude, they showed equivalent TPA cross-section. Interestingly, LGC-MC-05 the highest TPA cross-section among them, shows the smallest Q.E. This result needs to be noted and further studied to cover the reason as to why this is. Light emitting film were fabricated by adding the materials into PMMA by using simple spin coating methods. OLED : PMMA ratios is 1:20 and chloroform was used for better spin coating quality. After spin coating, the film was left inside a vacuum chamber for 24 hours at room temperature to allow the solvent evaporation. For all measurements, the OLED materials and PMMA ratio was fixed to prevent the ratio dependent fluorescence decay rate change[11, 12]. Two-photon NSOM microscopy has been used to excite the excited population of the OLED materials and measure the fluorescence decay rate depending on the exposure time.
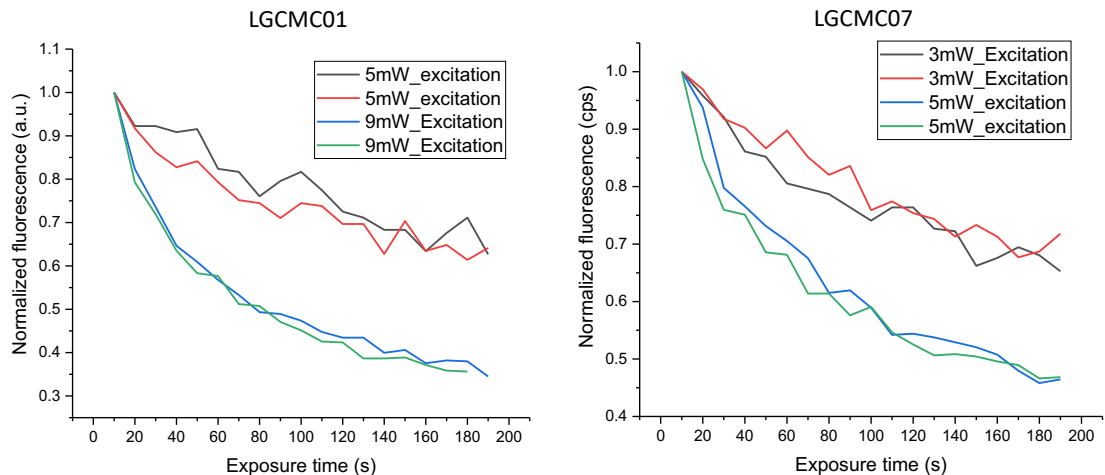
Figure 5-7. *Fluorescence decay curve of LGC-MC-01 and LGC-MC-07 in different laser excitation power.*

800nm 100fs-pulse laser from Spectra-Physics was used for the measurement. Figure 5-6. shows the NSOM fluorescence measurement of the LGC-MC-01 doped PMMA film when the exposure power is 15mW. 5um x 5um area was scanned using the NSOM system. Very uniform fluorescence distribution indicates the uniform distribution of the OLED material in PMMA matrix.

Intrinsic	**Extrinsic**
Electrochemical (Oxidation, Reduction)	Encapsulation (Water, O_2)
Thermal	Impurities
Interfacial (Chathode delamination)	Vacuum level
Photochemical	Substrate
Carrier/Charge Balance	Operation condition (Voltage, Currents)

Table 5-2. *Intrinsic and Extrinsic factor for OLED stability.*
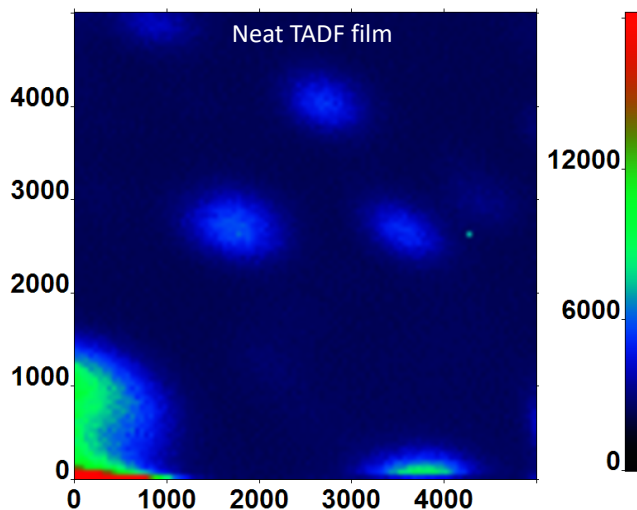
Figure 5-8. *Neat OLED materials NSOM fluorescence measurement results.*

To estimate the LGC-MC-01 fluorescence decay rate on multiple position was measured from different laser excitation power. For the LGC-MC-01 initial fluorescence was ~1430 cps and ~4610cps when the excitation power was 5mW and 9mW, respectively. This results shows the traditional quadratic two-photon absorption feature. The initial excitation is almost same in different position of the OLED film samples as shown in figure 5-6. Interestingly, the fluorescence decay rate is proportional to the initial fluorescence intensity. In two-photon absorption regime, the excitation population is directly related with the excitation power. The fluorescence decay rate is critically related to the molecular system deformation inside of the film, although it is not directly related to the molecule's electro luminescence[13, 14]. Additionally, although there are many intrinsic and extrinsic factors that affect an OLED lifetime[6] as shown in Table 5-2, NSOM fluorescence microscopy excitation and measurements are mostly affected by the localized molecular interaction in the film due to its high spatial resolution. This indicates that the fluorescence decay rate is essentially correspondent with the excited state population. This is why high light intensity in
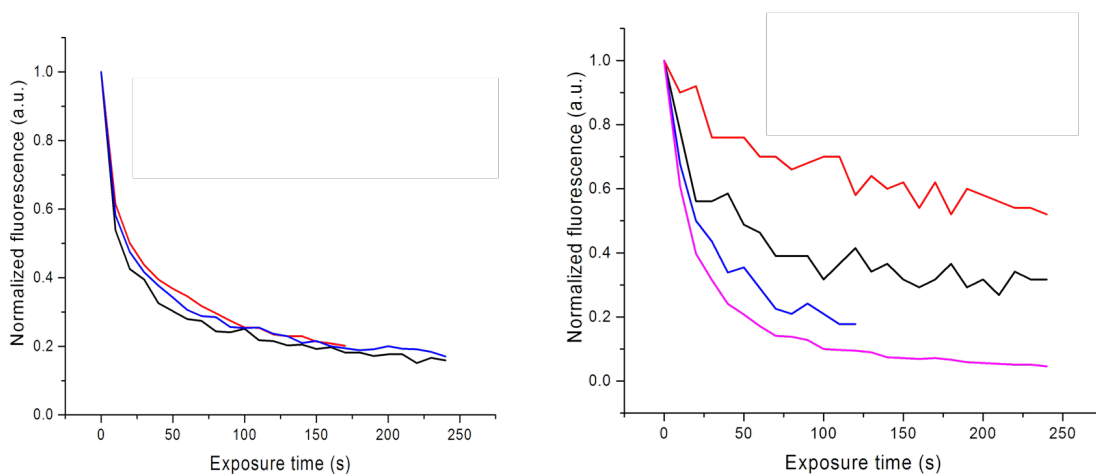
Figure 5-9. *Fluorescence decay dynamics of same initial fluorescence intensity in different position of OLED doped PMMA film and neat OLED film.*

OLED device facilitate its degradation. This hypothesis has been proved in the measurement of the different OLED samples in neat OLED film without PMMA matrix. LGC-MC-07 shows also same trends. Initial fluorescence intensity of LGC-MC-07 is ~2050cps and ~4690cps from 3mW and 5mW laser excitation, respectively. Same initial intensity has been shown in different measurement position. For the OLED molecules higher initial intensity sample position also shows faster fluorescence decay curve. More interesting results were obtained for neat OLED materials samples as shown in Figure 5.8. The NSOM fluorescent map has been processed from the neat OLED materials not from the OLED doped PMMA. Small aggregates below 1um were shown in the map. Each aggregates shows different fluorescence intensity. This is not shown in the OLED materials doped PMMA. Molecular interaction and orientation should be different in different aggregates. Hence charge transfer, molecular vibration and energy
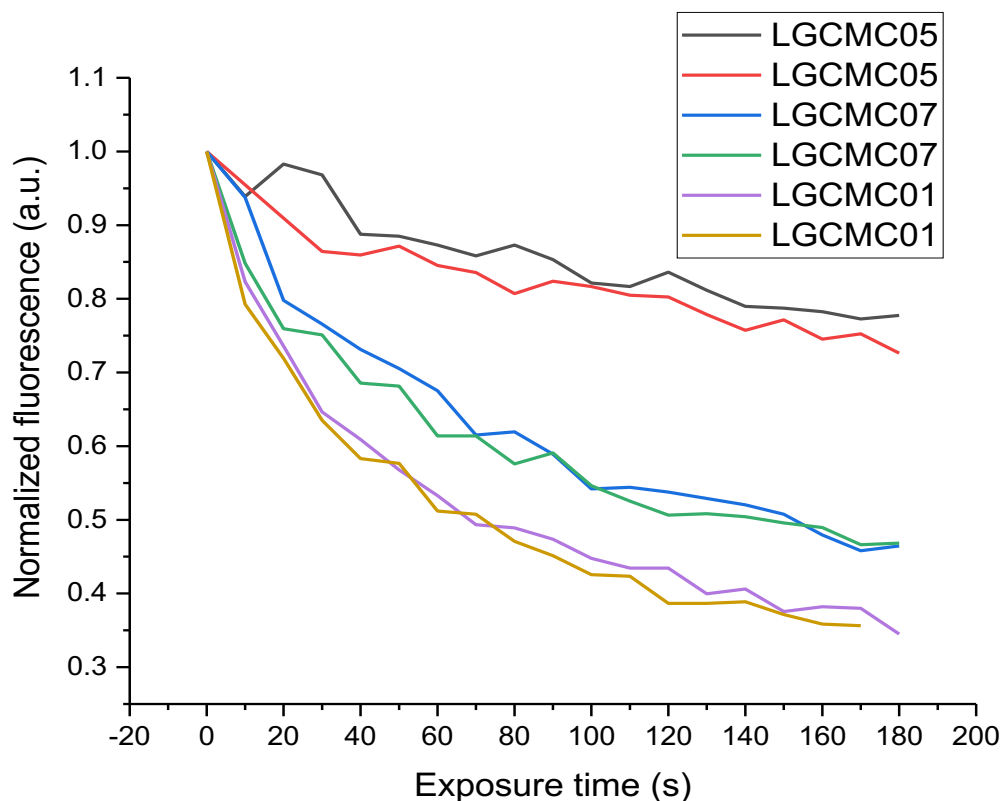
Figure 5-10*. Fluorescence decay rate of the LGC-MC-01, 05 and 07 doped PMMA films.*

transfer are also different in the different aggregates. This may lead the fluorescence difference in the aggregates. The results in Figure 5-9 is more intriguing. In the figure, fluorescence decay of the two different OLED film were illustrated for the OLED material doped PMMA film and neat OLED film. The OLED materials doped in PMMA film show similar fluorescence decay rate even in different positions. However, neat film fluorescence decay rate is very dependent on the measurement position. It should be noted that the fluorescence intensity in different positions is adjusted with similar value of about 5000 cps. We can assume the homogeneity of molecular interaction in the PMMA films and heterogeneity of molecular interaction in neat OLED films. The difference fluorescence decay rate in the neat OLED films infer the importance of the

intermolecular interaction of OLED materials. It is also hypothesized that localized fluorescence measurement using NSOM microscopy may depict the OLED devices operational stability. Three different kinds of OLED doped PMMA film have been fabricated using spin coating methods. Their initial fluorescence decay was measured using NSOM fluorescence microscopy by adjusting the fluorescence to a similar level with ~3000CPS. Figure 5-10. shows the measurement results. For the sample films, their decay rates look similar, although the three materials show different decay curves. In the figure LGC-MC-05 shows the slowest decay rate and LGC-MC-01 illustrates the fastest decay rate. This decay rate is highly correlated to the real device operational stability measurement as shown in Table 5-3. In the real device operation, we used traditional OLED device structure as shown in Figure 5-2. As the host materials of the emissive layer 3,30-bis(8a,9a-dihydro-9H-carbazol-9-yl)-1,10 -biphenyl (mCBP) was used for the device fabrication. LT90 of the LGC-MC-05 is the longest 11.1hrs and LGC-MC-01 is the shortest 0.94hrs. This results correlates well with the OLED doped PMMA film measurement using NSOM microscopy. NSOM microscopy measurement is based on the OLED materials doped in PMMA film while real OLED devices are using multiple layer structure. This simple structure for the measurement crucially reduces the sample fabrication time. Additionally, conducting LT 90 measurements required at several hours, while NSOM microscoy for measuring the fluorescence decay requires only several minutes.

| | | | QE(%) | | LE(lm/W) | | J(Cd/A) | | @ 3000cd/m² |
| | V(V) | Color coordinates (x,y) | | | | | | | LT90 (hrs) |
			3000cd	Max	3000cd	Max	3000cd	Max	
LGC-MC-01	7.3	(0.32,0.56)	6.6	7.5	8.9	13.4	20.7	23.5	0.94
LGC-MC-05	9.2	(0.39,0.57)	2.1	2.3	2.3	4.9	6.9	7.6	11.1
LGC-MC-07	6.4	(0.30,0.56)	13.5	14.1	20.7	26.9	42.1	44.2	4.2

Table 5-3. *Real OLED device performance measurement results.*

Hence we can save tremendous amount of time in estimating the OLED material stability when we using the NSOM microscopy method. It is necessary to understand why the NSOM microscopy fluorescence decay corresponds with the OLED device operation lifetime. As shown in Table 5-2, there are intrinsic and extrinsic factors to consider in the OLED materials' stability in diode operation. Extrinsic factors such as humidity, leakage current due to the dust and surface roughness are generally not related to the material properties because of their random occurrence not related with the materials itself properties. Additionally, intrinsic properties such as electro- and photochemical reaction, charge balance and thermal degradation may be a critically affected by intermolecular interaction in the local level. In this regime, high spatial resolution NSOM microscopy interrogates the localized intermolecular interaction with highly localized light-matter interaction. Therefore, we can get a more reliable signal depicting OLED materials stability from the NSOM systems.

5-3.   Conclusion

In this chapter, a simple method to estimate the molecular system stability for OLED devices. NSOM microscope fluorescence measurement methods has been introduced for measuring the OLED materials' stability. It has been shown that localized fluorescence measurement using NSOM is efficiently used for this purpose. Using this methods it is expected that the measurement time for OLED stability is minimized. Hence it is expected to decrease the amount of time spent in making devices to test their stability (LT90) and facilitate the development of more materials.

5.4.   References

1.   Kwong, R. et. al. High operational stability of electrophosphorescent devices. *Appl. Phys. Lett.*, 2002, 81, 162-164.

2.   Ràfols-Ribé, J. et. al. High-performance organic light-emitting diodes comprising ultrastable glass layers. *Sci. Adv.*, **2018**, 4, eaar8332.

3.   Minaev, B.; Baryshnikovb, G.; Agrena, H. Principles of phosphorescent organic light emitting devices. *Phys. Chem. Chem. Phys.*, **2014**, 16, 1719-1758.

4.   Lee, J.; Jeong, C.; Batagoda, T.; Coburn, C.; Thompson, M.; Forrest, S. Hot excited state management for long-lived blue phosphorescent organic light-emitting diodes. *Nat. commun.*, **2017**, 8, 15566.

5.   Uoyama, H.; Goushi, K.; Shizu, K.; Nomura, H.; Adachi, C. Highly efficient organic light-emitting diodes from delayed fluorescence. *Nature*, **2012**, 492, 234-238.

6.   Xia, S. et. al. OLED Devices Operational Lifetime: Insignts and Chanllenges. 2007 IEEE International Reliability Physics Symposium Proceedings. 45th Annual.

7.   Chen, X.; Kim, D.; Brédas, J. Thermally Activated Delayed Fluorescence (TADF) Path toward Efficient Electroluminescence in Purely Organic Materials: Molecular Level Insight. *Acc. Chem. Res.*, **2018**, 51, 2215-2224.

8.   Noda, H.; Nakanotani, H.; Adachi, C. Excited state engineering for efficient reverse intersystem crossing. Sci. Adv., 2018, 4, eaao6910.

9.   Byeon, S.; Lee, D.; Yook. K.; Lee, J. Recent Progress of Singlet-Exciton-Harvesting Fluorescent Organic Light-Emitting Diodes by Energy Transfer Processes. *Adv. Mater.*, **2019**, 1803714.

10.   Zhao, C.; Li, C.; Li, Y.; Qiua, Y.; Duan, L. Understanding the operational lifetime expansion methods of thermally activated delayed fluorescence sensitized OLEDs: a combined study of charge trapping and exciton dynamics. *Mater. Chem. Front.*, **2019**, 3, 1181-1191.

11.   Nakanotani, H.; Masui, K.; Nishide, J.; Shibata, T.; Adachi, C. Promising operational stability of high-efficiency organic light-emitting diodes based on thermally activated delayed fluorescence. *Sci. Rep.*, **2013**, 3, 2127.

12.   Godumala, M.; Choi, S.; Cho, M.; Choi, D. Recent breakthroughs in thermally activated delayed fluorescence organic light emitting diodes containing non-doped emitting layers. *J. Mater. Chem. C*, **2019**, 7, 2172-2198.

13.   Burrows, P.; Sapochak, L.; McCarty, D.; Forrest, S.; Thompson, M. Metal ion dependent luminescence effects in metal tris-quinolate organic heterojunction light emitting devices. *Appl. Phys. Lett.*, **1994**, 64, 2718.

14.   Kwong, C. et. al. Efficiency and stability of different tris(8-hydroxyquinoline) aluminium (Alq3) derivatives in OLED applications. *Mater. Sci. Eng. B,* **2005**, 116, 75–81.

CHAPTER VI

Orientation of the carbazole donor and triazine acceptor based

TADF deformation.

6-1. Introduction

Organic light-emitting diode (OLED) is a very important class of display devices, which has properties such as a high color quality and rapid electrical response time over their LCD(Liquid Crystal Display) counterparts.[1,2] These superior operational features have attracted industrial as well as academic interest since the Forrest group was able to harvest triplet-excited states in OLEDS via phosphorescence.[3-5] Recently, an unconventional way for harvesting the non-emissive triplets in organic materials has been developed. Thermally Activated Delayed Fluorescence (TADF) is the idea that room thermal energy may facilitate the non-emissive triplet conversion into emissive singlets in a reverse intersystem crossing (rISC) mechanism if the energy level difference between the triplet-singlet manifold is sufficiently small ($\Delta E_{ST} < 0.2$ eV).[6–9] OLEDs using organic TADF emitters have been able to pair the high EQE (External Quantum Efficiency) of their phosphorescent counterpart without the need of any additional coupling optics[6]. However,

the remaining key challenge precluding its commercialization is their poor device operational stability.

It was interesting to note that while many studies have been conducted to understand how the rISC of the TADF emitters may influence the device performances, not too many studies have been done in understanding the effect of aggregation on the device stability [10-14]. Adachi et al, reported photophysical properties and device efficiencies highly dependent on the type of host utilized for the device characterization.[10,11] Hidach et al. have shown that increasing the TADF emitter *wt* % in the emissive layer (EML) may increase the operational stability of the OLED[12]. Increment in the device stability was reported by Cui et al. when n-type host was used in the EML instead of traditional hosts[13]. These findings have been explained in terms of increased device stability due to an expansion of the electron and hole recombination zone[11,13]. Zhang et al. emphasizes the importance of steric hindrance effect on the TADF stability[14]. The study shows that the additional carbonyl group increase the OLED device operational life time by at least one order of magnitude. Most of these results have focused on structure-function properties. However, little to none has been done in understanding the excited state dynamics of TADF emitters upon aggregation and how they may influence the device operation.

In this chapter, we used multiple ultrafast spectroscopic techniques, with emphasis on the fluorescence upconversion and TA (Transient Absorption), to understand the excited state dynamics of multiple TADF isomer emitters shown in Fig. 5-3 upon aggregation. The TADF isomers are based on carbazole, benzonitrile, and Triazine, and were designed by the systematic modulation of their molecular structure. Their excited state dynamics were correlated with their device operational stability. We found particular differences in the excited state dynamics upon enhancing their intermolecular interaction that may dictate their device operational stability.

6-2.   Time-Resolved Fluorescence and Phosphorescence Measurements

The ultra-fast fluorescence upconversion (UpC) setup was used to measure the fluorescence with

ps time resolution as it has been previously described.[15] A mode-locked Ti-sapphire femtosecond

laser (Spectra-Physics Tsunami) was used to generate 80 fs pulses at 800 nm with a repetition rate

of 82 MHz. This Ti-sapphire mode-locked laser was pumped by a 532 nm CW laser (Spectra-

Physics Millennia), which has a gain medium of neodymium-doped yttrium vanadate (Nd:YVO4).

After the 800 nm pulsed beam is generated, a second harmonic (β- barium borate crystal) generates

a 400 nm excitation pulse. The residual 800 nm beam is directed to pass through a computer-

controlled motorized optical delay line. A Berek compensator controlled the polarization of the

800 nm excitation beam power varied between 33 to 40 mW. The fluorescence emitted by the

sample is upconverted by the residual 800 nm beam by a nonlinear crystal of β-barium borate. It

is important to mention that the 800 nm beam is passed by the optical delay line with a minimum

gate step of 6.25 fs. The monochromator is used to select the wavelength of the up-converted beam

of interest, and the selected beam is detected by a photomultiplier tube (R152P, Hamamatsu,

Hamamatsu City, Japan). The photomultiplier tube (PMT) converts the detected beam into photon

counts, which can be read from a computer. Coumarin 30 was used for calibrating the laser for the

range of emission wavelengths in this study. The instrument response function (IRF) has been

determined from the Raman signal of water to have a width of 110 fs.[16] Lifetimes of fluorescence

decay were obtained by fitting the fluorescence decay profile to the most accurate fit.

The time-correlated single photon counting (TCSPC) technique was used to study the

fluorescence and phosphorescence of the investigated chromophores. The laser used for the

TCSPC measurement was a Home-built mode-locked Ti-sapphire laser. The output beam from the laser was at 800 nm wavelength has a pulse duration of ~30 fs. The 800 nm output beam was frequency-doubled using a nonlinear barium borate crystal to obtain a 400 nm beam. Focus on the sample cell (quartz cuvette, 0.4 cm path length) was ensured using a lens of focal length 11.5 cm. Collection of fluorescence was done in a direction perpendicular to the incident beam into a monochromator, and the output from the monochromator was coupled to a photomultiplier tube, which converted the photons into electrical signals (counts). The Time Harp 200 is the PCI-board in charge of the histogram of photon creation (65,000 max) and its subsequent conversion into electrical signals. This electronic conversion process allows other electronic equipment in the room to interfere with the detection if the histograms are not finished fast enough. Therefore, electronic interference could be detected depending on how much time it takes to create the histogram (collect the 65,000 photons). The high density of photons by the excitation source make the IRF detection fast enough so no electronic interference is detected. In contrast to the IRF detection, the histogram created for the investigated samples are usually significantly slower than that of the IRF.

6-3.   Femtosecond Transient Absorption Measurements

Transient absorption measurement was carried out to observe the excited-state dynamics within one ns after photoexcitation of the TADF chromophores. A known procedure for this setup has been described in the literature.[16–17] Our system contains 1 mJ, 100 fs pulses at 800 nm with a repetition rate of 1 kHz. The output beam was split to generate pump (85 %) and probe beam (15 %) pulses with a beam splitter. An optical parametric amplifier (OPA-800C) was used to generate he pump beam. It was obtained from the fourth harmonic of the signal-idler beams and focused onto

a 2 mm quartz cuvette containing the sample. For the continuous white light generation, the probe beam was delayed with a computer-controlled motion controller and then focused into a sapphire plate. The white light was then overlapped with the pump beam in the sample cuvette, and the change in absorbance for the signal was collected by a charge-coupled device detector (Ocean Optics). Data acquisition was controlled by specialized software from Ultrafast Systems Inc. The typical power of the probe beam was < 0.1 μJ, and that of the pump beam was between 0.1-0.4 μJ per pulse. Magic angle polarization was maintained between the pump and probe beam using a wave plate. The pulse duration was around 130 fs. The sample was stirred with a rotating magnetic stirrer to prevent degradation.

6-4.   Results and discussion

All samples show similar absorption spectrum in chloroform and toluene (See Figure 5-4) except for the well-known charge transfer absorption region beyond the 380nm[10]. This indicates that the ground state molecular orbital is not critically changed by environment polarity and donor-acceptor orientation but critically affect the CT (Charge Transfer) state strength. Interestingly the different charge transfer absorption affects the TADF fluorescence spectrum and intensity of the TADF isomer. If the CT band in the absorption spectrum is strong the fluorescence intensity is strong as well, otherwise, the fluorescence intensity is very weak. The fluorescence spectrum of the compound with the stronger intensity is more blue color. This indicates that ΔE_{st} between the singlet and triplet or LE (Localized Excitation) of
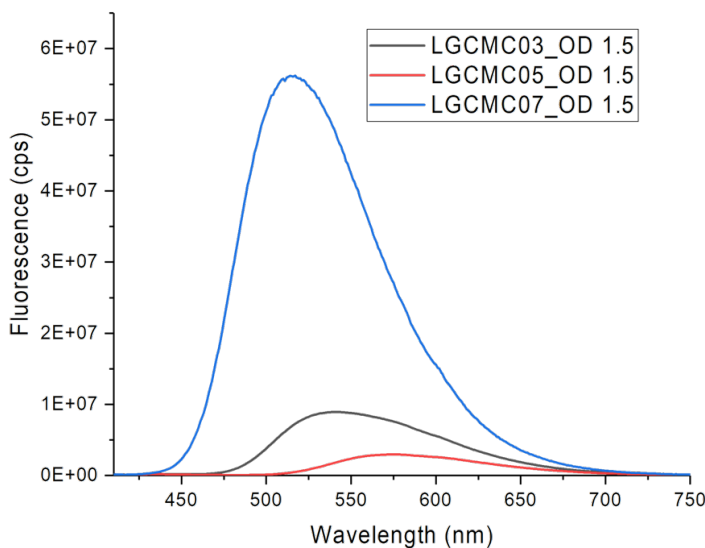
Figure 6-1. *Fluorescence spectrum of LGC-MC-03, LGC-MC-05 and LGC-MC-07.*

the molecular system[10, 11, 18-20] has been increased. To estimate the molecular interaction in similar

molecular distance, we adjusted the different molecule's absorption around 360nm to 1.5 O.D. We

believe that similar absorption coefficient leads to similar concentration of the different molecular

TADF isomers. Steady state fluorescence results in Figure 6-1. show the different fluorescence

spectra. The lowest fluorescence intensity of LGC-MC-05 indicates that its molecular systems has

higher ΔE_{ST} among the samples and stresses the importance of the localized triplet level of the

TADF molecules. To verify that the samples thus indeed have the TADF properties, single photon

counting used to measure the fluorescence decay dynamics. All samples were investigated at

ambient condition. Figure 6-2. shows that the fluorescence decay dynamics of the samples. All

samples show the traditional fluorescence decay dynamics of TADF OLED molecules, a prompt
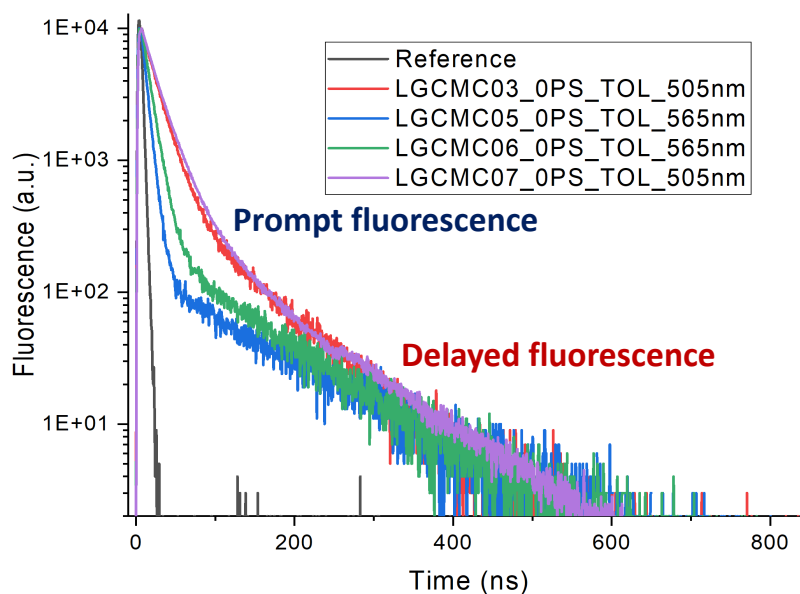
and delayed fluorescence.

Figure 6-2. *Fluorescence decay dynamics of the TADF OLED isomers.*

The samples have prompt fluorescence decays of ~50ns and delayed fluorescence decay component after the prompt fluorescence decay which shows much slower decay rate. Interestingly, LGC-MC-03 and 07 showed longer prompt fluorescence, then LGC-MC-06 and 07 followed. The delayed component of the isomers is opposite in comparison with the prompt fluorescence. This shows the relationship between the prompt and delayed fluorescence decay time in RISC regime. If the RISC rate is higher the delayed fluorescence decay time will be smaller due to its fast up-conversion from triplet to singlet. The prompt fluorescence decay time is highly correlated with the fluorescence intensity in same concentration of the isomer samples. It is well known that the higher rate of the TADF donor in the emissive layer of OLEDs increases the operational life time of the OLED devices[12, 13]. Adachi et al. explains that increasing TADF concentration expands the hole-electron recombination region[11-13]. This increases device operational life time. However, the intermolecular interaction such as pi-pi stacking due to increasing of the aggregation or crystalline rate inside of the layer cannot be neglected[21].
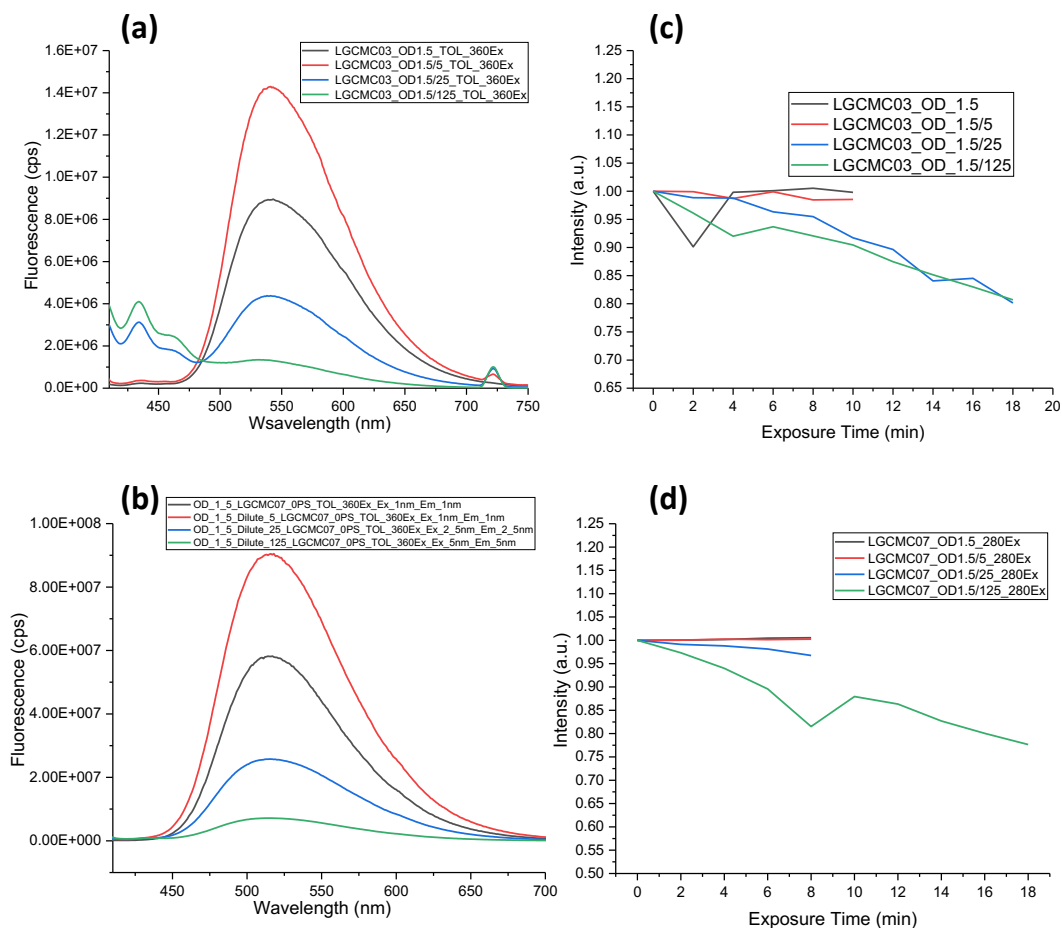
Figure 6-3. *Concentration dependent spectrum of LGC-MC-03(a) and 07 (b) and degradation late from UV-Exposure(c),(c).*

We therefore prepared the samples which have different concentration in toluene. Very high concentration sample were made and tested using steady state fluorescence analysis. Optical Density of the peak absorption of the samples was adjusted to 1.5. The TADF samples showed similar absorption spectrum except for the well-known CT absorption (Figure 5-4). Then, the samples were diluted by 5, 25, 125 times. We measured the fluorescence spectrum of the different concentration samples for LGC-MC-03 and LGC-MC-07. Figure 6-3. shows the steady state fluorescence spectrum. Interestingly, LGC-MC-03 and LGC-MC-07 shows very different

spectrum, LGC-MC-03 shows red shift fluorescence peak (~535nm), while LGC-MC-07 shows

505nm fluorescence maximum peak. If we assume that the fluorescence peak has been from the

singlet CT state, the triplet CT state might be closer to the ~505nm peak based on the TADF

efficiency equation[6]. This was also supported by the LGC-MC-06 results which shows that the

sample has a more red shifted fluorescence peak relative to LGC-MC-03, and shows very poor

fluorescence intensity due to larger ΔE_{ST}. More interesting results are shown on the different

concentration fluorescence spectrum results. For LGC-MC-03 lower concentration samples show

additional fluorescence spectrum around 450nm. The lower concentration, the more intense the

peak strength. However, LGC-MC-07 does not show the critical additional peak in comparison to

the LGC-MC-03. The sample LGC-MC-07 shows only tiny additional fluorescence in very diluted

(125 times) samples (Figure 6-3). However, the sample LGC-MC-03 shows fast fluorescence

decay from 280nm deep U.V. exposures (Figure 6-3) while LGC-MC-07 does not. It is surprising

that similar trends were introduced in the TADF OLED devices in different publication by Adachi

et al.[12] although the authors did not critically focus on the feature. In the publication, low

concentration samples which has additional fluorescence band shows faster degradation rate of the

fluorescence intensity. Core materials of the samples in the publication is carbazole and

benzonitrile. The structure of their core materials is very similar with the TADF isomers

investigated in this chapter. Hence we conclude that the additional fluorescence is detrimental to

the molecular stability for TADF fluorescence scheme. However, it is unclear why the dual

fluorescence cause less stable feature of the TADF molecules. To verify this, it is necessary to

understand the origin of the dual fluorescence. There are several reports of TADF showing dual

fluorescence[22, 23]. In the papers, additional fluorescence in blue region originates from the LE state
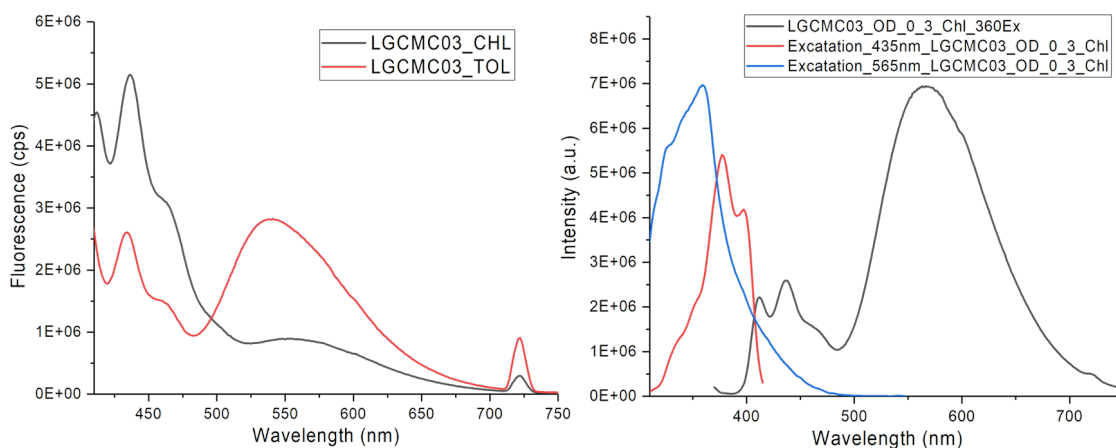
or CT state[22, 23].

Figure 6-4. *Fluorescence and excitation spectrum of LGC-MC-03.*

It is essential to verify the origin of the additional fluorescence. To verify that the additional fluorescence is caused from LE or CT, we measured the fluorescence spectrum and excitation of LGC-MC-03 in different solvents as shown in Figure 6-4. It is noteworthy that the main TADF fluorescence peak shifted from ~540 to 555nm in different polarity of solvent (chloroform and toluene). However, the additional spectrum from low concentration samples does not shift. That feature shows that the fluorescence spectrum is not related to the CT state fluorescence. Additionally, excitation measurements result supports that the additional fluorescence is originated from the LE state. Because the excitation spectrum resembles a mirror image of the additional fluorescence around 450nm while the excitation spectrum of the main TADF band is very similar to the absorption spectrum of the molecular system. These two features strongly support that the additional fluorescence caused form LE state of the TADF isomer. However, the reason as to why additional fluorescence from the LE state facilitate the fragmentation of the OLED materials is not clear yet. To verify this we need to understand the excited state dynamic of the TADF OLED molecules.
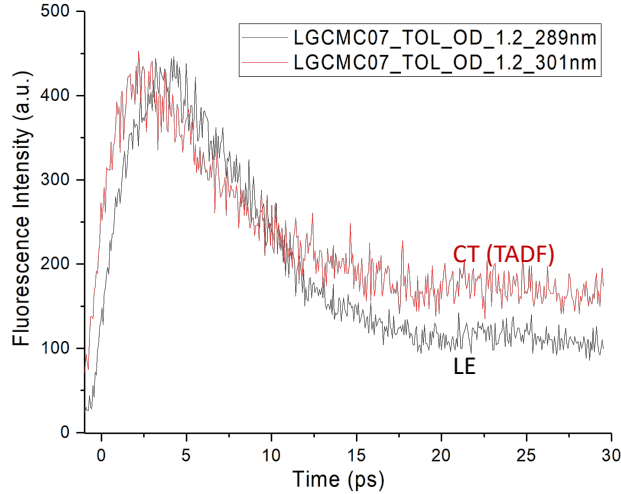
Figure 6-5. *Upconversion fluorescence measurement of the LGC-MC-07.*

We hence investigate the excited state fast dynamics of the two fluorescence spectrum area of the LGCMC07 using upconversion fluorescence spectroscopy. Although LGC-MC-03 shows the fastest degradation rate, its quantum efficiency is too low. It is difficult to achieve enough upconversion signals from the sample. We hence measured the fluorescence signals from LGC-MC-07. Figure 6-5. shows two fluorescence state decay dynamics of the two different wave length. Based on the eqation 2-2 and 2-3, 289nm and 301nm are responsible to the LE state and CT state fluorescence in Figure 6-4, respectively. The rise time to the peak fluorescence intensity is ~2.5ps and ~3.75ps for CT and LE state, respectively. This similar rise time shows that the two states are competitive for the very initial excited state. The fluorescence upconversion dynamics in different concentration has also been measured for the LGC-MC-07 and shown in Figure 6-6. Interestingly, the amount of upconversion fluorescence photon of the samples below 15ps is increased if the concentration is decreased. This means that the fluorescence intensity from the LE states has been increased in comparison with the higher concentration by consideration of the LE and TADF time domain.
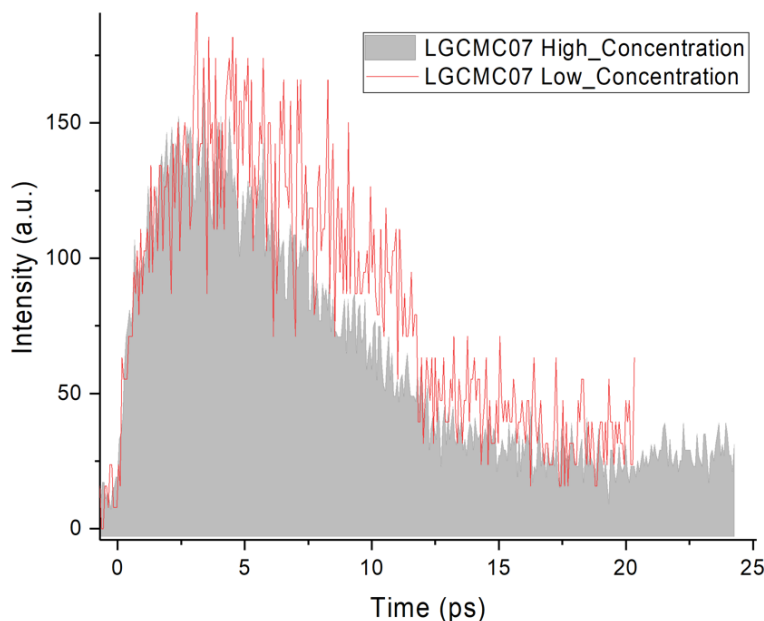
Figure 6-6. *Upcoversion fluorescence measurement results of LGC-MC-07 in different*

concentration.

These results are well correlated to the steady state fluorescence results of the TADF isomers. Additionally fs-transient absorption analysis supports that the low concentration TADF samples show more fluorescence orienting form the LE state. Figure 6-7. shows the fs-transient spectrum measurement results in visible and near IR. The TADF isomer shows almost similar transient absorption profile in very initial time (<10ps) for all concentration. All samples shows very similar ESA (Excited state absorption) spectrum. The ESA spectrum around 750nm might be assigned to the cationic carbazole moiety and the spectrum below 450nm, the benzonitrile moiety[10, 24]. Broad absorption between the two spectrum looks like the CT state absorption of the TADF molecules. There is no significant ESA spectrum due to the LE state in the fs-Transient absorption, however, we can deduce relative LE state population, if the LE and CT states are competitive.
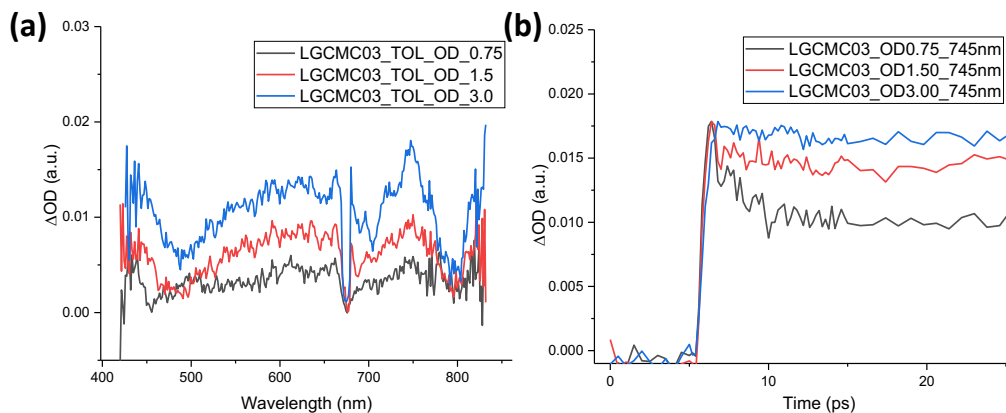
Figure 6-7*. Ultra-fast transient absorption of LGC-MC-03 in different concentration. a) Initial transient absorption on (<10ps). b) Transient-absorption dynamics at 745nm in different concentration.*

Fast excitation decay of the CT state has been interpreted as relatively higher LE state population. It is clear that a lower the TADF molecule concentration facilitates the rapid ESA decay at 745nm (Cationic Carbazole) from the figure 6-7. The cationic carbazole can be interpreted as the TICT (Twisted Intermolecular Charge Transfer) state[10]. This also supports that the higher LE state ratio on low concentration TADF samples if the CT state for TADF luminescence and LE state are competitive. All of the results from steady state, fs-upconversion fluorescence measurement and fs-transient has supported that low concentration TADF samples show the higher LE state emission. However, we need to verify why higher LE state emission increases the TADF molecular degradation. Firstly, the higher LE state emission can be induced from the poor LE state and CT state coupling. Monkman et al. insists that the spin forbidden RISC of the TADF is critically assisted by the LE and CT state coupling[18-20]. In this regime the higher LE state emission decreases the coupling rate, hence, the RISC rate. Hiroyuki et al. showed that higher RISC rate is important to enhance the TADF molecular stability[11].
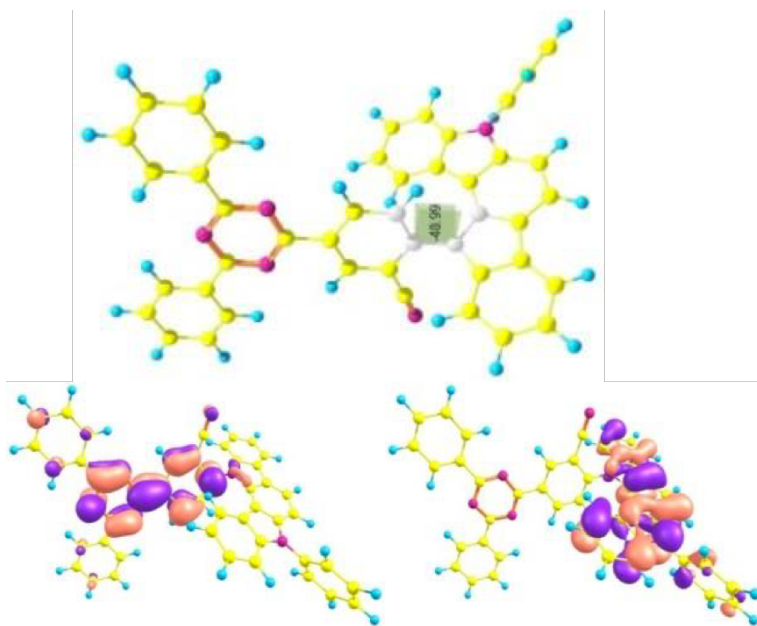
Figure 6-8*. DFT (Density Function Theory) calculation of the LGC-MC-07.*

It is clear that this decoupling between the LE and CT state is detrimental to the TADF molecular system stability. Secondly, we can get an idea of the structural orientation of the TADF materials. Core structure of the TADF has carbazole donor and benzonitrile and triazine acceptor. The structure is very similar with DMABN ((Dimethiamino)benzonitrile) representative dual fluorescence materials from LE and CT states[25-26]. Many publication insists that the CT state molecular structure is mostly TICT(Twist Intermolecular Charge Transfer) State that has high dihedral angle between donor acceptor bonding. In the molecule LE state has been oriented from planar structure[25-26]. Additionally, another TADF OLED molecule which has dual fluorescence has TADF features from quasi-equatorial TICT states and non-delayed fluorescence from the quasi axial structure[22]. Hence, it is rational to state that the TADF fluorescence caused from the TICT states and its dihedral angle is close to 90º and LE fluorescence of the molecules is via the planar structure of the molecules. These feature explain why low concentration samples shows much higher LE emission for the materials. Based on the DFT (Density Functional Theory) the

TADF isomers' ground state dihedral angle is between 40~60º (shown in Figure 6-8). Higher concentration might increase molecular aggregates leading to a more planar structure formation, while low concentration leads to a less intermolecular interaction. When we consider the different molecular structured orientation of each state, additional fluorescence may lead to more molecular structural change. By consideration of the very fast rise and relaxation time of the LE state, this structural change has increased the molecular bonding dissociation. Additionally, bond dissociation energy between the carbazole and benzonitrile also supports that the higher LE state emission is detrimental to molecular stability. Alexandra Ya. et al. calculates the bond dissociation energy of the phenyl and carbazole. In the paper the bond dissociation energy in neutral state is lower than the radical ionic states between the carbazole and phenyl bonding[27]. Although the molecular structure in the paper is not exactly same, it is noteworthy that the unexpected feature of the bond dissociation energy has been correlated with our measurement data. Finally, our DFT calculation data shows that the dihedral angel beyond a specific angle (~50 degree) is inversely proportional of the delayed fluorescence decay time. We believe that the higher dihedral angle favors the TICT state rather than planar LE state. As a consideration that the shorter delayed fluorescence decay time leads to a higher RISC rate which is beneficial to the TADF stability[11], it might also be noteworthy that additional fluorescence from the LE state is not a good sign for TADF molecular stability.

6-5.   Conclusion

In this chapter the origin of the TADF molecules fragmentation mechanism from LE state fluorescence using ultra-fast femtosecond spectroscopic analysis has been proposed. Our findings show one possible TADF molecular degradation pathway from the LE state in ps time scale. DFT calculation, upconversion fluorescence measurement and fs-transient results support the relationship of the concentration dependent LE state population and TADF degradation. Our measurements shows that the degradation also highly affected by the fast time scale at the LE states. Higher LE state induces molecular structural change within 10ps and leads unstable planar structure of the TADF. The structural change in such very fast time scale might cause additional TADF molecular instability. To this regards, our results may give a new design rule of the TADF materials to solve the current poor operational life time problem.

6-6. References

1.   Minaev, B.; Baryshnikov, G.; Agren, H. Principles of phosphorescent organic light emitting devices. *Phys. Chem. Chem. Phys.*, **2014**, 16, 1719-1758.

2.   Vicca, P.; Steudel, S.; Genoe J.; Heremans, P. Adhesion Promoting Polymer Interlayers for Ag Layers Deposited in OLED Processing. *J. Adhes. Sci. Technol.,* **2010**, 24 , 1145.

3.   Baldo, M. et. al. Highly efficient phosphorescent emission from organic electroluminescent devices. *Nature*, **1998**, 395, 151.

4.   Kim, S. et. al. Degradation of blue-phosphorescent organic light-emitting devices involves exciton-induced generation of polaron pair within emitting layers. *Nat. Commun.*, **2018**, 9, 1211.

5.   Klimes, K.; Zhu, Z.; Li, J. Efficient Blue Phosphorescent OLEDs with Improved Stability and Color Purity through Judicious Triplet Exciton Management. *Adv. Funct. Mater.*, **2019**, 29, 1903068.

6.   Uoyama, H.; Goushi, K.; Shizu, K.; Nomura, H.; Adachi, C. Highly efficient organic light-emitting diodes from delayed fluorescence. *Nature*, **2012**, 492, 234-238.

7.   Di, D. et. al. High-performance light-emitting diodes based on carbene-metal-amides. *Science*, **2017**, 356, 159-163.

8.   Hamze, R. et. al. Eliminating nonradiative decay in Cu(I) emitters: >99% quantum efficiency and microsecond lifetime. *Science,* **2019**, 363, 601-606.

9.   Yang, Z. et. al. Recent advances in organic thermally activated delayed fluorescence materials. *Chem. Soc. Rev.*, **2017**, 46, 915-1016.

10.   Hosokai, T. et. al. Evidence and mechanism of efficient thermally activated delayed fluorescence promoted by delocalized excited states. *Sci. Adv.*, **2017**, 3, e1603282.

11.   Noda, H.; Nakanotani, H.; Adachi, C. Excited state engineering for efficient reverse intersystem crossing. *Sci. Adv.*, **2018**, 4, eaao6910.

12.   Nakanotani, H.; Masui, K.; Nishide, J.; Shibata, T.; Adachi, C. Promising operational stability of high-efficiency organic light-emitting diodes based on thermally activated delayed fluorescence. *Sci. Rep.*, **2013**, 3, 2127.

13.   Cui, L. et. al. Long-lived efficient delayed fluorescence organic light-emitting diodes using n-type hosts. *Nat. Commun.*, **2017,** 8, 2250.

14.   Zhang, D.; Cai, M.; Zhang, Y.; Zhanga, D.; Duan, L. Sterically shielded blue thermally activated delayed fluorescence emitters with improved efficiency and stability. Mater. Horiz., 2016, 3, 145-151.

15.   Vázquez, R. et. al. Evaluating the Effect of Heteroatoms on the Photophysical Properties of Donor–Acceptor Conjugated Polymers Based on 2,6-Di(thiophen-2-yl)benzo[1,2-b:4,5-b′]difuran: Two-Photon Cross-Section and Ultrafast Time-Resolved Spectroscopy. *J. Phys. Chem. C*, **2017**, 121 , 14382 -14392.

16.   Flynn, C.; Ramakrishna, G.; Yang, H.; Northrop, B..; Stang, P.; Goodson, T. Ultrafast Optical Excitations In Supramolecular Metallacycles with Charge Transfer Properties. J. *Am. Chem. Soc.*, **2010**, 132, 1348– 1358.

17.   Keller, B. et. al. Investigating the Optical Properties of Thiophene Additions to s-Indacene Donors with Diketopyrrolopyrrole, Isoindigo, and Thienothiophene Acceptors. *J. Phys. Chem. C,* **2018**, 122, 27713−27733.

18.   Gibson, J.; Monkman, A., Penfold, T. The Importance of Vibronic Coupling for Efficient Reverse Intersystem Crossing in Thermally Activated Delayed Fluorescence Molecules. *Chem. Phys. Chem.*, **2016**, 17, 2956 –2961.

19.   Penfold, T.; Dias, F.; Monkman, A. The theory of thermally activated delayed fluorescence for organic light emitting diodes. *Chem. Commun.*, **2018**, 54, 3926-3935.

20.   Etherington, M.; Gibson, J.; Higginbotham, H.; Penfold, T.; Monkman, A. Revealing the spin–vibronic coupling mechanism of thermally activated delayed fluorescence. *Nat. Commun.*, **2016**, 7, 13680.

21. Godumala, M.; Choi, S.; Cho, M.; Choi, D. Recent breakthroughs in thermally activated delayed fluorescence organic light emitting diodes containing non-doped emitting layers. *J. Mater. Chem. C*, **2019**, 7, 2172-2198.

22. Tanaka, H.; Shizu, K.; Nakanotani, H.; Adachi, C. Dual Intramolecular Charge-Transfer Fluorescence Derived from a Phenothiazine-Triphenyltriazine Derivative. *J. Phys. Chem. C*, **2014**, 118, 15985-15994.

23. Li, X. et. al. A three-dimensional ratiometric sensing strategy on unimolecular fluorescence–thermally activated delayed fluorescence dual emission. *Nat. Commun.*, **2019**, 10, 731

24. Kohler, G.; Grabner, G.; Rotkiewicz, K. Nonradiative deactivation and triplet states in donor-aryl-acceptor compounds (dialkylaminobenzonitriles). *Chem. Phys.*, 1993, 173, 275-290.

25. Zachariasse, K.; Druzhinin, S.; Kovalenko, S.; Senyushkina, T. Intramolecular charge transfer of 4-(dimethylamino)benzonitrile probed by time-resolved fluorescence and transient absorption: No evidence for two ICT states and a $\pi\sigma^*$ reaction intermediate. *J. Chem. Phys.*, **2009**, 131, 224313.

26. Segado, M.; Mercier, Y.; Gómeza, I.; Reguero, M. Intramolecular charge transfer in aminobenzonitriles and tetrafluoro counterparts: fluorescence explained by competition between low lying excited states and radiationless deactivation. Part II: influence of substitution on luminescence patterns. *Phys. Chem. Chem. Phys.*, **2016**, 18, 6875.

27. Freidzon, A. et. al. Predicting the Operational Stability of Phosphorescent OLED Host Molecules from First Principles: A Case Study. *J. Phys. Chem. C*, **2017**, 121, 40, 22422-22433.

CHAPTER VII

Conclusion

In this dissertation the localized molecular interaction of organic electronic materials has been investigated. The main purpose of this dissertation is a give a pathway to understand and utilize the organic molecular system better. Using different sets of experiments, I studied several important issues to answer the question raised in this dissertation. Near field optical scanning microscope in two-photon mode by a sequence of phase-locked femtosecond pulses allows us to measure the coherence dynamics at the local level including the coherent energy transfer in DPDI acceptor film, as well as obtaining the dephasing time for the acceptor in the photovoltaic blend. The experiment clearly shows the feasibility of detecting the coherent contribution to the local excitation energy transport on the femtosecond time scale and measuring the dephasing time on a spatial scale of tens of nm in photovoltaic systems. More importantly the effect of local structural properties on the coherent transport contribution in multi-chromophore systems were probed with this approach. I believe that the work opens important avenues in the investigation of functionalities of solar and energy conversion devices enhanced by the quantum coherence as well as the fast processes in other classical and quantum related phenomena in the solid state. Additionally, the time-resolved spectroscopy and microscopy investigation presented in this dissertation have provided information on coherent transport properties of dendritic

121

macromolecules in solution and in organic films. Through this comparison, the dendron structures lead to longer exciton mobility properties due to stronger intra-and inter-molecular couplings occurring in the solid-phase with respect to dendrimer structure. This result shows the importance of combining liquid and solid phase spectroscopy results. This combination of powerful spectroscopic methods could yield an efficient way of improving the potential of this class of organic macromolecules for light harvesting applications. A simple method to estimate the molecular system stability for the OLED devices has also been proposed. NSOM microscopy for fluorescence measurement in molecular level shows its powerful possibility to measure the OLED materials stability without real OLED device fabrication. Using this methods it is expected to minimize the measurement time for the OLED properties measurement, and therefore, decrease the device measurement time to facilitate more material development. Finally, the origin of the TADF molecules fragmentation mechanism has been proposed using ultra-fast femtosecond spectroscopic analysis. The findings show one possible TADF molecular degradation in fast time scale. Our measurements shows that the degradation is also highly affected by the fast time scale of LE states population dynamics. Higher LE state population induces molecular structural change within 10ps and leads unstable planar structure of the TADF. Overall, my work in this dissertation is mainly focused on the verification of the intermolecular interaction of organic molecules aggregates and indicates the importance of fundamental physical investigation of the materials. The results in this dissertation may give a new design rule of the TADF and light-harvesting materials to solve the current poor operational life time problem and relatively low efficiency. At the moment in which the field of organic electronic materials is still burgeoning, I wish that the fundamental physical investigation assist the development of highly applicable materials for the organic electronic devices which has the potential to make our life more valuable.